Flat-Plate as a Lift Generating Device for Low Reynolds Number Applications

A Thesis
Submitted in Partial Fullfillment of the Requirements for
The Award of the Degree of

Doctor of Philosophy

By

Bastav Borah
Regn. No. 186103009

Department of Mechanical Engineering
Indian Institute of Technology Guwahati
Guwahati- 781039, Assam, India

Department of Mechanical Engineering
Indian Institute of Technology Guwahati
Guwahati-781039, India

DECLARATION

I hereby certify that the research presented in this dissertation, titled: Flat-Plate as a Lift Generating Device for Low Reynolds Number Applications, was conducted under the supervision of Prof. Vinayak N. Kulkarni and Prof. Ujjwal K. Saha in the Department of Mechanical Engineering at the Indian Institute of Technology Guwahati, India.

This work is original and has not been previously submitted for any degree, diploma, associateship, fellowship, or equivalent qualification at any other university or institution.

Date: June 26, 2025

Bastav Borah
Reg. No.: 186103009
Department of Mechanical Engineering
Indian Institute of Technology Guwahati

Department of Mechanical Engineering
Indian Institute of Technology Guwahati
Guwahati-781039, India

CERTIFICATE

It is certified that the work contained in the thesis entitled: Flat-Plate as a Lift Generating Device for Low Reynolds Number Applications, submitted by Mr. Bastav Borah to the Indian Institute of Technology Guwahati for the award of the degree of Doctor of Philosophy has been carried out under our Supervision in the Department of Mechanical Engineering, Indian Institute of Technology Guwahati. This work has not been submitted elsewhere for the award of any other degree or diploma.

Vinayak N. Kulkarni
(Professor)
Department of Mechanical Engineering
Indian Institute of Technology Guwahati

Ujjwal K. Saha
(Professor)
Department of Mechanical Engineering
Indian Institute of Technology Guwahati

ACKNOWLEDGEMENT

Completing this PhD thesis has been an extraordinary journey filled with challenges, growth, and learning. It is a culmination of the support, guidance, and encouragement I have received from numerous individuals and organizations, to whom I am deeply indebted.

First and foremost, I express my heartfelt gratitude to my advisors, Prof. Ujjwal K. Saha and Prof. Vinayak N. Kulkarni. Their invaluable guidance, profound knowledge, and unwavering support have been the cornerstones of my academic journey. Their insightful feedback, encouraging words, and constructive criticism have been instrumental in shaping the direction of this research and my growth as a scholar. I am truly fortunate to have had the privilege of working under their mentorship.

I am also sincerely thankful to the members of my dissertation committee—Prof. Niranjan Sahoo, Assoc. Prof. Pranab K. Mondal, and Prof. Bimlesh Kumar—for their thoughtful suggestions and constructive feedback. Their expertise and commitment to academic excellence have significantly contributed to the refinement and depth of this research.

To my dear friends Anand Verma, Ojing Siram, and Kavita Naik, along with many others who have been my pillars of support, I am profoundly grateful for your unwavering encouragement. Whether it was through motivating conversations that uplifted my spirits, late-night discussions that provided clarity, or moments of laughter that eased the pressures of academic life, your companionship has been a source of strength and joy throughout this journey. Your belief in me has been a constant source of motivation.

I am deeply appreciative of my colleagues and friends in the Department of Mechanical Engineering, IIT Guwahati, for their camaraderie, collaboration, and inspiration. Working alongside such talented and dedicated individuals has been an enriching experience. From engaging technical discussions to collaborative experiments and shared academic struggles, your presence has made this journey both rewarding and enjoyable.

I would also like to acknowledge the invaluable support of the technical and administrative staff in the Department of Mechanical Engineering and the Wind Tunnel Lab. Your tireless efforts, efficiency, and readiness to assist have ensured the smooth functioning of the lab and significantly contributed to the progress of this research.

To my family, words cannot fully express my gratitude for your unconditional love, patience, and belief in me. You have been my anchor through the most challenging moments, providing the strength and encouragement I needed to persevere. Your sacrifices and constant support have been the foundation upon which this journey was built.

Finally, I would like to extend my gratitude to every individual who has contributed to this journey in ways both big and small. From mentors and colleagues to friends and well-wishers, each of you has played a part in shaping this journey.

This thesis is not merely a reflection of my efforts but also a testament to the support, belief, and encouragement of all those who have stood by me. Thank you for being part of this incredible journey.

Bastav Borah

ABSTRACT

The flow of fluids has always been an interesting and complex topic for research. With respect to fluid flow in the field of aerodynamics, a lot of research work has been carried out to determine the shape and size of aerofoils that can extract the maximum amount of performance. As is the case with most studies, majority of these investigations were driven by market forces or the prevailing requirements of the time period. As a result, a remarkable section of these studies was conducted for flows around the Reynolds number (*Re*) of 10^6, at which the commercial airliners operate. This has resulted in extremely optimised wing designs that operate at their maximum efficiency.

For the flows at *Re* lesser than 10^6, the design ideas from the above studies cannot be directly implemented. This region of *Re* is generally observed in Micro Aerial Vehicle (*MAV*) operations, small sized micro wind turbines with an overall restriction in the size of the devices. Staying within these dimensional constraints, similar level of optimised performance cannot be obtained by implementing the configuration and design modifications of normal sized aircraft wings. A number of experimental studies have established the fact that simply downsizing a regular wing into smaller size will not yield identical results.

In the *Re* range of 10^4-10^6, it was observed via experimental studies that a normal flat-plate has better lift-to-drag ratio (*L/D*) than the conventional streamlined wings. A typical fixed-wing low-speed aircraft has a maximum *L/D* ratio which is greater than 10. But for the range of *Re* under consideration, insects and birds usually have this ratio lower than 10. The separation of flow and subsequent generation of laminar separation bubble is different at different *Re*. At these *Re*, the flow is laminar and a transition to turbulent flow will help in overcoming the flow separation. A flat-plate is observed to offer better and a fairly constant L/D ratio in this spectrum of *Re*.

Wind tunnel experiments are conducted to study the flow around a flat-plate to understand the aerodynamic behaviour around it. In this regard, the frequency of vortex shedding is measured for flat plates at different aspect-ratios. A channel of inverted-dimples is placed on the suction side of the flat plate to initialise transition to turbulent flow and the lift/drag forces are measured. Subsequently, an attempt is made to improve the performance of the flat-plate so that it can be effectively used as a lift generating device for low *Re* flow. Inspiration is taken by emulating natural design elements found in birds. The wing-tip feathers of long-distance soaring birds are mimicked to increase the lift force while maintaining a relatively consistent drag force. The improvement in the fields of information technology, manufacturing processes and general computing power has brought an increase in the use of *MAV*s. The scope of adopting flat-plate as a lift generating device for *MAV*s can be definitely explored due to its design and fabrication simplicity.

CONTENTS

NOMENCLATURE

Notations

C_D	Coefficient of Drag
C_{Dmax}	Maximum Coefficient of Drag
C_L	Coefficient of Lift
C_{Lmax}	Maximum Coefficient of Lift
C_p	Pressure Coefficient
e	Oswald's Efficiency Factor
Re	Reynolds Number
St	Strouhal Number

Abbreviations

AoA	Angle of Attack
AR	Aspect Ratio
CFD	Computational Fluid Dynamics
CTA	Constant Temperature Anemometer
DAQ	Data Acquisition System
DARPA	Defense Advanced Research Projects Agency
FFT	Fast Fourier Transform
HWA	Hot Wire Anemometer
L/D	Lift-to-Drag
L/D_{max}	Maximum Lift-to-drag
LE	Leading Edge
LSB	Laminar Separation Bubble
MAV	Micro Aerial Vehicle/ Micro Air Vehicle
NACA	National Advisory Committee for Aeronautics
NASA	National Aeronautics and Space Administration
PIV	Particle Image Velocimetry
PSD	Power Spectral Density
RANS	Reynolds Averaged Navier-Stokes
SD	Standard Deviation
TE	Trailing Edge
UAV	Unmanned Aerial Vehicle

LIST OF FIGURES

LIST OF TABLES

Chapter 1: Introduction

Chapter Outline

Overview:

With the advancement of material science and computation power, there has been a considerable rise in the number of research studies at low Reynolds number which was not feasible in earlier times. The fact that a low Reynolds number flow has certain distinct and peculiar behaviours when compared with flows at higher Reynolds number, makes this an interesting field for research. The primary push for low Reynolds number application is the recent increase in the adoption of Micro Aerial Vehicles in various domains right from a predominant military use to civilian applications such as last mile delivery option, flood reconnaissance, medical supply in far flung areas etc. This chapter gives a brief summary about low Reynolds number flows and its association with Micro Aerial Vehicles. The final section will outline the research objectives along with the roadmap and blueprint of the thesis.

1.1 Motivation

Since the advent of human flight, improvement in the design of efficient wings has been an ongoing process. Numerous studies and research work have been put into intricately studying the air flow characteristics and finding out design modifications which can bring an improvement in the performance of wings. In this regard, aerodynamicists have been working on airfoils as well as on 3-dimensional wings via different methods and ideas to bring an efficient enhancement in performance. This has been a continuous process since the time of Wright brothers. The commercialisation of the aviation industry led to a race of improvement in design particularly with respect to increasing the wind speed at higher Reynolds number (*Re*). These led to the relegation of studies in the lower *Re* range, i.e. around 10^4–10^5. Only in the recent times, with an increase in the demand for low speed applications, research in low *Re* flow has generated an interest.

The rise in the use of Unmanned Aerial Vehicles (*UAV*)/ Micro Aerial Vehicles (*MAV*) in a variety of civil (Figure 1.1) and military applications have primarily pushed the demand of research into low *Re* flows (McMasters and Henderson, 1979).

Figure 1.1: Use of MAVs in flood and forest fire
source: indiatoday, cba

The commercial airline industry operates at *Re* higher than 10^6, whereas the *UAV*s/*MAV*s operate at *Re lower t*han 10^5 (Figure 1.2). A number of studies have established the fact that conventional airfoils designed for high *Re* applications do not perform well at lower *Re* (McMasters and Henderson, 1979; Mueller, 2004, 1999). There is ample scope for investigating design of airfoils that can provide adequate performance improvements in *MAV*s at lower Re. Most of the work related to low *Re* was being done with respect to *MAV* application and that too was concentrated in the defence sector (Grasmeyer and Keennon, 2001). The military use of *MAV* requires highly complicated and state-of-the-art technologies to remain ahead of the game, which is not in case of its civilian applications. The use of *MAV*s in the field of flood warning, forest fire reconnaissance, wild life preservation have already started and the primary requirement of these applications is durability, simple design and a longer flight time.

The use of flat-plates as lift generating devices has been studied by a number researchers (Lam and Leung, 2005; Lam and Wei, 2010; Nakamura et al., 1991). The results obtained in these studies show that there is a possibility of using flat-plate with *MAV*s by making certain alterations in its geometry. A regular flat-plate is the simplest of all geometrical shapes and even with certain elementary modifications, its fabrication will not be very costly. A *MAV* assembled with a flat-plate wing will drastically reduce its cost and can give a huge boost to the applicability of *MAV*s.

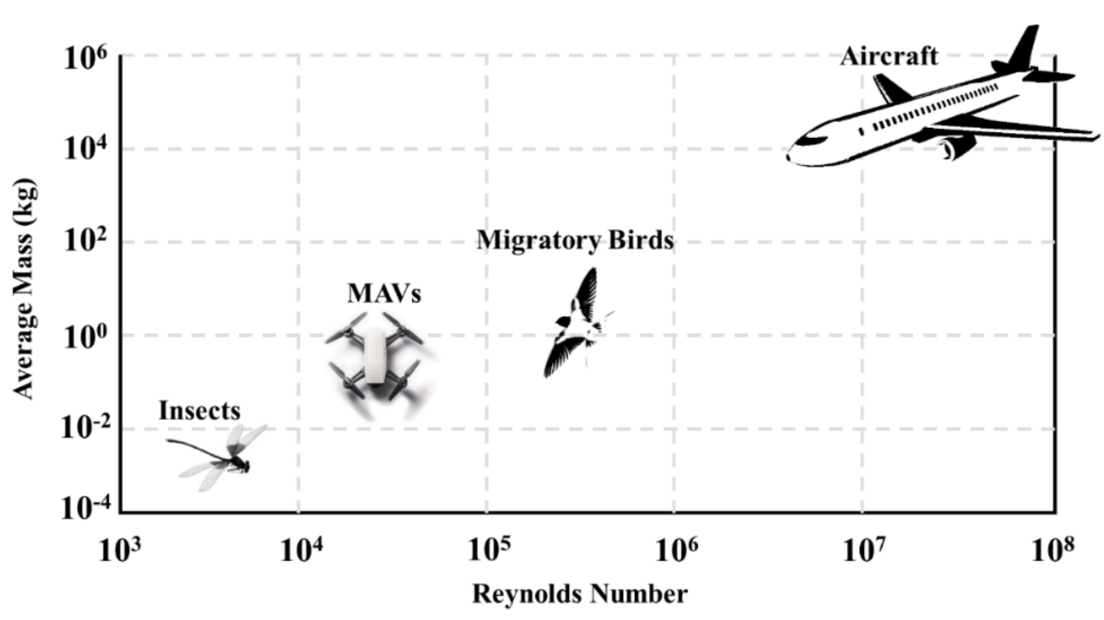

Figure 1.2: Distribution of aerodynamic applications
(Adapted from Mueller 1999)

1.2 Challenges

Flow separation poses a great challenge particularly with respect to aerodynamic application. It leads to an increase in pressure drag for airfoils due to the modified pressure field. Even loss of lift or stall condition may be reached because of this situation. As the flow gets separated from the surface, eddies and vortices are formed which begin to shed off from the bounded surface. These phenomena are known as Karman vortex street and it happens at a certain frequency. If this frequency matches with the resonance frequency of the structure, it may lead to structural failures.

The increased pressure drag causes a lot of unwanted conditions, right from loss of lift to even stalling of aerial vehicles. This issue multiplies exponentially with respect to low *Re* applications such as *MAV*s. The low speed flow doesn't lead to reattachment as in the case of flows at higher *Re*. Due to overall dimensional restriction, the chord length of *MAV* wings is shorter with respect to their span. This results in less lift generation compared to conventional larger aspect ratio (*AR*) aerial vehicle wings. This issue is again compounded by flow separation leading to further reduction in lift. The lesser surface area available for lift generation in case of low *AR* wings is further reduced by the separated flow. Hence, keeping the flow attached with the surface and thereby increasing the surface area for lift generation will greatly improve the performance of an *MAV*. Flow separation from a flat-plate is shown in Figure 1.3.

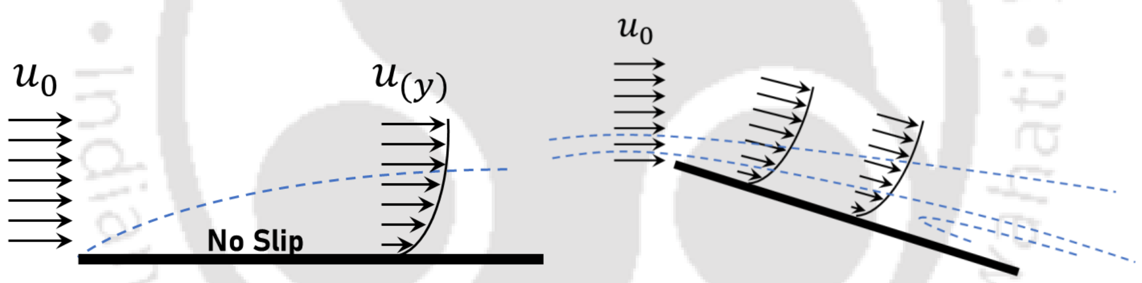

Figure 1.3:Flow separation from a flat-plate

In case of flow around a flat-plate, the sharp leading edge (*LE*) prompts faster separation of the flow. A number of studies have shown that a thinner flat plate (Laitone, 1997; Sunada et al., 2000, 2002) with a rounded *LE* has better flow characteristics than an unmodified flat-plate, when lift-to-drag (*L/D*) ratio is considered. The bluntness at the *LE* of a regular flat-plate initiates earlier flow separation which is then unable to reattach to the surface, at higher Angle of Attack (*AoA*). Particularly in the case of integrating a flat-plate as a wing on *MAV*s the span of the wing has to be shorter as *MAV*s has overall size restrictions. As per the classification, *MAV*s are low powered unmanned autonomous flying vehicles having a linear dimension of around 15 cm, gross take-off weight of approximately 100 g with a payload of 20 g. Surveys of the available research work on *MAV*s and flat-plate wings have shown that there is a dearth of scientific work in these field.

An inevitable consequence of lift generated by a planform is induced drag. Due to the pressure difference between suction (top) and pressure (bottom) side of the wing, air leaks from the pressure side to the suction side via the wingtips. The air flowing over the top has a tendency to curl up inwards, whereas the air below flows outward and curls towards the top, this phenomenon is shown in Figure 1.4.

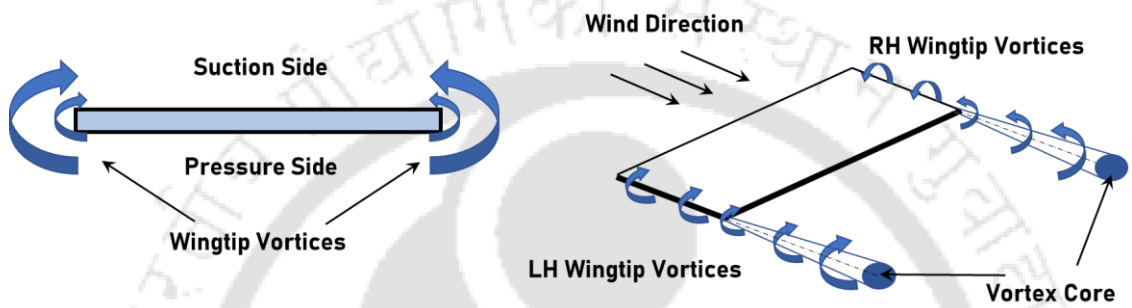

Figure 1.4: Illustration of air leakage from bottom to top

This results in a continuous spillage of high pressure air which causes a reduction of the effective lift produced by the planform, essentially creating a form of drag named as induced drag. Vortices are formed at the trailing edge (*TE*) due to the different streams of air flowing from the top and bottom surfaces of the planform. These vortices has a clockwise and anti-clockwise sense of rotation at the left and right ends of the wing, respectively, when viewed from the rear. These tip vortices are responsible for the formation of induced drag, also known as lift independent drag. One way to overcome this challenge is through the use of high *AR* wings which reduces this spillage and provides a greater surface area for lift generation. However, generally speaking aircrafts have a practical limit on size and more specifically in the case of *MAVs* there is further reduction in the availability of space as well as weight. Inspiration can be found from nature to conquer these hurdles in the form of birds' wingtips.

1.3 Biomimetics Solution: Birds' Wingtip to Flat-plate Winglets

Nature has always provided solutions to the challenges of man. With respect to improving performance of flat-plate wings, we look at the configuration of a birds' wingtip feathers. A few feathers extend from the tip of the wings which has been observed to be beneficial for soaring. In Figure 1.5, the wingtip feathers of a variety of birds can be seen to be spread, like the spread of fingers of a human beings' hand. These birds can soar for a long period of time without any significant use of energy. A significant reduction in lift-induced drag was thought to be achieved by the wingtip feathers slotted configuration (Tucker, 1995).

Figure 1.5: Wingtips of birds in flight

The slots also appeared to reduce the component of drag that was due to vertical vortex shedding. Wind tunnel experiments have been conducted which showed that the removal of wingtip slots in birds lead to an increase in the drag. A corollary that can be derived from these studies is that the addition of feather like attachments to the tip of a flat-plate can bring in improvement in its *L/D* ratio. Birds have some amount of control on the movement of these wingtip feathers, but similar handling is not possible in case of an *MAV*. Nonetheless, the implementation of rigid wingtip devices provide certain benefits which can be achieved without any sort of control.

1.4 Present Objective and Road Map

Humans have always looked at birds while fantasizing about soaring in the sky. In the present study, an attempt is made to enhance the performance parameters of a flat-plate as a lift generating device, particularly with respect to its application on *MAV*s. The shape and geometrical simplicity of a flat-plate will curtail the overall fabrication costs of *MAV* which can intensify the widespread use of *MAV* applications. Flow in the *Re* range of 10^4-10^5 is widely termed as low *Re* flow. In the research works conducted till now, for low *Re* aerodynamic applications, mostly conventional airfoils have been studied. Notable investigations in this field have been conducted by Sunada et al. (2000, 2002), Badrya et al. (2018), Okamoto and Azuma, (2005, 2011), O'Meara & Mueller (1986), Ananda et al. (2015), Ananda et al. (2012), Pelletier and Mueller (2000) among others.

Based on these studies, in the present investigation, a study is conducted on flat-plate wings to gauge its applicability for low *Re* applications, specifically for fixed-wing *MAV* use. In this regard, initially, a computational comparative study is conducted between a flat plate and an S5010 airfoil to measure the performances of these airfoils at low *Re*. Thereafter, experimental studies are conducted on flat-plate wings to measure its coefficient of lift (C_L) and drag (C_D). This would help in calculating the *L/D* ratio of the wings which will act as the baseline data. Further, certain bio-inspired modifications are carried out on the flat-plate wings to improve its performance.

1.5 Organisation of The Thesis

The central theme of this thesis is the improvement in *L/D* of a flat-plate wing. There are eight chapters in this thesis which are summarised as below:

The study begins in Chapter 1 with an introduction to fundamental aerodynamic principles, focusing on lift and drag, and the significance of flat plates in aerodynamic design. Chapter 2 provides a literature review, highlighting current applications of flat plates and identifying gaps in existing research. Chapter 3 outlines the research methodology, detailing computational and experimental setups. Chapters 4 through 7 explore various flat-plate wing configurations: Chapter 4 analyzes computational findings, while Chapters 5, 6, and 7 examine experimental results of wings with inverted dimples, planar attachments, and non-planar attachments, respectively, assessing their impact on aerodynamic performance. Chapter 8 concludes by synthesizing insights, emphasizing advancements in flat-plate wing designs, and inspiring future research in aerodynamic innovation.

1.6 Road Map

The roadmap of the investigation is visually depicted in Figure 1.6, serving as a navigational guide through the research process. This illustration presents a graphical representation of the sequential steps and key milestones achieved throughout the study. It outlines the flow of the research, from the initial objectives and methodology to the analysis and conclusions drawn. By providing a comprehensive overview of the research trajectory, the figure aids in understanding the organization and progression of the investigation, highlighting how each component contributes to the overall findings. This visual tool enhances the reader's ability to grasp the structure of the research and its systematic approach.

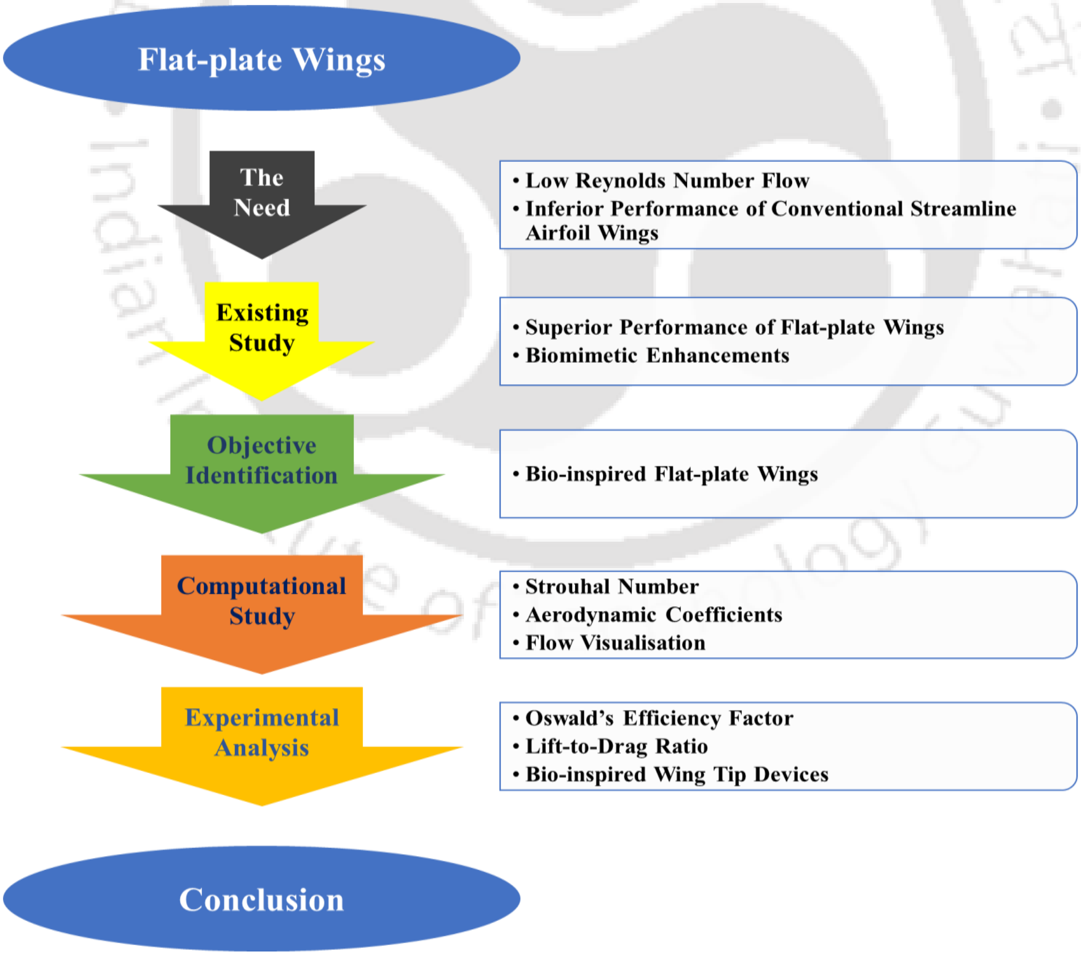

Figure 1.6: Roadmap of the present investigation

Chapter 2: Literature Review

Chapter Outline

Overview:

A significant portion of aerodynamic research focuses on high Reynolds number flows exceeding 10^6*, which aligns with the operating conditions of the commercial aviation industry. In contrast, flows with Reynolds number below* 10^6*, the typical domain for Micro Air Vehicles, often involve studies primarily conducted by defence-related organizations like DARPA and NASA, formerly known as NACA. While some of these studies are publicly accessible, a large portion remains classified due to their sensitive nature. These studies usually focus on advanced technologies and highly specialized applications, which may not be relevant for civilian use. This chapter presents a comprehensive literature review of aerodynamic studies related to flat-plate wings, with a focus on lift generation capabilities. Additionally, it covers biomimetic research aimed at enhancing aerodynamic characteristics. A collection of general studies on low Reynolds number aerodynamics is also included. The chapter concludes by identifying research gaps in existing literature and outlining the objectives for further exploration.*

2.1 Introductory Remark

Flat plate wings, with certain modifications, hold significant potential as lift-generating devices in low *Re* applications. However, to realize this potential, a deeper understanding of flow behaviour at low *Re* is essential. Extensive experimental and computational analyses have been carried out to study low *Re* fluid dynamics, but this report can only cover the most accessible references due to the vastness of the literature. The continuous improvement in computational power has led to the development of advanced *CFD* schemes, allowing for a more accurate representation of low *Re* flows. Despite these advancements, properly conducted experimental studies remain the most reliable source of data for validating these simulations.

In this section, a comprehensive overview of both experimental and computational studies that explore the use of flat-plate wings as lift-generating devices is provided. This includes a review of existing methodologies, as well as newer approaches inspired by avian biomimetics, which are covered in the following section. The goal is to offer insights into the current state of research and identify potential areas for further exploration. In addition to summarizing previous research, this section seeks to highlight the key trends and gaps in the study of flat-plate wings for low *Re* applications. It outlines the challenges associated with experimental setups and computational models, emphasizing the need for robust experimental validation to support computational findings. Furthermore, this section examines the impact of various modifications on the lift-generating capacity of flat plates, drawing parallels with natural phenomena through biomimetic studies. Ultimately, these insights aim to guide future research efforts and encourage innovative solutions in the design and application of low *Re* lift-generating devices.

2.2 Studies on Flat-plate

For *Re* in the range of 10^6, a wealth of experimental data is available. However, data becomes increasingly sparse as you move beyond this range, especially at lower *Re*. Historically, low speed aerodynamic testing was relatively uncommon, often dismissed as representing "off-design" conditions. Nevertheless, given that the rectangular flat plate is a fundamental model for studying aerodynamic behaviour, researchers have conducted numerical analyses to bridge the data gap and better understand these lower-speed regimes.

Schmitz (1967) carried out a series of experiments involving three distinct airfoils: a slender flat plate, a slender cambered plate, and a conventional N60. These experiments were conducted across a *Re* spectrum spanning from 2×10^4 to 2×10^5. One of the key findings from this investigation was that the performance of slender plate airfoils consistently outshone others at *Re* below 10^5. A similar observation was also noticed by McMasters and Henderson while compiling a review article on the performance of low-speed airfoil shapes available at that time. They observed that the flat-plate has a better *L/D* when compared to smooth airfoils in the *Re* range of 10^3–10^5 (McMasters and Henderson, 1979). These conventional streamlined smooth airfoils used in the aviation industry tends to underperform at low *Re* as seen in Figure 2.1.

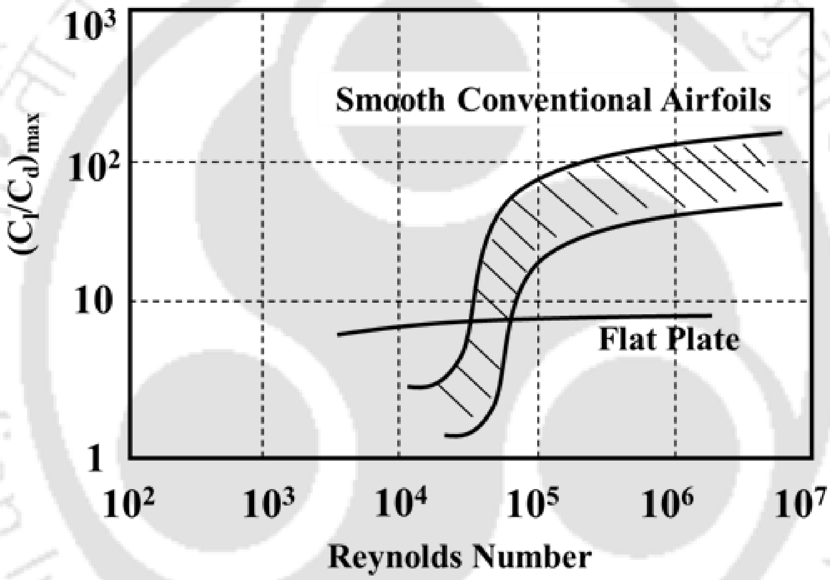

Figure 2.1: Variation of *L/D* ratio with *Re*
(McMasters & Henderson, 1979)

Another noteworthy observation by Hoerner (1985) was that cambered plates exhibited minimal variations in the C_l and C_d in relation to the *Re*, while flat plates demonstrated a nearly constant behavior unaffected by changes in the *Re*. Hoerner demonstrated that within the *Re* range of 4×10^4 to 1.2×10^5, the cambered plate experienced a notable 4% increase in the maximum lift coefficient (C_{lmax}), whereas the N60 airfoil exhibited a remarkable surge of over 180% in its C_{lmax}. There is a notable scarcity of data regarding fixed low-aspect-ratio wings for the low *Re* range of 10^4–10^5. Selig et al. examined the aerodynamic characteristics of various airfoils across a *Re* range from approximately 6×10^4 to 3×10^5, including a 2% thick flat-plate airfoil (Selig et al., 1989). While the results were promising, they did not provide specific outcomes for low-aspect-ratio wings. Selig and his co-researchers have conducted several aerodynamic studies at low *Re*, offering valuable insights into airflow behavior around wings in this range (Ananda et al., 2012, 2015; Giguère and Selig, 1997; Gopalarathnam et al., 2003; Selig et al., 1989; Selig et al., 1996). These studies have contributed to the development of new conventional streamlined airfoil sections. However, the same level of progress has not been achieved for flat-plate wings, indicating a gap in research and understanding in this area.

Nakayama et al., (1993) explored unsteady viscous flow around flat plates by numerically solving the incompressible two-dimensional Navier-Stokes equations using finite-difference computations. While conducting this study at the low *Re* of 200 and 400, it was found that Strouhal number (*St*) remained constant for the lower *Re* whereas this dimensionless parameter increased stepwise in the case of the higher *Re* (Figure 2.2).

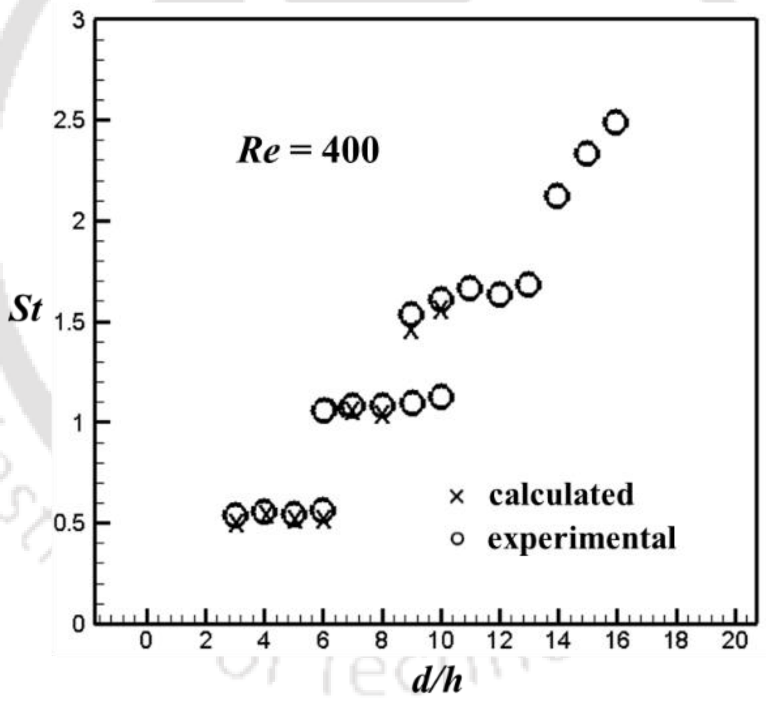

Figure 2.2: Variation of *St* with *d/h*
(Nakayama et al., 1993)

With advancements in experimental techniques and enhanced precision of measuring instruments for low-speed flows, there emerged a trend of conducting experimental studies to validate the numerical results. *St*, which gives us an idea about the oscillatory nature of the flow, was analysed in the wake of a flat-plate with beveled edges by Chen and Fang (1996). This study was conducted at *Re* = 3.5×10^3 to 3.2×10^4 for *AoA* = 0º–90º. The investigation was carried out over a range of *Re* spanning from 3.5×10^3 to 3.2×10^4, encompassing *AoA* from 0° to 90°. Laitone (1995, 1997) observed in his study that at the *Re* of 20,700, the NACA 0012 wing had worse aerodynamic qualities when compared with a thin flat-plate. While the 0012 had a *L/D* of 7.45 at a C_l of 0.40, in comparison the 1% flat-plate achieved an *L/D* of 8.25 (Figure 2.3). The observation also revealed a positive correlation, the thinner the flat plate, the higher its *L/D*. Pelletier and Mueller (2000) conducted experiments to study low *AR* thin flat-plates at low *Re*, and compared the results with cambered plates. These experiments, conducted at *Re* = 60,000 and 200,000, showed that the cambered plates offered better performance. They also made an important observation that the *TE* geometry didn't affected the lift and drag forces in the case of thin plates. A study was conducted by Sunada et al. (2000), on the aerodynamic features of airfoils at *Re* = 4×10^5, with variations in parameters related to airfoil shape such as thickness, camber, and roughness. *LE* vortices was observed to significantly influence airfoil performance at this *Re*. For optimal performance at this *Re*, an airfoil exhibited characteristics such as reduced thickness, a sharp *LE*, and approximately 5% camber with the maximum camber positioned near mid-chord.

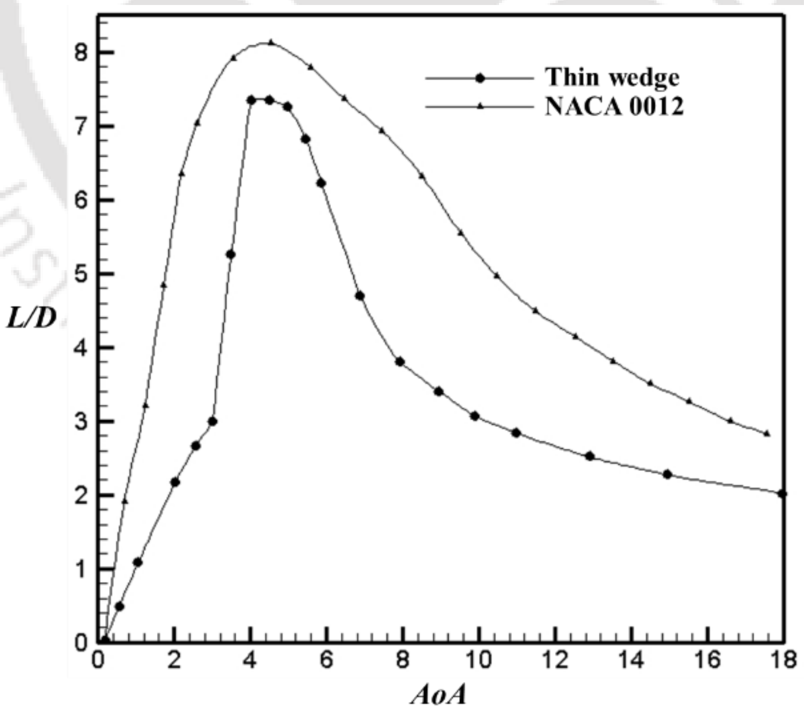

Figure 2.3: Variation of *L/D* with *AoA* (Laitone 1995, 1997)

Torres and Mueller (2004) presented an analysis of lift, drag, and pitching moment characteristics for wings with low *AR* operating at the low *Re* range of 7×10^4 to 2×10^5. The data are derived from wind tunnel experiments involving flat-plate wings with 2% thickness, varying *AR*s from 0.5 to 2.0, and four distinct planforms. The findings revealed significant nonlinearities in the lift curves, particularly noticeable for *AR*s below 1.25. Wings with these low *AR*s demonstrated elevated C_{lmax} and corresponding *AoA*. While for the higher *AR*s of 1.75 and 2.0, the rectangular planform achieved a higher C_{lmax}.

Lam and Leung (2005) performed experiments to explore the vortex shedding wake behind an elongated flat plate at a *Re* of 5,300. They observed that in the wake, a distinctive vortex street pattern emerges, characterized by a sequence of *LE* vortices interspersed with *TE* vortices. The *TE* vortex originates directly from the sharp *TE*, whereas the formation and shedding of the *LE* vortex appear to involve a more intricate mechanism, as indicated by available evidence. The shedding of the *LE* vortex appears to originate from a position axially near the *TE*. Following shedding, these vortices are transported downstream in the wake, propelled at a convection speed approximately equal to 0.8 times the free-stream velocity.

Cosyn and Vierendeels (2006) performed a computational analysis to investigate the flow characteristics around low *AR* wings, with a specific focus on the resulting forces of lift and drag. The computational simulations were carried out, comparing the responses of a flat plate and a reflex-type low *Re* profile, S5010, representative of a flying-wing Micro Air Vehicle (*MAV*). The outcomes revealed that, for *AR* of 0.5 and 1.0, the C_l values were comparable for both wing profiles (Figure 2.4). Notably, as observed in the figure, in the case of the flat-plate wing, the C_l values were higher at elevated *AoA*.

Thin, flat-plate wings of different planforms such as rectangular, elliptical, and Zimmerman, was assessed by Gresham et al. (2010) through wind tunnel experiments. Rectangular wings with rounded leading-edges exhibited non-zero trim angles at low incidences due to asymmetric development of a three-dimensional separation bubble at low *Re*. As *AoA* increased, the bubble elongated, leading to loss of reattachment and the onset of large amplitude roll oscillations. These oscillations, with a *St* around 10^{-2}, are comparable to those encountered by small aircraft in atmospheric gusts.

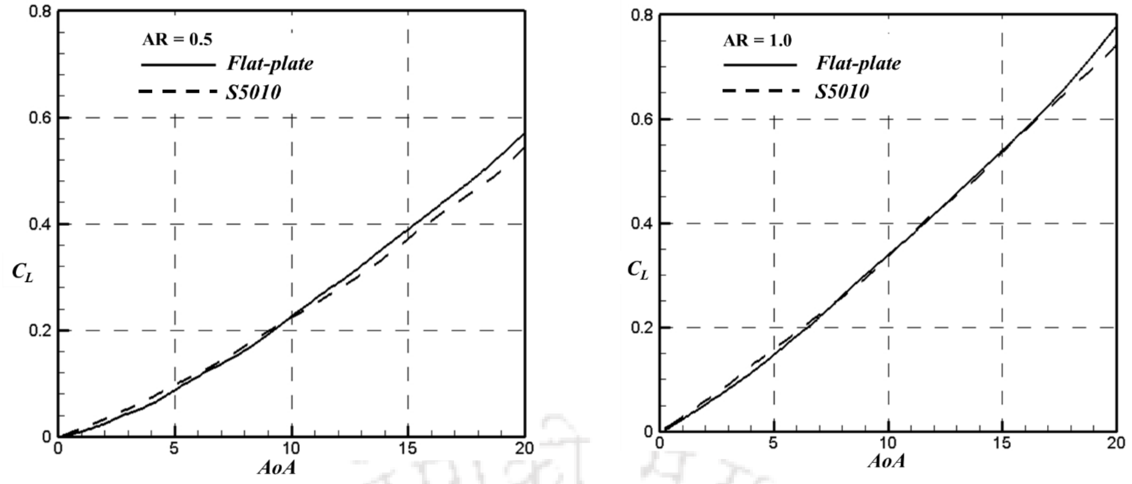

(a) AR = 0.5 (b) AR = 1.0

Figure 2.4: Comparison of C_L with *AoA* for a Flat-plate and S5010 simulations at *Re* = 10^5 for different *AR*s (Cosyn and Vierendeels, 2006)

Okamoto and Azuma (2011) performed a study to analyse the aerodynamic coefficients at a low *Re* of 10^4, that employed elliptical, rectangular, and triangular planforms with diverse *AR*s, along with a swept rectangular (parallelogram) wing featuring an *AR* of 4. All models utilized thin rectangular airfoil sections. Flow visualization in low *Re* conditions confirmed that the leading-edge separation vortex was unable to reattach to the wing surface, resulting in the emergence of numerous small vortices from the separated region. In one such study, analyses have been conducted to compare flat plates with alternative airfoil designs such as NACA0012 by Lee and Su (2012). In this, it was observed that the flat-plate wings were providing similar C_l figures as the symmetrical airfoil at the *Re* of 29,000 and 54,000. For the flat plate, at the lower *Re*, the *L/D* was higher than the conventional airfoil at lower *AoA*s (Figure 2.5(a)), although the C_d was slightly higher (Figure 2.5(b)).

Zhang et al. (2012) conducted a study examining membrane and rigid flat-plate wings with varied *AR*s at the low *Re* of 31,000 and 51,000. In contrast to the rigid flat plate, the membrane wing exhibited superior characteristics, including a higher lift curve slope, increased stall-region lift, and enhanced aerodynamic efficiency, for all the studied *AR*s. A similar study was undertaken by Mizoguchi and Yamaguchi (2012) where the effect of *AR* on rectangular wings at a *Re* of 7.6×10^4 and 5.2×10^4 was studied. They observed that wing stall characteristics are notably influenced by *AR* when *AR* ≤ 2.0, with an additional impact on lift slope observed when $AR \leq 1.5$. Moreover, C_{lmax} values experience an increase under conditions where $AR \leq$ 1.0.

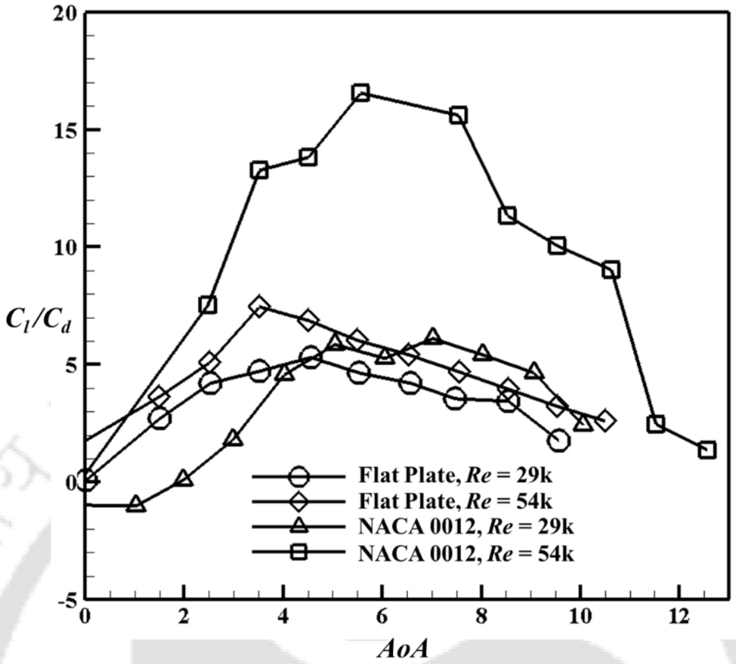

(a) Variation of *L/D* with *AoA*

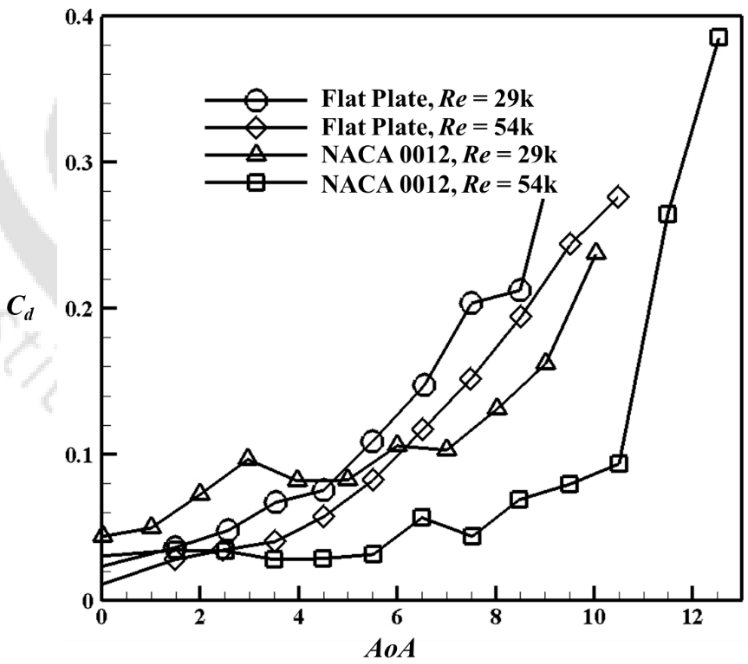

(b) Variation of C_d with *AoA*

Figure 2.5: Aerodynamic loading coefficients of NACA 0012 airfoil and flat plate at different *Re* (Lee and Su, 2012)

Ananda et al. (2012, 2015) undertook a research initiative to investigate the aerodynamics at low *Re* of 60,000 and 160,000, focusing on ten flat-plate wings with *AR*s spanning from 2 to 5. The primary findings derived from the wind tunnel experiments pertain to Oswald's efficiency factors (*e*), extracted from the measurements. Notably, the wind tunnel data revealed substantial sensitivities in the *e* for flat-plate wings concerning variations in *AR* (Figure 2.6).

It was observed that *e* exhibited a decreasing trend with increasing *AR*, dropping from around 0.81 for a wing with an *AR* of 2 and taper ratio of 1 to approximately 0.33 for a wing with an *AR* of 5 and taper ratio of 1. Mizoguchi and Itoh (2013) conducted wind-tunnel testing on thin rectangular wings within the scope of low *Re* flow, ranging from 2.6×10^4 to 7.6×10^4. The primary objective of their study was to experimentally explore the influence of *AR* variations on the aerodynamic characteristics of these wings. For wings with an *AR* of 3.0 and above, the *AR*'s impact is minimal, leading to qualitatively similar aerodynamic characteristics (Figure 2.7). However, there is *AoA* dependent variation in the pitching moment coefficient, attributed to low *Re* flow effects. Low-aspect-ratio wings show unique aerodynamic traits influenced by wingtip vortices, notably pronounced around an *AR* of 1.0. This results in significant increases in the C_{lmax} and stall angle for *AR* less than or equal to 1.0.

Traub (2013) did an analytical study to examine the impact of wing *AR* on performance at low *Re*. The analysis incorporated a consideration for airfoil pressure drag through the application of a leading-edge suction approach. It was observed that moderate wing *AR*s are favoured to minimize the sectional pressure-drag penalty, as low airfoil efficiency becomes apparent.

Chen et al. (2016) examines the three-dimensional flow behavior and aerodynamic characteristics of a NACA0003 wing with an *AR* of 1 at *Re* of 1.0×10^5, using both experimental and numerical methods. Results indicate that the three-dimensional wing-tip vortex notably delays the formation of the laminar separation bubble (*LSB*). However, as *AoA* increases, the *LSB* expands downstream chordwise and spanwise outboard. In contrast to higher *AR* wings, the wing-tip effect on the low *AR* wing significantly influences separation bubble development, as the flow near the wing's central section tends towards two-dimensional flow.

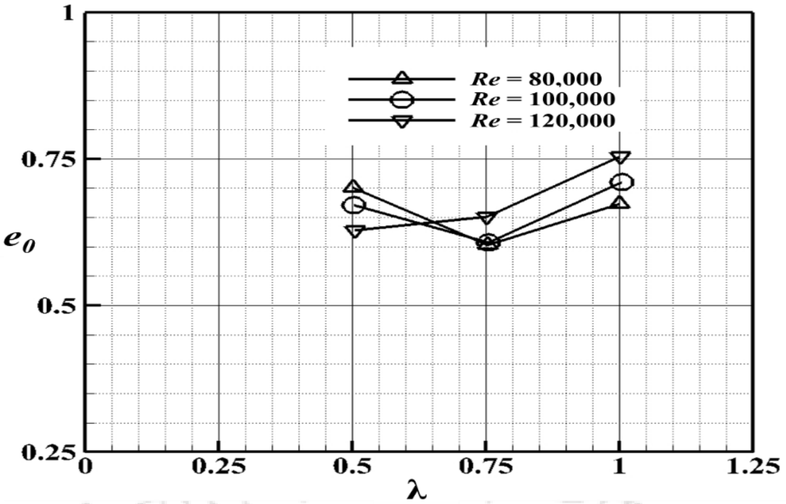

(a) *AR* = 2.0

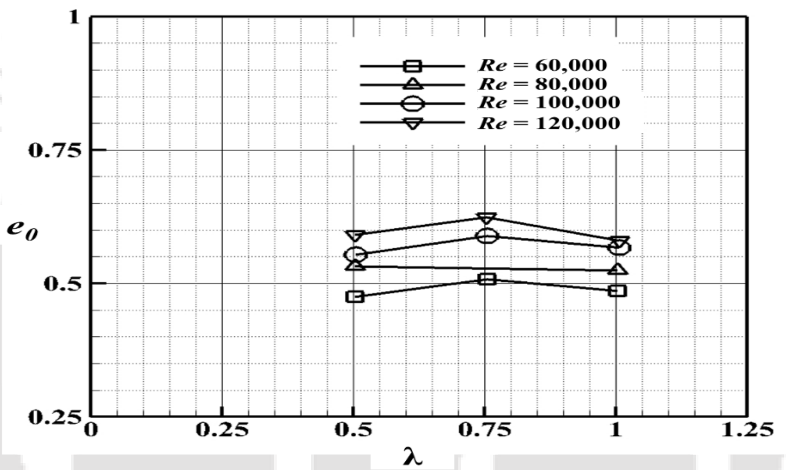

(b) *AR* = 3.0

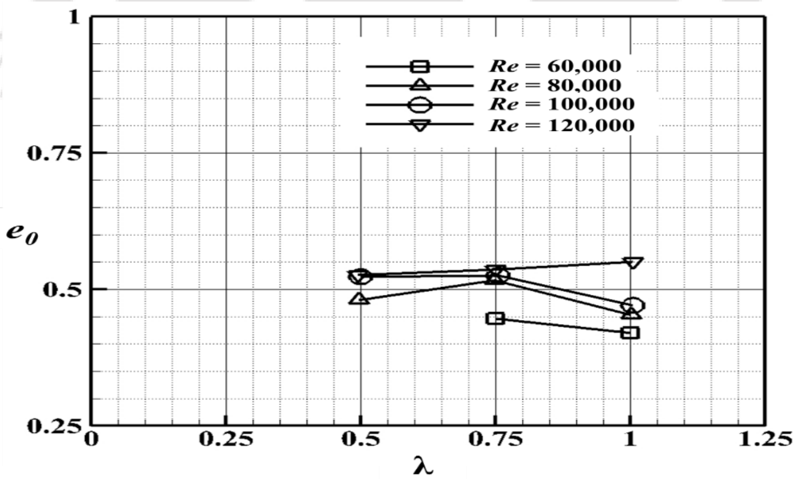

(c) *AR* = 4.0

Figure 2.6: Variation of *e* with *Re* for different *AR*s (Ananda et al., 2012, 2015)

Experimentally, the mean-flow reattachment of low *AR* wings (*AR* = 0.75–2.5) was examined using planar *DPIV* at the mid-span plane, with a chord-based *Re* = 80,000 and *AoA* ranging from 0° to 45° for each wing by Devoria and Mohseni (2017). Lift generation at high incidences is sustained solely by wings with *AR* < 1.5, as tip vortex downwash maintains reattached mean flow, while fully separated flow occurs for larger *AR*.

The *AoA* and *AR* critical for reattachment at high incidences also depend on *Re*, with turbulence transition in the leading-edge shear layer aiding the reattachment process. Okamoto et al. (2019) conducted wind tunnel tests to analyze the aerodynamic characteristics of rectangular wings with *AR*s ranging from 0.5 to 2, simulating insect-sized wings at low *Re* between 1×10^3 and 1×10^4. They observed that *Re* significantly influences the aerodynamics of low *AR* wings, particularly evident with specific *AR* wings. For wings with an *AR* of 1, the disappearance of vortex lift at lower *Re* leads to decreased C_{Lmax}. Tip vortices predominantly affect wings with *AR* ≤ 1, while a chord-wise vortex direction influences those with *AR* > 1 (Figure 2.8).

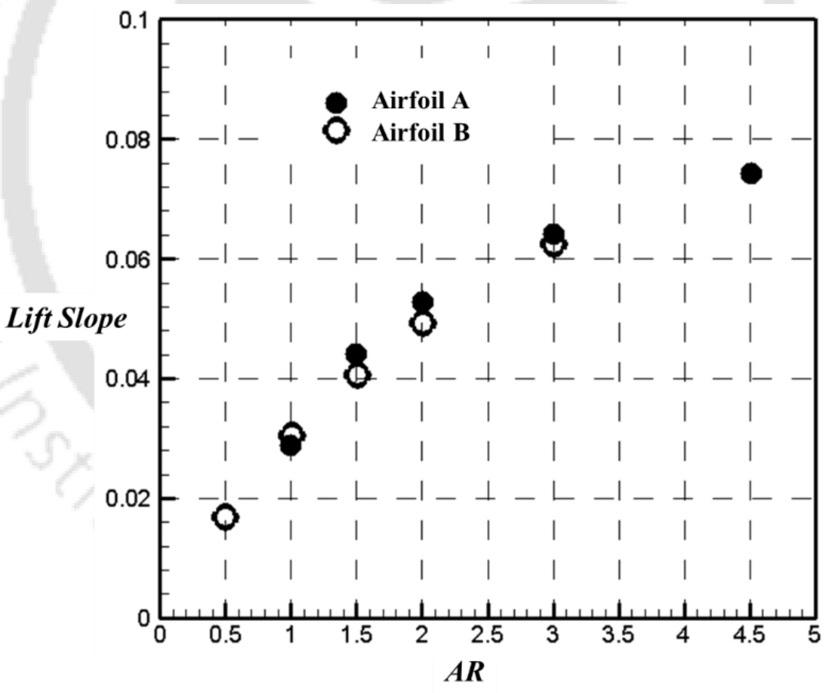

Figure 2.7: Lift Slope at *Re* = 5.2×10^4
(Mizoguchi and Itoh, 2013)

In another study, particle image velocimetry was employed to investigate the interaction of three-dimensional vortical structures over a low *AR* thin wing at a chord *Re* of 10^5 (Dong et al., 2020). The thin wing exhibits maximum lift at an *AoA* of 42°. Flow separation occurs at the

LE, forming a prominent leading-edge vortex crucial for lift generation. Findings indicate an increase in induced velocity of the tip vortex with *AoA*, aiding flow reattachment and sustaining the leading-edge vortex.

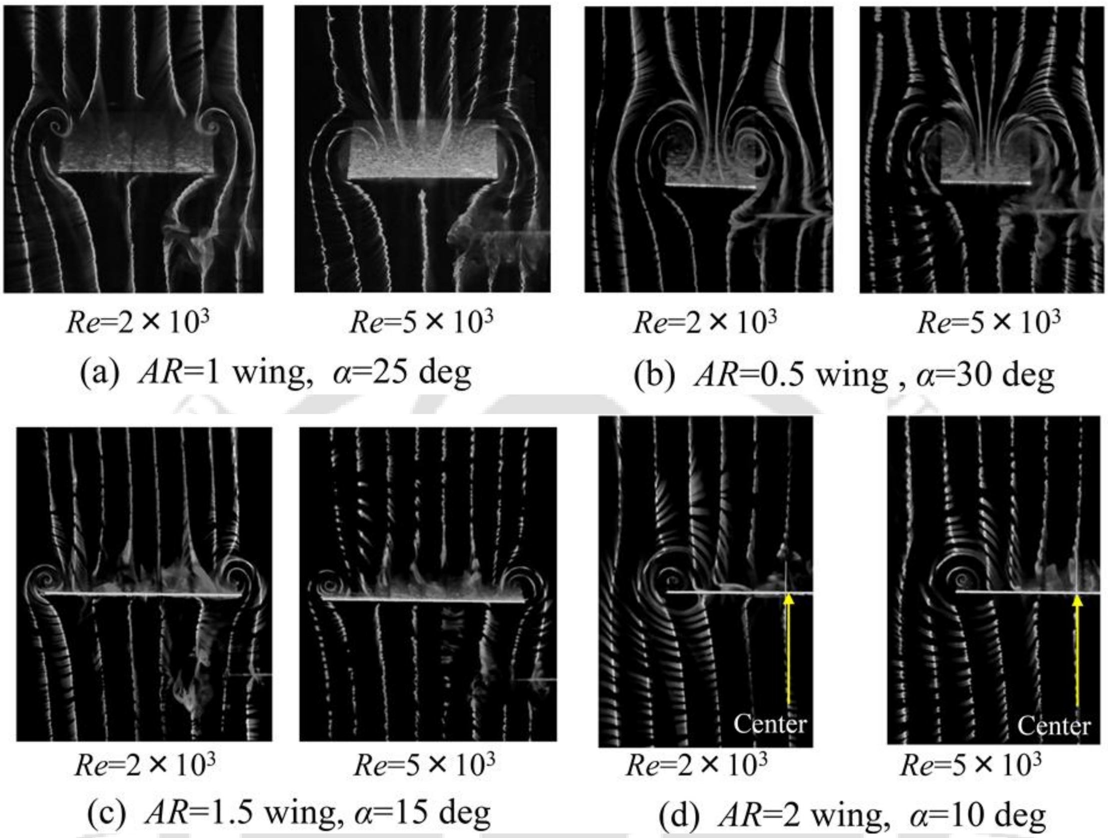

Figure 2.8: Tip vortices in the vertical plane of the wing *TE* (Okamoto et al. 2019)

Gutierrez-Castillo et al. (2021), experimentally determined the C_L for a flat-plate at low *AoA*s across different *AR*s of 1, 2, 4 and 8, and within the range of moderate *Re* = 40×10^3 to 200×10^3. They have introduced a correlation aimed at determining the slope for various *Re* and *AR*, incorporating two free parameters: α_1 and α_2. This correlation comprises two components; the first adjusts the $C_{L\alpha}$ value to consider finite wings, aligning with the outcomes anticipated by Prandtl's lifting line theory. The second part is solely dependent on the *Re*. The proposed correlation demonstrates the capability to forecast the $C_{L\alpha}$ value with an average error of 4.1% within the examined range. Santos et al. (2021) conducted experiments to investigate how different wingtip geometries affect aerodynamic coefficients. They specifically examined the wingtip taper ratio, discovering that a moderate taper ratio provided more favourable aerodynamic outcomes compared to a higher taper ratio. A moderate wingtip taper ratio (0.50) provides greater wing area and wingspan compared to wings with highly tapered wingtips, even when the *AR* is the same. This increase in wing surface area and span does not significantly impact profile drag. However, the slight increase in wingspan encourages an outward shift in the tip vortex, slightly enhancing wingspan efficiency.

In recent works, Traub investigated the lift components of low *AR* rectangular wings (Traub, 2023). The calculations were performed for *AR* 0.5 to 3 wings at *Re* that varied from 3000 to 2.16×10^6, using analysis methods based on the *LE* suction analogy. The results showed good similarities with the works of Torres and Mueller (2004), Lamar (1974), Shields and Mohseni (2012) among others. Solis et al. (2024) investigated the impact of spanwise wing deformation on wingtip vortex behavior in a towing tank at $Re = 20 \times 10^3$, employing models with a semi *AR* = 2 and varying levels of spanwise deformation. Analyzing the influence of spanwise deformation on a NACA 0012 wing model at low *Re* reveals the complexity, necessitating further detailed studies to understand varying flow patterns, particularly concerning *AoA* effects. A maximum tip deflection of 4.5% was observed in this study, indicating that deformations of this magnitude significantly affect lift and the associated wingtip vortex for a semi *AR* of 2. Zhu et al (2024) performed a study that examined three-dimensional flow characteristics over four low *AR* rectangular plates of 1.00, 1.25, 1.38 and 1.50 at an *AoA*= 6° and chord *Re* = 5400, employing both tomographic and planar Particle Image Velocimetry (*PIV*) techniques. The study unveiled the interaction between spanwise fluid transport and downwash stemming from wingtip effects, marking the first observation of such dynamics. It identifies two key mechanisms: first, spanwise fluid transport intensifies reversed flow, bolstering shear layer roll-up and vortex shedding; second, near-wall spanwise flow interacts with shed C-shape vortices, reinforcing vortex heads.

Research on flat plate wings encompasses various studies aimed at understanding and optimizing their aerodynamic characteristics, especially for low *Re* applications. These studies explore a range of topics, including the influence of wing thickness, *AR*, and wingtip configurations on lift, drag, and overall efficiency. One focus area is the experimental analysis of flat plate wings, where wind tunnel experiments and other testing methods are used to assess their aerodynamic performance. These experiments help determine the *L/D* ratios and the effects of flow separation, vortex formation, and wake characteristics. They also examine the impact of different wingtip designs, such as planar and non-planar attachments, on the aerodynamic properties of flat plate wings. Another important area involves computational studies using techniques like Computational Fluid Dynamics (*CFD*). These studies enable detailed simulations of airflow around flat plate wings, providing insights into pressure distribution, flow patterns, and the impact of wing modifications on aerodynamic coefficients. Overall, these studies contribute to a better understanding of flat plate wings' behavior and potential applications, particularly in contexts like *MAV*s and other low *Re* environments. The findings from these studies are critical for informing the design and optimization of flat plate wings for various engineering and scientific applications.

2.3 Studies on Wingtip Devices

From an aerodynamic perspective, while enhancing the lift characteristics of a flat-plate is desirable, it often comes with the drawback of increased lift-induced drag. This type of drag arises from wingtip vortices, which are a consequence of airflow leakage from the pressure side to the suction side of finite wings. These vortices contain a high-velocity, low-pressure core and create a downward flow, or downwash, contributing to induced drag. To address this challenge, researchers have been exploring various methods and innovative devices aimed at mitigating lift-induced drag by targeting wingtip vortices.

As early as the late 1800s, Lanchester (1907) devised winglets as a solution to mitigate this induced drag. Once the effectiveness of winglets in reducing induced drag while maintaining lift was established, ongoing research endeavours have consistently focused on refining winglet designs for further optimization.

Winglet designs inspired by nature often draw on the observation of bird wings and their unique adaptations to improve aerodynamic efficiency. By studying birds, engineers have gained insights into how nature minimizes induced drag through wingtip shapes and structures. Birds like hawks and eagles, for example, have feathers at their wingtips that spread out, creating a natural form of winglet that reduces vortices and enhances lift. These natural designs inform the development of engineered winglets that aim to reduce induced drag, increase lift, and enhance fuel efficiency in aircraft. Engineers use biomimicry to create winglets that mimic these natural features, with the aim of achieving better aerodynamic performance. Such designs can lead to improved fuel efficiency, reduced noise, and enhanced aircraft manoeuvrability. By taking inspiration from nature, researchers can develop innovative winglets that offer significant benefits in various aeronautical applications, from commercial aviation to unmanned aerial vehicles (*UAVs*) and small-scale aircraft. The slotted high-lift wing represents a natural concept that can be integrated into flat-plate wing designs to enhance their lift generation capabilities (Savile, 1957). Indeed, based on the functional attributes of wings, Savile categorized them into soaring wings, high-speed wings, elliptically shaped wings, and high-lift wings, which are naturally seen in albatrosses, falcons, crows, and eagles, respectively. This classification underscores the diverse aerodynamic strategies employed by birds and suggests potential applications for improving the lift characteristics of engineered flat-plate wings.

By incorporating winglet designs (Figure 2.9), Whitcomb's study demonstrated a reduction of approximately 20% in induced drag through the use of these devices (Whitcomb, 1976). The experiments which were conducted at a Mach number of 0.78 resulted in an increase of nearly 9% in the wing's *L/D* ratio. Spillman and Allen adopted a natural solution (Figure 2.10) in wing designs and observed a reduction in drag and an increase in lift (Spillman and Allen 1978). In recent times, a similar approach was also taken by Hossain et al. (2011) and was able to achieve identical results. This indicates that applying these bio-inspired engineering designs to flat-plate wings has the potential to boost their performance. However, it's worth noting that most studies in this domain focus on the application of winglets in conventional airfoil wings, leaving a gap in research related to flat-plate wings.

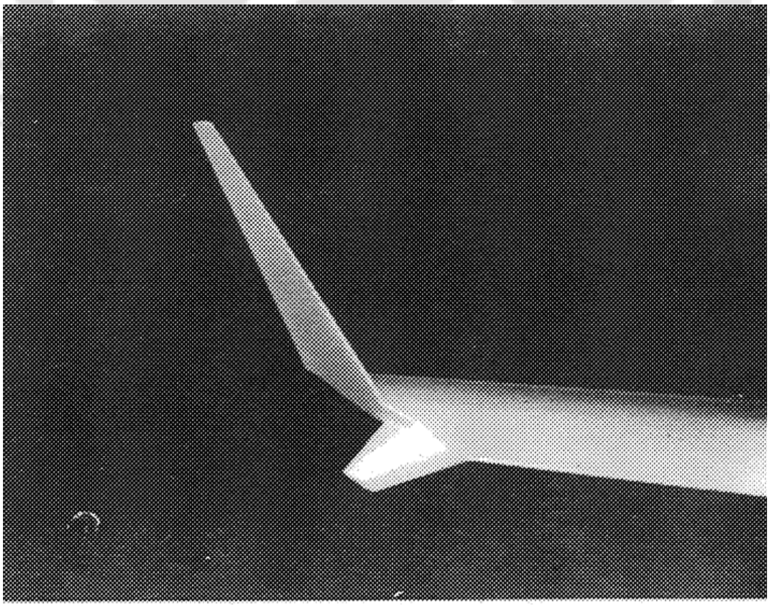

Figure 2.9: Winglet investigated by Whitcomb (1976)

The slotted configuration refers to a wing structure where the outer feathers are spread apart, resembling the fingers of a human hand. This feature significantly influences the drag experienced by birds during flight (Tucker, 1993, 1995). The slots are thought to mitigate the lift-induced drag generated by wingtip vortices, leading to more efficient flight. Tucker observed that the induced drag was reduced when using non-planar slotted winglets in a Harris Hawk. This configuration facilitated the dispersion of wingtip vortices in both horizontal and vertical directions, contributing to a decrease in induced drag.

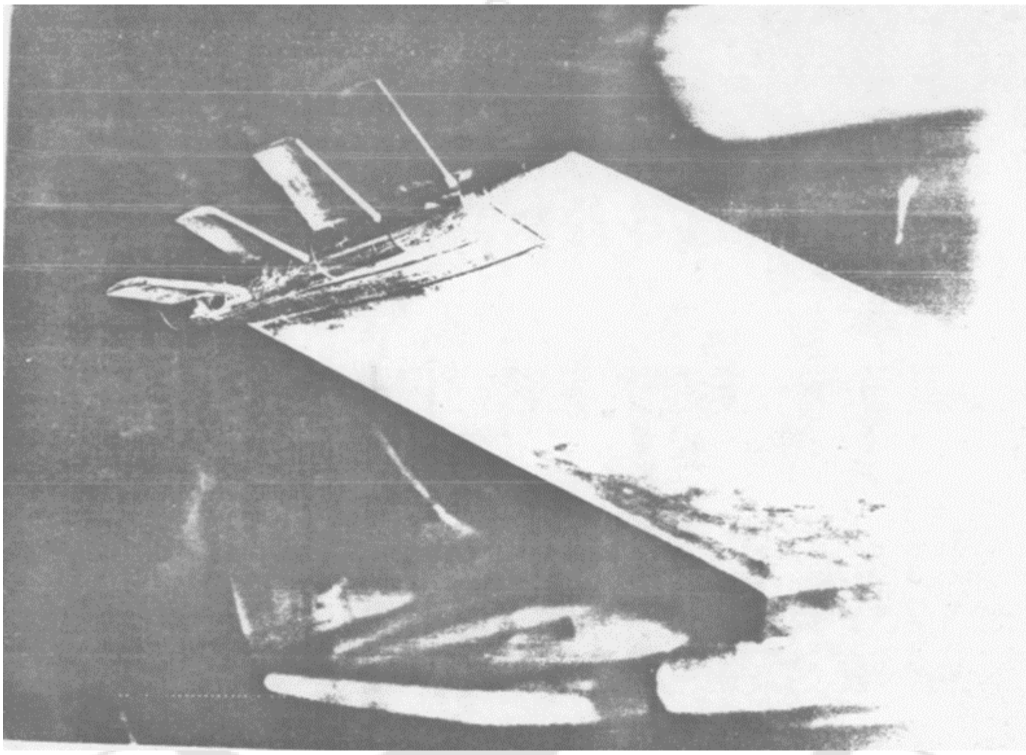

Figure 2.10: Wingtip array of 4 shorter sails (Spillman and Allen 1978)

La Roche and Palffy (Roche, 1996; Roche and Palffy, 1996) conducted a study at *Re* below 2×10^6, examining the use of wingtip devices to minimize induced drag. They named and patented this configuration as "Wind-Grid". Smith et al. performed a study to understand the performance upgrades in a wing with multiple winglets (Smith et al., 2001). This study explored the potential of multi-winglets to reduce induced drag without increasing the wingspan of aircraft. Wind tunnel models were constructed using a NACA 0012 airfoil section for the untwisted, rectangular wing and flat plates for the winglets. Testing was conducted over a range of *Re* from 1.61×10^5 to 3×10^5. A substantial increase in the lift curve slope was observed with the dihedral spread of winglets set at zero incidence relative to the wing, which also helped distribute the tip vortex. Flat plate winglets at zero incidence improved the lift curve slope and generated more lift than an equivalent area of the baseline wing.

Kroo (2001, 2005) provided an overview of various studies on nonplanar wing designs aimed at improving wing efficiency. Kroo illustrates examples of the potential capabilities of nonplanar systems based on the height-to-span ratio in Figure 2.11(a). For a given height and span, the box-plane configuration achieves the lowest vortex drag, as observed by von Kármán and Burgers (1935). These studies addressed induced drag, the component of drag caused by lift. Despite covering a range of contemporary concepts, the focus was predominantly on high *AR* subsonic wings. A key observation from these studies was that as lift force increases, drag force also tends to increase. Similar to airfoil research, most studies on winglets focused on high *Re,* typically exceeding 10^6. A maximum induced drag reduction of approximately 11% compared to an elliptically loaded planar wing was achieved either by extending the span by 15−20% or by adding winglets with a height equal to 20% of the semi-span, without any span extension (Figure 2.11(b)).

The effect of different winglet shapes on the flowfield behind a tapered wing has been experimentally investigated by Soltani et al. (2004). The tip vortices formed by various winglet shapes differ significantly and impact the flowfield over the wing surface. These vortices change with varying *AoA,* and the total pressure measured behind each winglet indicates differences in induced drag. Winglets also displace and alter the shape of the primary tip vortex compared to the bare wing model, with each winglet producing distinct variations in these characteristics. In wind tunnel tests, conducted to evaluate the reduction of induced drag using wing-tip blowing, as well as fixed and adaptive multi-winglets, it was observed that both systems were able to minimize induced drag (Ceron-Munoz et al., 2013). Tip blowing achieved the largest gains, but multiwinglets are a promising design for reducing vortex drag. Despite offering less drag reduction compared to tip blowing, multiwinglets do not require an external power source, which is a significant advantage, especially for light airplanes. Wind-tunnel tests of the semispan wing demonstrated a 55% increase in effective *AR* with the use of multiwinglets. Fluck and Crawford (2014) performed numerical studies using the extended lifting line model to investigate the performance of wings with slotted wingtips. The study, conducted at a *Re* of 1.3×10^6, revealed that spreading additional wingtip feathers further apart provided aerodynamic benefits.

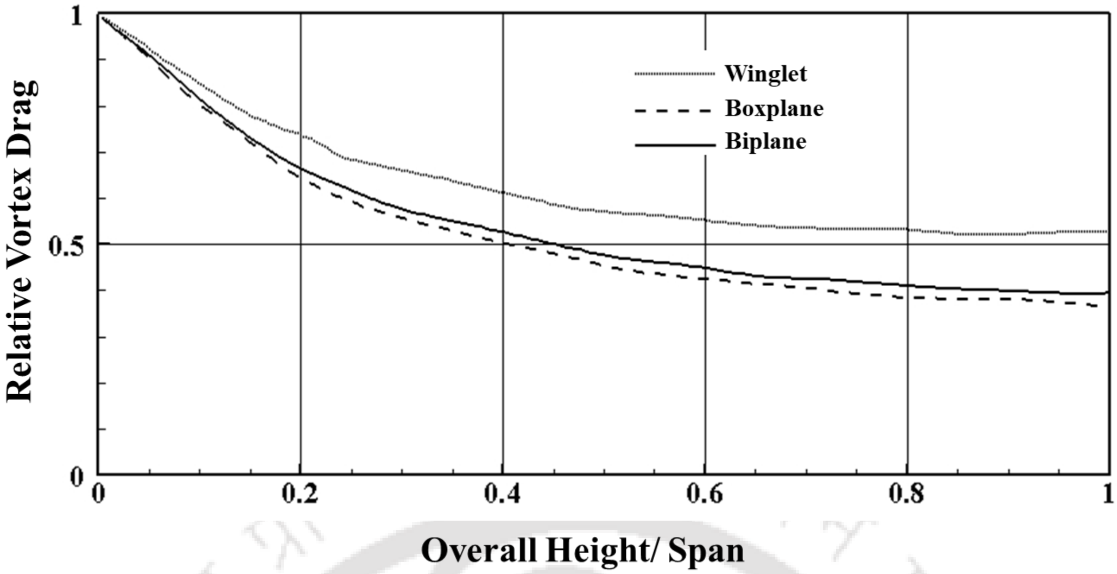

(a) Induced drag variation with allowable height for nonplanar systems (Kroo 2001)

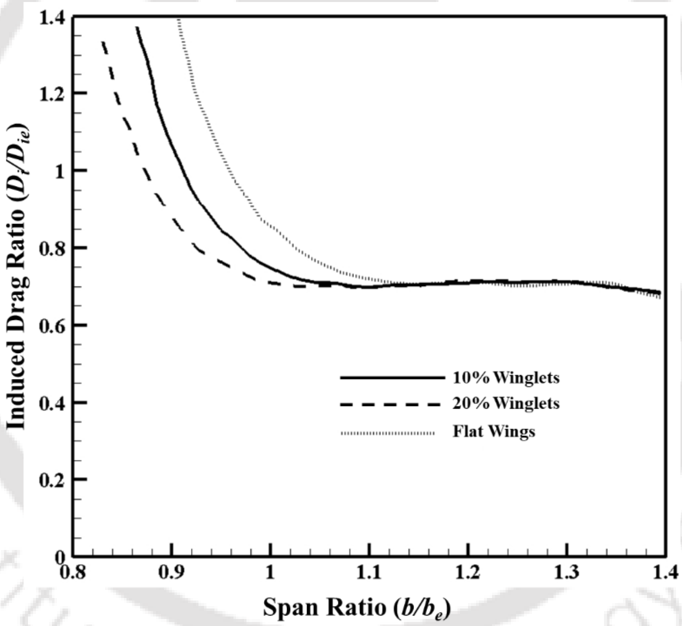

(b) Variation in induced drag for wings and wings with winglets (Kroo 2005)

Figure 2.11: Study conducted by Kroo for increased aircraft efficiency

Reddy et al performed a numerical analysis to study various configurations of aircraft wingtip devices (Reddy et al., 2015). The wingtip device in this study inspired by soaring birds, features three smoothly blended elements. Each multi-winglet configuration was integrated into a complete aircraft model. Computational results show that the multi-winglet design significantly increases the C_L (Figure 2.12(a)) and aerodynamic performance (L/D) (Figure 2.12(b)) and more effectively diffuses the vortex core compared to other winglet configurations. However, adding more winglet elements could make them thinner and more delicate, requiring greater caution.

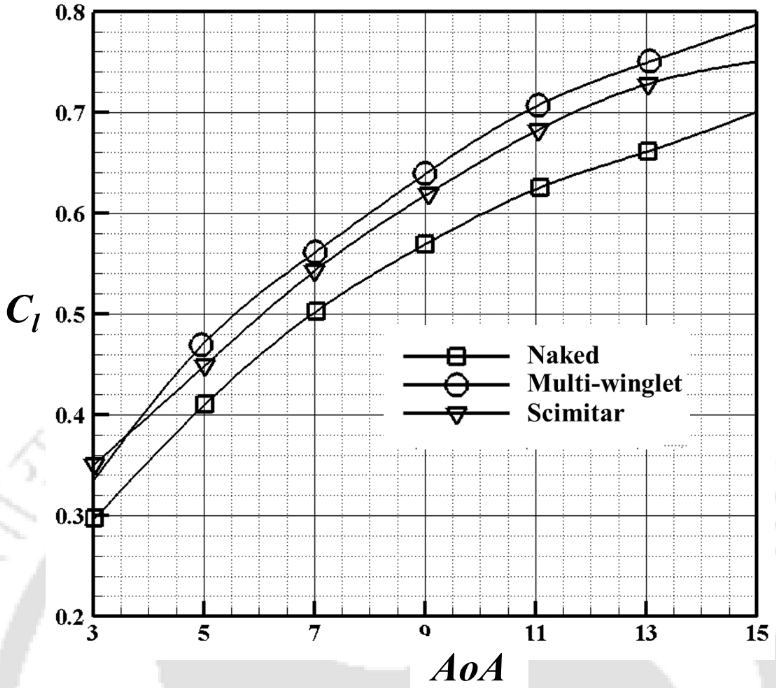

(a) Variation of C_l vs *AoA*

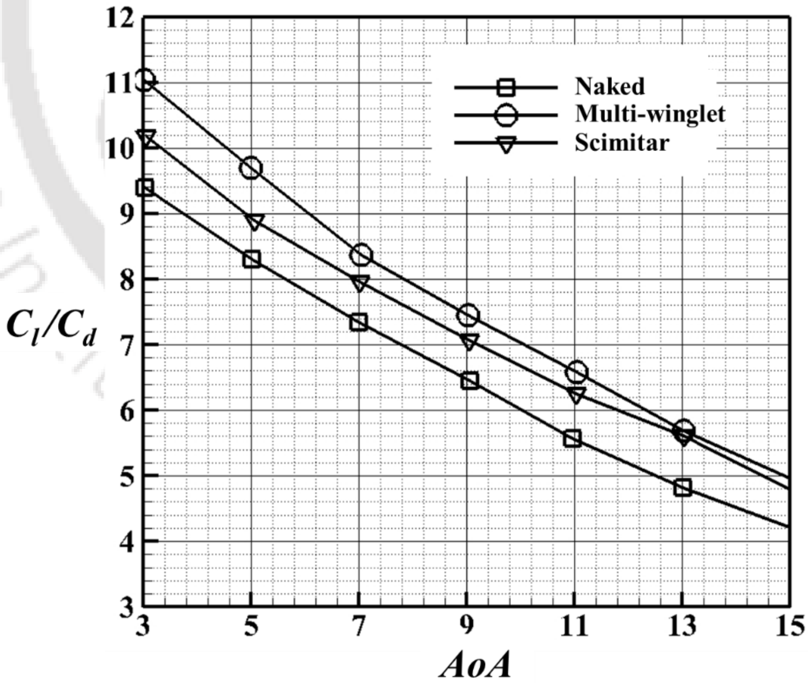

(b) Variation of *L/D* vs *AoA*

Figure 2.12: Computational analysis of Reddy et al. (2015)

In an experimental study by Siddiqui et al. (2018), rigid and flexible wingtip devices with both flat and curved shapes were tested on a base flat plate wing. This study, which involved a base wing with an *AR* of 3.0 at a *Re* number of 3×10^5, offers results that are compared in the current analysis. Siddiqui et al. (2017) conducted a review of various studies focusing on bio-inspired wingtip extension devices, primarily in the context of aircraft wings and typically at high *Re* numbers. The wingtip devices used in these experiments were largely inspired by bird wings. Birds can manipulate their wingtip feathers in several ways for aerodynamic control, a complex process that is challenging to replicate artificially. Helal et al. conducted Numerical studies to identify the optimal aerodynamic performance of a subsonic aircraft wing with various winglet cant angles (Helal et al., 2017). This study uses NACA 653218 airfoil section coordinates for both the wing and the blended winglet design. *CFD* models were run at a Mach number of 0.2 at sea level, where the air pressure and temperature are 101,325 Pa and 288.2 K, respectively. The results indicate that wings with winglets can increase the *L/D* by approximately 6% to 15% compared to wings without winglets, depending on the *AoA* during different flight phases. The most efficient *AoA* was found to be 4 degrees.

Birds with high-lift wings, like eagles and hawks, are known to operate under conditions that resemble those in *MAV* applications with high payload demands (Lynch et al., 2018). A notable characteristic of high-lift wings is the presence of wingtip gaps in a slotted configuration. The NACA 0012 airfoil was used as the base semi-span wing, achieving an increase in the lift curve slope in the range of 10%-22%. They used both planar and non-planar wingtips (Figure 2.13) on a rectangular wing with an SD7032 airfoil. In the planar configuration, they observed a 7.25% improvement in the mean C_L in the pre-stall region. They concluded that the impact of wingtip gap size on aerodynamic performance is independent of whether the wingtips are planar or non-planar. A team of researchers fabricated a biologically inspired *MAV* at the Technical University of Madrid (UPM) (Sevillano et al., 2019). The primary goal of this study was to analyze a winglet configuration based on multiple grids that emulate birds' wingtip feathers, referred to as a wing-grid device. Biomimetic Unmanned Aerial Vehicles, which mimic bird flight, are characterized by their reduced size, low flight speed, and low *AR*s. These features make them ideal for various tasks that are challenging or impossible for humans to perform. In a similar research, Khan et al. (2019) investigates the C_L and C_D to optimize wing design and enhance aircraft performance. Reducing drag from wingtip vortices decreases fuel consumption and emissions. *CFD* results show that the plain wing produced the highest drag, while the blended winglet was the most beneficial wingtip device. The 30° cant angled blended winglet and 60° cant angled wingtip fence generated additional lift compared to their counterparts. These findings closely align with the established use of wingtip devices.

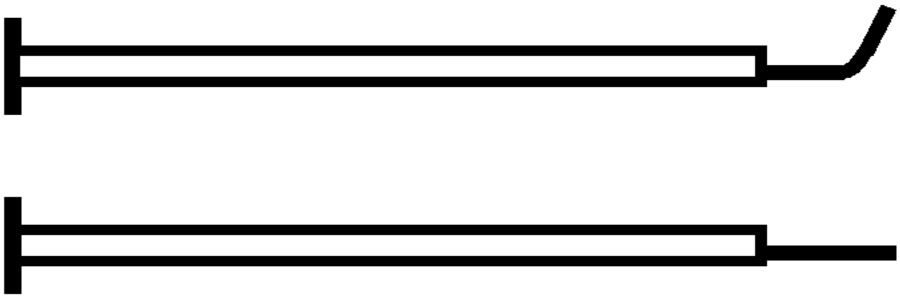

Figure 2.13: Nonplanar (top) and planar (bottom) wingtip configurations of Lynch et al. (2018)

Epple et al. (2022) performed an experimental study on a NACA 4412 airfoil to examine the effect of winglets on induced drag. They observed that the wing without winglets produced stronger wingtip vortices compared to the wing with winglets. The wingtip vortex of the wing without winglets exhibited greater intensity, with an increasing diameter as it moved downstream, running parallel to the wake. In contrast, the wing with winglets had a significantly weaker wingtip vortex, which was thinner and directed towards the central region of the wake, indicating a substantial reduction in induced drag. The use of wingtip type devices have been tried by Barroso-barderas et al. in their study on bioinspired *MAV*s (Barroso-Barderas et al., 2022). This research develops two bioinspired *MAV* prototypes featuring morphing wings and wing grid wingtip devices. The wing grid *MAV* is designed to minimize aerodynamic and weight penalties. A preliminary theoretical conceptual design verified the requirements, wind tunnel tests determined the aerodynamic characteristics, and suitable materials were selected.

In a recent study, Bardera et al. (2023) conducted a study that introduces several innovations, including the complete design of a *UAV* with biomimetic wingtip designs aimed at reducing induced drag from tip vortices. Inspired by birds' primary feathers, the *UAV* features three grids at the wingtips. The results demonstrate significant aerodynamic efficiency improvements during cruise and ascent phases (Figure 2.14). These improvements translate into enhanced autonomy and range for the *UAV* during missions.

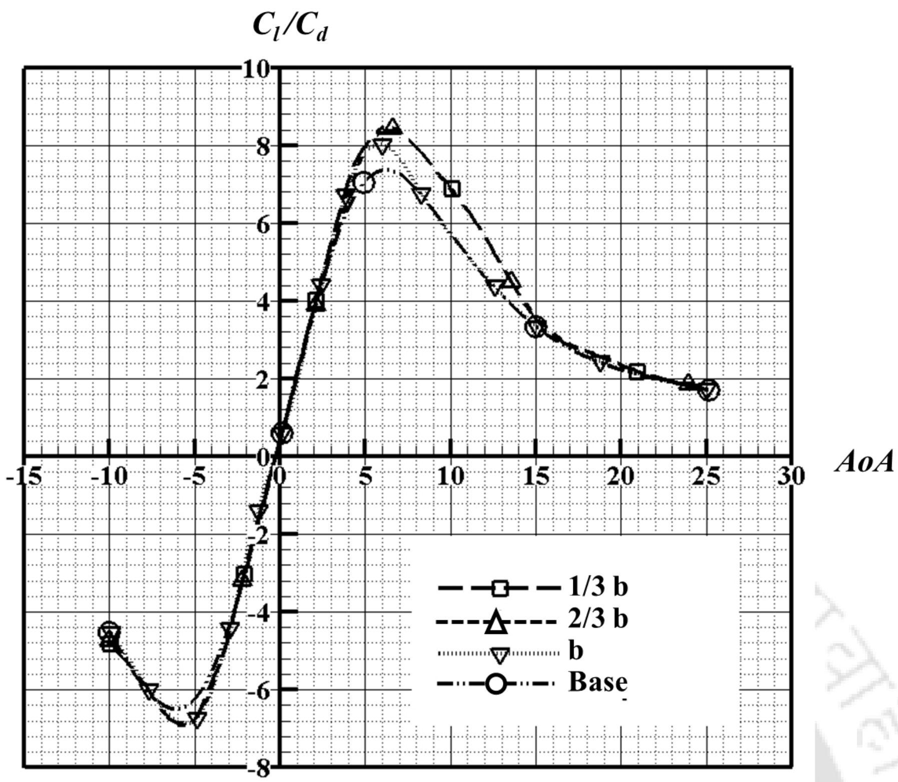

Figure 2.14: Aerodynamic efficiency of the *UAV* with base, b/3, 2b/3 and full extended grids (Bardera et al. 2023)

2.4 Gap in Research

The comprehensive literature review sheds light on the extensive body of research dedicated to optimizing airfoils and wings, predominantly focusing on higher *Re*. This emphasis on higher *Re* regimes is understandable given their prevalence in many aerospace applications. However, within the *Re* range of approximately 100,000, there appears to be a relative scarcity of studies addressing optimization techniques and modifications tailored to this specific regime.

This observation underscores a notable gap in current research efforts, signalling an opportunity for further exploration and innovation in aerodynamic design methodologies. Given the prevalence of applications operating within this *Re* range, such as small *UAV*s, *MAV*s, and certain low-speed aircraft, the need for optimized aerodynamic solutions tailored to this regime is evident.

Moreover, while conventional airfoil and wing optimization strategies may not be as effective within the lower *Re* number regime, there are indications of alternative approaches that hold promise. One such avenue involves the exploration of flat plates as viable wing configurations for generating lift. This unconventional approach challenges traditional design paradigms and opens up new avenues for enhancing aerodynamic performance in applications characterized by lower *Re*.

Therefore, the identified gap in optimized techniques and the potential of novel approaches, such as utilizing flat plates as wings, highlight the importance of further research and development efforts aimed at addressing the unique aerodynamic challenges associated with lower *Re* regimes. By bridging this gap and exploring innovative design strategies tailored to specific *Re* ranges, researchers can unlock new opportunities for improving the performance and efficiency of a diverse range of aerospace systems.

2.5 Scope of Work and Present Objective

Based on the identified literature gap, the primary focus of this research is to explore the use of flat-plates as viable wing configurations for generating lift in lower *Re* regimes, specifically within the range of approximately 100,000. The study aims to address the current gap in literature regarding optimization techniques tailored to this specific aerodynamic context, which is particularly relevant for applications such as small *UAV*s, *MAV*s, and certain low-speed aircraft.

Taking these requirements into account, the following objectives have been established:

- **Feasibility and Performance Evaluation**: Investigate the feasibility and performance potential of flat-plates as wings within the specified *Re* range. This research will include comparative studies between flat-plates and traditional airfoil shapes using computational simulations to assess key aerodynamic characteristics such as lift and drag.
- **Experimental Study by varying Aspect Ratio**: Conduct an experimental study to evaluate the aerodynamic performance parameters of flat-plate wings with varying ARs. This investigation will provide empirical data on lift, drag, and other relevant aerodynamic characteristics under controlled conditions, enhancing the understanding of how *AR* influences wing performance.

- **Evaluation of Inverted Dimples**: Investigate the impact of inverted dimples on the aerodynamic performance of flat-plate wings. This objective will involve experimental studies to analyze how the presence of inverted dimples influences lift generation, drag reduction, and overall flow characteristics. The findings will aim to establish the efficacy of inverted dimples as a design feature in enhancing the performance of flat plates in lower *Re* regimes.
- **Investigation of Wingtip Attachments**: Perform experimental investigations on flat-plate wings modified with wingtip attachments. These modifications will be implemented in both planar and non-planar configurations to explore their impact on aerodynamic performance. The results obtained from this analysis will be compared with those of the unmodified base wings to facilitate better optimization and refinement of the wing design.

2.6 Concluding Remark

By addressing these areas of research, this study aims to make incremental contributions toward filling the identified literature gap and advancing the state of the art in aerodynamic design methodologies tailored to the lower *Re* regime. This research endeavour has the potential to enhance our understanding of aerodynamic phenomena specific to this regime, leading to the development of more efficient and optimized aerodynamic solutions for a diverse array of applications, including small *UAV*s, MAVs, and other low-speed aircraft.

Furthermore, the insights gained from this research can pave the way for designing novel wing configurations and flow control techniques optimized for lower *Re*. By exploring innovative strategies such as the use of flat plates and inverted dimples, this study seeks to drive innovation and push the boundaries of aerodynamic performance in this critical domain. Ultimately, the findings could contribute to improved aircraft efficiency, performance, and overall operational capabilities, fostering advancements in the aerospace sector and beyond.

Chapter 3: Methodology

Chapter Outline

Overview:

The computational and experimental study on the flat-plate wings at low Reynolds number involved a multifaceted approach. In the computational domain, numerical simulations using state-of-the-art computational fluid dynamics techniques were employed to model the aerodynamic behavior of flat-plate wings. The simulations were conducted over a range of Reynolds number representative of low-flow applications. Concurrently, wind tunnel experiments were conducted to validate and complement the computational findings. The flat-plate wings, characterized by varying aspect ratios, were carefully designed and fabricated for the experimental phase. The wind tunnel testing provided empirical data on lift and drag characteristics. Both the computational and experimental results were critically analyzed to gain comprehensive insights into the aerodynamic performance of the wings at low Reynolds number, contributing to a holistic understanding of their behavior under these conditions.

3.1 Introductory Remark

The methodology encompasses both computational and experimental setups to ensure a comprehensive analysis of flat-plate wing aerodynamics. The computational setup employs advanced simulation tools, such as *CFD*, to model airflow, pressure differentials, and performance metrics like *L/D* ratios. Detailed meshing techniques and turbulence models ensure accuracy in capturing complex flow phenomena.

The experimental setup involves wind tunnel testing of flat-plate wing prototypes. These prototypes include configurations like inverted dimples, planar attachments, and non-planar attachments. High-precision sensors and data acquisition systems measure key parameters such as lift, drag, and flow patterns. The integration of computational and experimental approaches allows for robust validation of results, ensuring reliable and credible insights into aerodynamic performance.

3.2 Computational Setup

The study involves two-dimensional simulations of the flat-plate conducted using the commercial solver ANSYS FLUENT-14.5. FLUENT employs a finite volume formulation to solve the incompressible continuity and momentum equations in the 2D domain. The simulation includes a detailed description of the boundary conditions, specifying how the flat-plate interacts with its surroundings. Additionally, a carefully crafted meshing strategy is implemented to accurately represent the geometry and capture flow intricacies. The numerical methodology applied for the current simulation is detailed in subsequent sections.

3.2.1 Computational Domain

The computational domain and boundary conditions, detailed in Figure 3.1, showcase a rectangular configuration designed to model the two-dimensional flow over the flat-plate. The lateral extent of the domain is limited to ±10c, while along the flow direction, it spans from -3.33c to +16.67c. This sizing is carefully chosen to encompass the crucial regions where complex flow physics occur, including separation zones along the *LE* and *TE*, as well as the formation and behavior of vortices. The positioning of the flat-plate within this domain is strategically arranged to facilitate accurate capturing of flow dynamics, especially in the wake region where the interactions and effects are pronounced

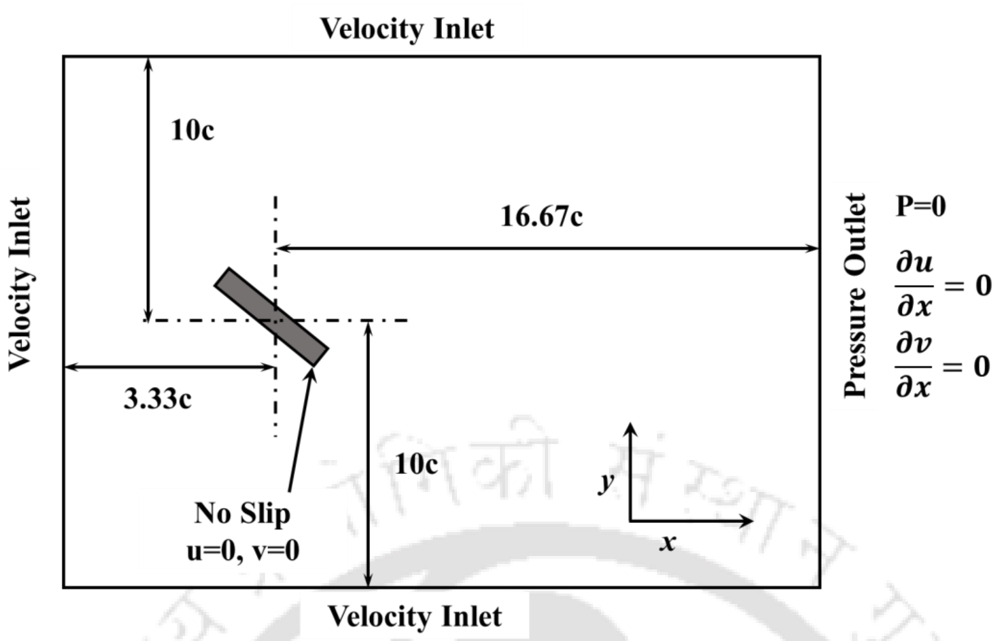

Figure 3.1: Computational domain and boundary conditions

Meshing is a fundamental step in *CFD* simulations, essential for accurately representing geometry and capturing flow intricacies. Utilizing advanced algorithms, meshing discretizes the computational domain into smaller elements through a process called mesh generation, ensuring suitable resolution for solving governing equations. The quality of the mesh profoundly influences simulation accuracy and convergence, making effective meshing critical for successful *CFD* simulations. In this study, the computational domain is discretized into structured quadrilateral grids using ICEM *CFD* meshing (Figure 3.2), incorporating face meshing and edge sizing operations to achieve the desired meshing level.

3.2.2 Solution Methods and Turbulence Model

The present study employs the unsteady 2D Reynolds Averaged Navier-Stokes (*RANS*) formulation using ANSYS-FLUENT version 14.5. A pressure-based solver is utilized for the simulation, solving the governing equations through pressure–velocity coupling with the SIMPLE scheme. Spatial discretization is carried out using second-order up-winding. The simulation adopts a conservative approach, with the temporal terms discretized using a second-order upwind scheme. Each time step undergoes 20 iterations, and convergence is achieved with a residuals criteria set at 10^{-6}. This computational setup ensures a comprehensive analysis of the unsteady flow characteristics around the flat plate.

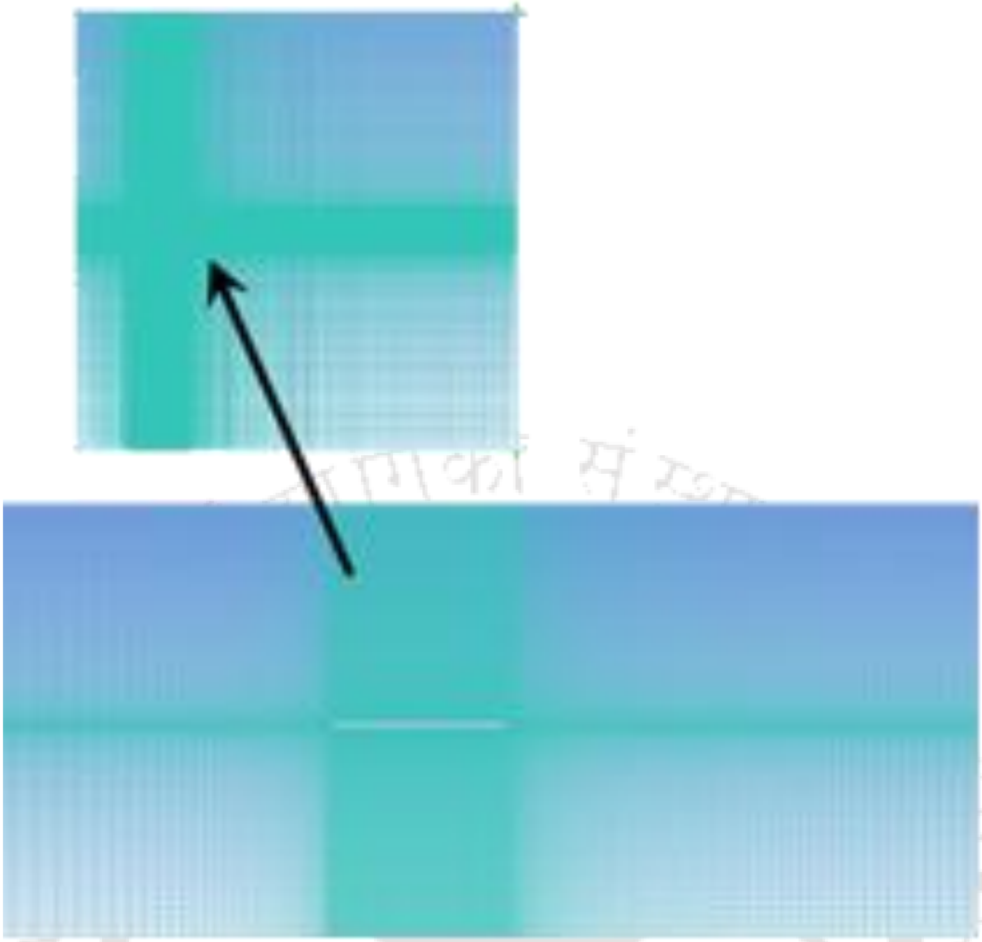

Figure 3.2: Computational grid with closed up view near the flat plate

In the current simulation, turbulence in the flow is modelled using the Spalart-Allmaras turbulence model with standard model constants (C_{b1} = 0.1355, C_{b2} = 0.622, C_{v1} = 7.1, C_{w2} = 0.3). This model, designed for aerospace applications dealing with boundary layers under adverse pressure gradients, simplifies the turbulence representation into a one-equation model solving for the kinematic eddy viscosity. The transport equation for the transported variable, $\tilde{\nu}$, is:

$$\frac{\partial}{\partial t}(\rho\tilde{\nu}) + \frac{\partial}{\partial x_i}(\rho\tilde{\nu}u_i) = G_\nu + \frac{1}{\sigma_{\tilde{\nu}}}\left[\frac{\partial}{\partial x_j}\left\{(\mu + \rho\tilde{\nu})\frac{\partial\tilde{\nu}}{\partial x_j}\right\} + C_{b2\rho}\left(\frac{\partial\tilde{\nu}}{\partial x_j}\right)^2\right] - Y_\nu + S_{\tilde{\nu}} \quad (3.1)$$

Where $\tilde{\nu}$ is identical to the turbulent kinematic viscosity except in the near-wall region, G_ν is the production of turbulent viscosity and Y_ν is the destruction of turbulent viscosity that occurs in the near-wall region due to wall blocking and viscous damping, $\sigma_{\tilde{\nu}}$ and C_{b2} are the constants and ν is the molecular kinematic viscosity. $S_{\tilde{\nu}}$ is a user defined source term.

3.2.3 Grid Independence Test and Validation

To determine the optimal mesh resolution, a grid independence test is conducted by varying the number of grid points from 57,400 to 128,016. The simulation focuses on the flow around a flat-plate with a 1% thickness ratio at a *Re* of 10^5. The analysis involves observing the variation of pressure coefficient (*Cp*) along the flat-plate edge. Notably, grids exceeding 77,576 points exhibit minimal changes in *Cp* values with further refinement, as depicted in Figure 3.3. Consequently, for the present study, a mesh with 77,576 cells is chosen, ensuring a balance between computational efficiency and accuracy based on this grid independence analysis.

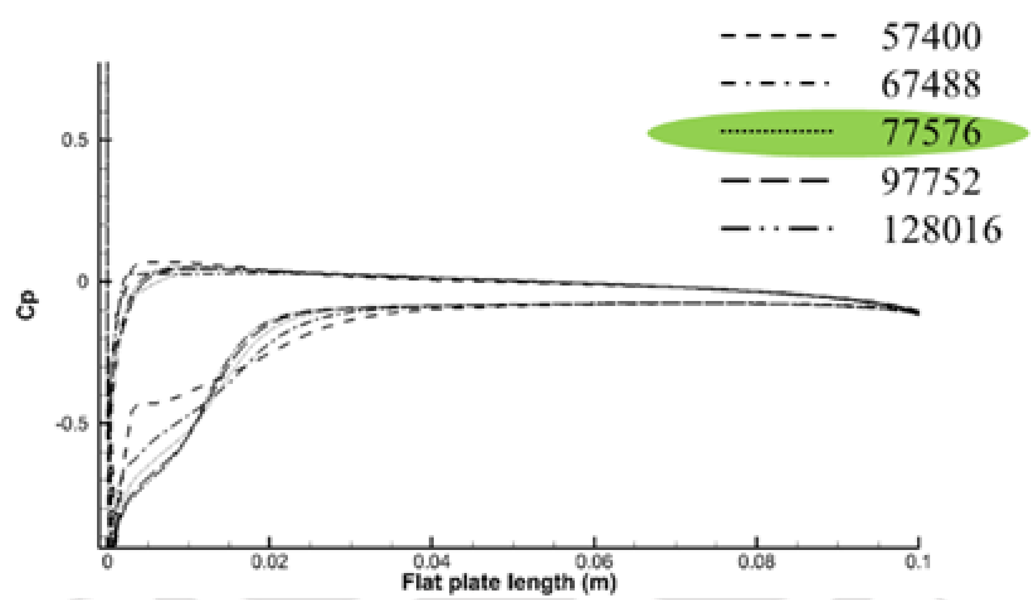

Figure 3.3: Variation of C_p along flat plate length (suction and pressure side) for different grid sizes

The reliability of the computational setup is validated against both computational results from Winslow et al. (2018) and experimental findings from Okamoto et al. (1996). Winslow et al. utilized a transonic unsteady rotor Navier-Stokes 2D (TURNS2D) in-house developed solver to investigate flow parameters around a flat plate with a 1% thickness ratio at $Re = 10^4$. Okamoto et al. conducted a similar experimental investigation. The current computational setup replicates the same analysis, and the resulting lift and drag coefficients are compared with the referenced results, as illustrated in Figure 3.4. Notably, the deviation of C_l and C_d obtained from the present setup is reasonably consistent with the findings of both Winslow et al. and Okamoto et al., affirming the validation and accuracy of the computational model.

3.3 Experimental setup

The experimental investigations were conducted in a subsonic open-circuit wind tunnel situated at the Department of Mechanical Engineering, IIT Guwahati. This section details the entire process from airfoil selection to wing model fabrication, outlining the experimental arrangement for aerodynamic analysis. The experimental methodology employed in this study encompasses a systematic approach to assess the performance of flat-plate wings within a low-turbulence wind tunnel facility.

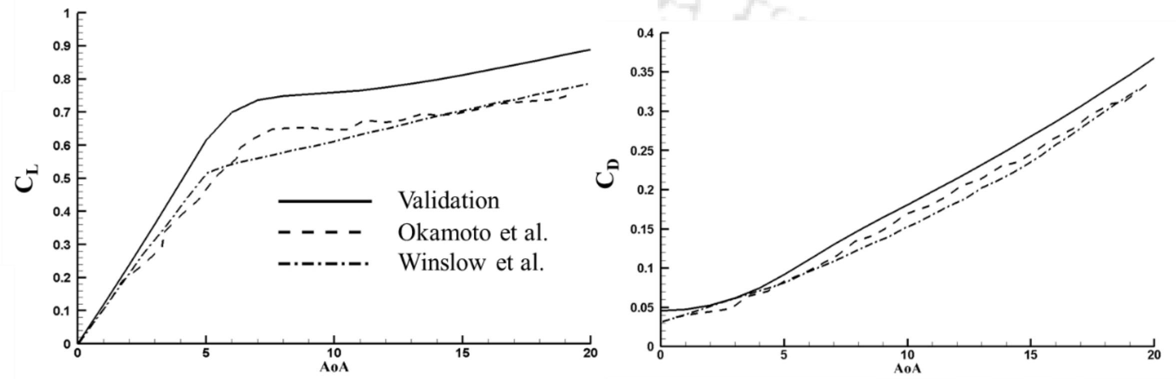

Figure 3.4: Comparison of C_L and C_D for a flat plate of 1% thickness ratio with the results of Okamoto et al. (1996) and Winslow et al. (2018)

The experimental setup for aerodynamic measurements of various wing models is illustrated in Figure 3.5. The balance is positioned beneath the test section, with the wing model affixed to the top portion of the balance. A wire connects the balancing mechanism to an electronic panel, which translates the voltage signals from strain gauge sensors into corresponding forces and moments. Subsequently, the data is recorded on a computer linked to the balance via an RS232 cable. The balance quantifies force and moment data in kg and kg-cm, respectively. To derive aerodynamic force coefficients, lift and drag forces are normalized using freestream dynamic pressure ($1/2\rho U^2_\infty$) and wing surface area (A).

The pitch angle of the model can be adjusted within a range of -10° to 30°, measured with a digital spirit level having an uncertainty of ±0.2°. To determine the frequency of shed vortices in the wake, a hot-wire probe is positioned in the wake region. Its movement is controlled by a 3D traverse mechanism mounted at the tunnel's top, providing mobility along streamwise (z), vertical (y), and spanwise (x) directions with a resolution of 0.05mm. The probe's non-dimensional location in the measurement region is denoted by x/c, y/c, and z/c for the respective directions. The coordinate system's origin is assumed at the intersection of the mid-plane of the span and the *LE* of the airfoil with zero pitch angle. Data acquisition is performed using the hot wire setup, and the frequency response of shed vortices is obtained through power spectral density (*PSD*) analysis of the velocity signal using the *FFT* approach, with a maximum deviation of ±4% for the current flow conditions.

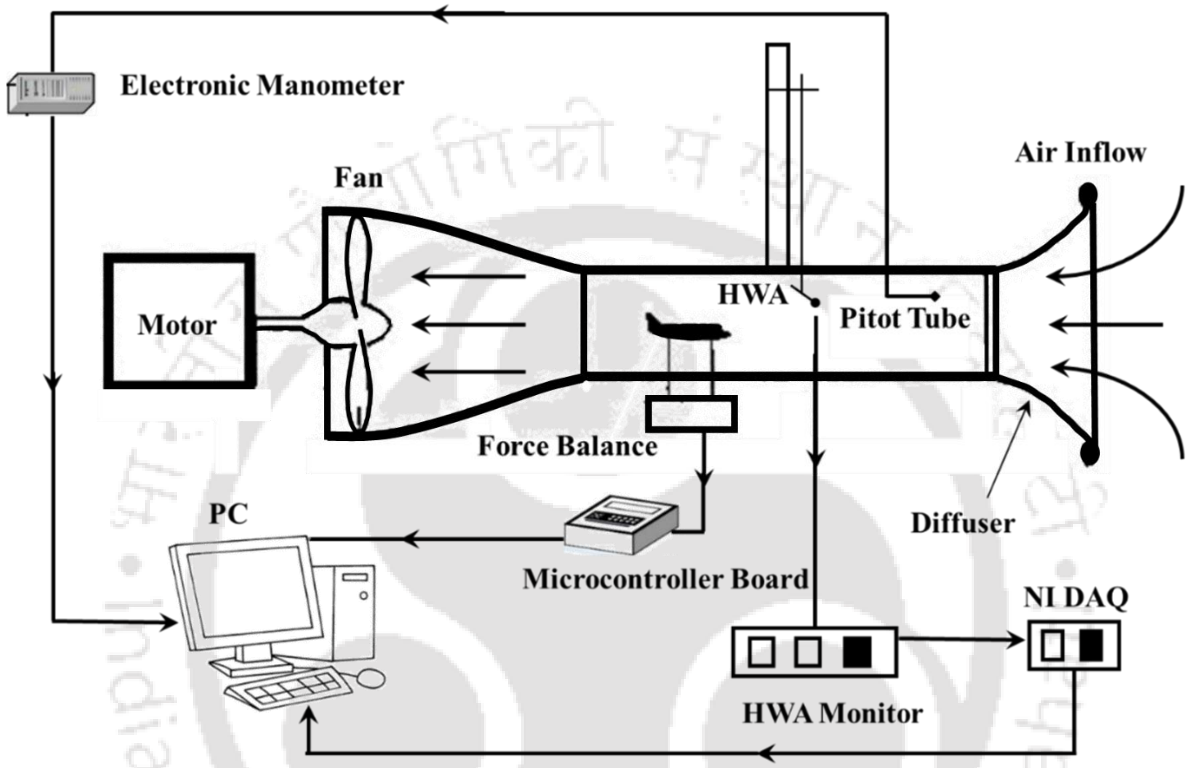

Figure 3.5: Experimental setup

In wind tunnel testing, the blockage effect, caused by limited space between the tested model and tunnel walls, can lead to variations in airflow compared to open-air conditions. This effect is crucial to assess for accurate aerodynamic measurements. The blockage ratio, representing the ratio of the wing's projected area to the tunnel test section's cross-sectional area, is employed for this evaluation. In the current study, the maximum blockage ratio is 2.7% for *AR* = 2.0 at 20° *AoA*, decreasing to 2.2% for *AR* = 0.5 at 26°. The diminishing blockage effect with decreasing *AoA* and *AR* suggests reduced interference during wind tunnel testing. For finite wings, the blockage ratio remains lower even at higher *AoA*, indicating minimal or no need for blockage correction, consistent with the reported negligible influence when the blockage ratio is below 5% (Barlow et al. 1999; Chen and Liou 2011; Jeong et al. 2018).

3.3.1 Wind Tunnel

To evaluate the aerodynamic performance of the wing models, experiments were conducted in a low-turbulence wind tunnel facility, ensuring controlled and consistent inflow conditions for accurate measurement. This subsonic wind tunnel features a 3-phase 30 HP induction motor powering the tunnel fan, as illustrated in Figure 3.6. Operating on an open-circuit principle, the wind tunnel achieves a maximum wind speed of 50 ms^{-1} at the test section. Velocity measurements are conducted using an electronic manometer with a sampling frequency of 100 Hz. The dimensions of the tunnel test section are 600 mm in width, 600 mm in height, and 2000 mm in length. The average standard deviation (*SD*) in wind flow measurements using a pitot-static tube is approximately 1.2%, indicating a relatively low level of variability in the recorded data. In comparison, the standard deviation for rpm measurements is around ~2%, reflecting a slightly higher degree of variability in the rotational speed measurements. These values suggest a reasonable level of precision and consistency in the wind flow measurements, with slightly more variability observed in the rpm data.

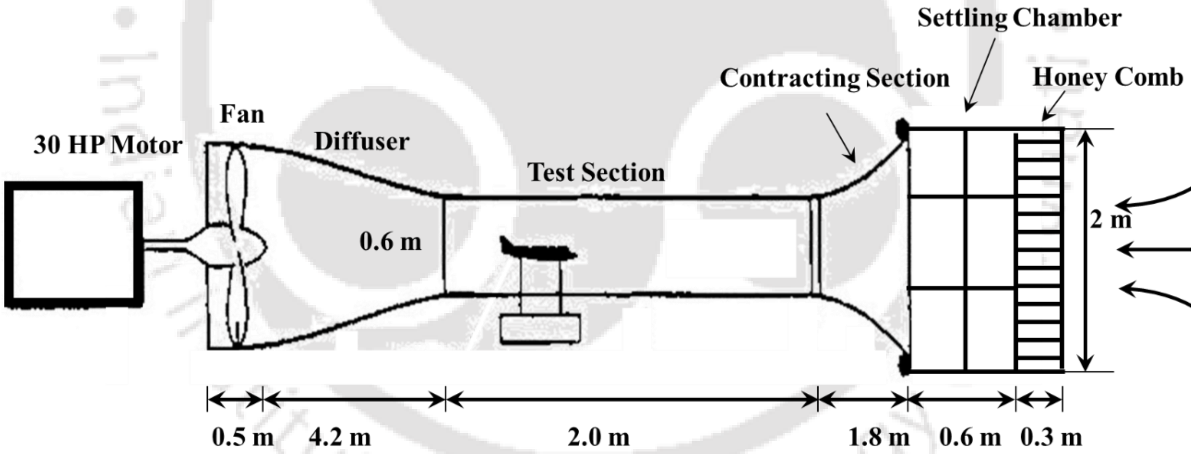

Figure 3.6: Schematic of wind tunnel

The turbulence level in the wind tunnel is assessed using a hot-wire anemometry system. The observed turbulence intensity is found to be less than 0.3% for the current wind tunnel studies. This level of turbulence is considered quite low and meets acceptable standards, ensuring that all flow physics phenomena and aerodynamic characterizations of models are accurately captured (Bruun, 1995). For the present study, experimental investigations are conducted in a flow velocity range of 5-13 ms^{-1}. The wind tunnel is calibrated for a wind speed range of 3-15 ms^{-1}, achieved by adjusting the tunnel fan rpm. The maximum rotational speed of the tunnel fan can reach up to 480 rpm in this speed range. The tunnel calibration curve for the current flow regime is depicted in Figure 3.7, with a correlation factor (R^2) of 0.9998. The close-to-unity R^2 value indicates a highly linear relationship between the tunnel fan RPM (N) and the corresponding freestream velocity (U_∞).

3.3.2 Force Balance System

Evaluating the aerodynamic characteristics of wing models requires precise measurement of the forces they experience in moving air. A three-component strain gauge-based force balance (Model: WBAL-00103, Make: Sunshine Measurements) is employed for this purpose, estimating lift, drag, and pitching moment with load capacities of 1 kg, 0.4 kg, and 5.0 kg-cm, respectively.

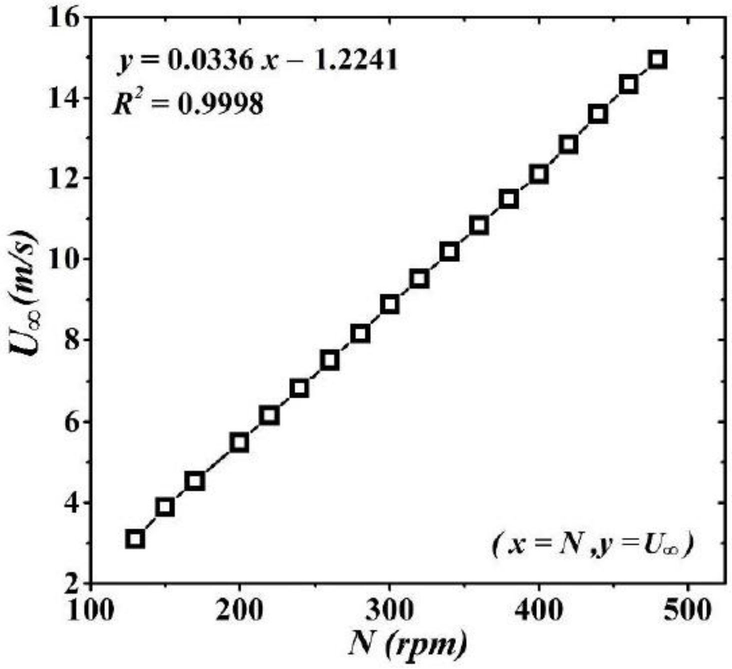

Figure 3.7: Calibration of wind tunnel

The model is mounted to the balance's top portion using a support plate and this plate is linked to a vertical load-carrying bar and a vertical strut, facilitating controlled pitch adjustments during testing. The lower part of the load-carrying bar is fixed to a metric plate, transmitting all model loads to this point. These loads are then transferred through link elements to strain gauge sensors. The balancing mechanism connects to an electronic panel via a 25-pin connector, converting instantaneous voltage signals from strain gauges into corresponding forces and moments. Output data is stored in a computer connected to the balance via an RS232 cable. The gain value, set at 400 for signal amplification, is manually adjusted using a gain switch. Potential biases or disturbances in the strain signal, occurring when the model is mounted, can be rectified with the zero adjustment switch. The pitch angle of a mounted model can be adjusted between -10° and 30° to the flow direction using a pitch controller.

To calibrate the 3-component force balance, a calibration body is mounted onto the balance, as illustrated in Figure 3.8. The calibration body features three pans, labelled P_1, P_2, and P_3. P_1 and P_2 are connected to the body via calibration arms, while P_3 is linked to an arm through a string passing over a pulley. The balance is configured with a sampling frequency of 100 Hz, and data acquisition is conducted over a 10-second sampling duration, utilizing a gain value of 400 for calibration. This duration effectively reduces minor fluctuations caused by load pans not being fully stabilized or small electronic fluctuations.

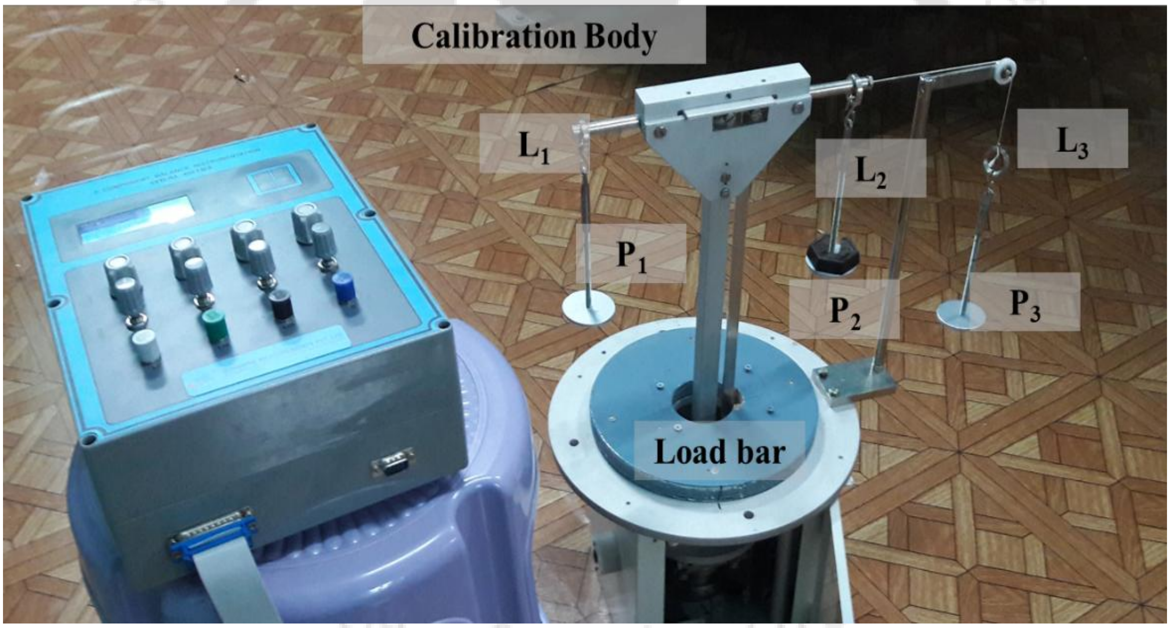

Figure 3.8: Calibration setup of force balance

Known loads, denoted as L_1, L_2, and L_3, are applied to their respective pans, and the output load and moment are recorded in the microcontroller-based LCD panel. L_1 and L_2 represent vertical loads associated with lift and moment, while L_3 pulls the body horizontally, representing the drag force. The calibration covers a load range of 5−500 gm for lift measurements and 5-250 gm for drag force in this study. The maximum calibration error is less than 4% for lift and pitching moment, and less than 2% for drag force.

3.3.3 Hot Wire Anemometer

The primary purpose of a hot-wire anemometer (*HWA*) is to monitor flow velocity fluctuations, providing valuable insights into turbulence, boundary layers, and other dynamic fluid flow phenomena. Operating on the principle of convective heat transfer through a heated fine wire in a fluid flow, the *HWA* system detects instantaneous changes in heat transfer rate caused by alterations in fluid flow behavior. The convective heat loss from the wire surface is expressed as I^2R, where I is the current through the wire and R is the wire's resistance (Bruun 1995; Russo 2011). Depending on whether the current or resistance is kept constant, *HWA* can operate in two modes. In constant temperature mode, the resistance is maintained constant, allowing the current to fluctuate with flow velocity. For this study, a constant temperature anemometer (*CTA*) setup is utilized to investigate and analyze the flow field mapping. In this setup, as wind speed increases, enhancing heat transfer, the probe sensor tends to cool down, decreasing its resistance. To maintain a consistent resistance, the amplifier sends more current into the wire, resulting in a higher potential difference across the resistor. The output voltage across the probe is the amplifier output voltage or the voltage necessary to maintain the desired current through the wire. The single wire/channel *CTA* probe, made of platinum-coated tungsten wire, is tested for flow field mapping estimation. The probe is connected to the hot-wire system through a BNC socket, and the *HWA* unit captures both instantaneous and fluctuation signals. These signals are acquired using a data acquisition (*DAQ*) system (Model: DAQ6363, Make: NI) with a maximum sampling frequency of 2 MHz.

King provided a simplified form of the analytical relationship between the electric power supplied to the probe sensor and the speed of the surrounding fluid flow, as expressed in Eq. 3.2 (King, 1914). This equation depicts the linear variation of the dependent variable E^2 with the independent variable U_∞, where E is the voltage across the hot-wire, U_∞ is the free stream velocity, and A and B are calibration constants. The sensitivity (S) of the hot-wire probe is obtained by taking the derivative of Eq. 3.2 with respect to the freestream velocity, as given in Eq. 3.3 (Lee and Ken Kauh, 1997; Wagner and Kent, 1988).

$$E^2 = A + B\sqrt{U_\infty} \tag{3.2}$$

$$S = \frac{dE}{dU_\infty} = \frac{B}{4E\sqrt{U_\infty}} \tag{3.3}$$

The *HWA* calibration involves measuring the tunnel's velocity using a Pitot-Static probe, establishing the relationship between voltage changes in the *HWA*, and aiming for a correlation R^2 value close to unity. The probe sensor is positioned within the tunnel with its axis normal to the freestream flow direction, ensuring uniform heat transfer. For this study, the anemometer is calibrated for wind speeds of 3−15 ms^{-1}, capturing signals at a sampling rate of 10 kHz for 10 seconds. Post-processing is done using the NI-LabVIEW program. Figure 3.9 illustrates a typical calibration curve for the hot-wire in the present flow conditions. The variation of mean voltage response of the hot-wire anemometer (*HWA*) corresponding to freestream velocity is depicted in Figure 3.9(a). The polynomial equation derived from this curve is utilized to determine the sensitivity of the hot-wire probe at a given velocity. Additionally, the calibration curve for the hot-wire is presented in terms of E^2 and U_∞ in Figure 3.9(b).

This curve demonstrates a correlation factor R^2 close to unity, indicating a strong linear relationship between these two variables. The calibration constants A and B, determined as 1.5139 and 0.6248, respectively, are used to estimate probe sensitivity, turbulence intensity, and other essential flow field parameters.

3.3.4 Wing Model Design

A rectangular flat-plate wing is characterized by its simple and straight geometry. It has a constant chord length and *AR*, with equal spans across its wingspan. In the present experimental study, a flat-plate wing measuring 150 mm, chordwise, with a thickness of 5 mm is investigated which results in a thickness ratio of approximately 3.33%. Notably, the thickness of this flat-plate is comparable to 2.72% of the wing used in a prior study by Siddiqui et al. (2018). The material chosen for both the wing and its attachments is plexiglass due to its widespread availability. Three types of modifications were implemented on the flat-plate wing to evaluate performance improvements from each change. These modifications included adding an array of inverted dimples on the suction side and incorporating planar/non-planar wingtip attachments.

The array of inverted dimples was strategically positioned along the span at multiple locations on the suction side of the flat-plate wing of *AR* = 2, aimed at initiating an early transition to turbulent flow. The inverted dimples have a diameter of approximately 1.0 mm and a height of about 0.5 mm (Figure 3.10). A total of 15 dimples are arranged along the span at three chordwise positions: 0.25c, 0.5c, and 0.75c. These dimples are distributed in various combinations, as mentioned below, to study their effect on optimizing flow control and promoting early transition to turbulent flow:

a) Single row at location 0.25c from *LE*.
b) Single row at location 0.5c from *LE*.
c) Single row at location 0.75c from *LE*.
d) Double rows at location 0.25c and 0.5c from *LE*.
e) Double rows at location 0.5c and 0.75c from *LE*.

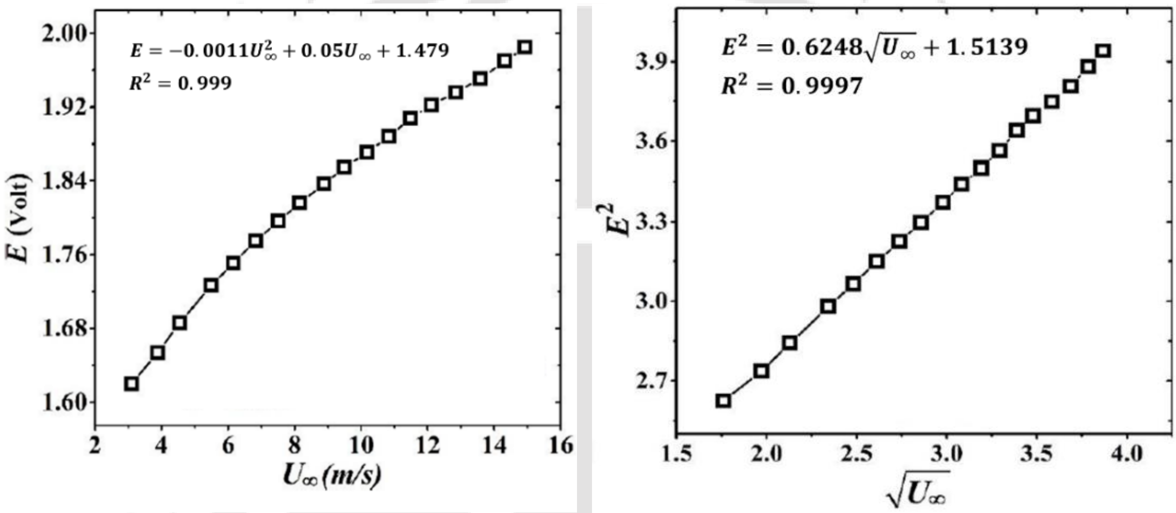

(a) Variation of mean voltage as a function of pitot-static probe velocity

(b) Relation of mean voltage and velocity as per King's law

Figure 3.9: *HWA* calibration

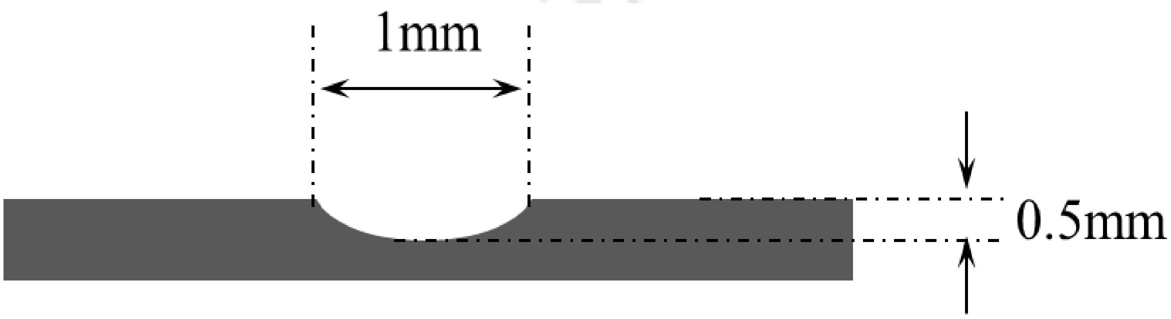

Figure 3.10: Cross sectional view of inverted dimples

Each of these combinations is tested, and the aerodynamic coefficients are analyzed and compared to determine any resulting improvements. The arrangement of the inverted dimples is illustrated in Figure 3.11 (schematic diagram) and Figure 3.10 (real image).

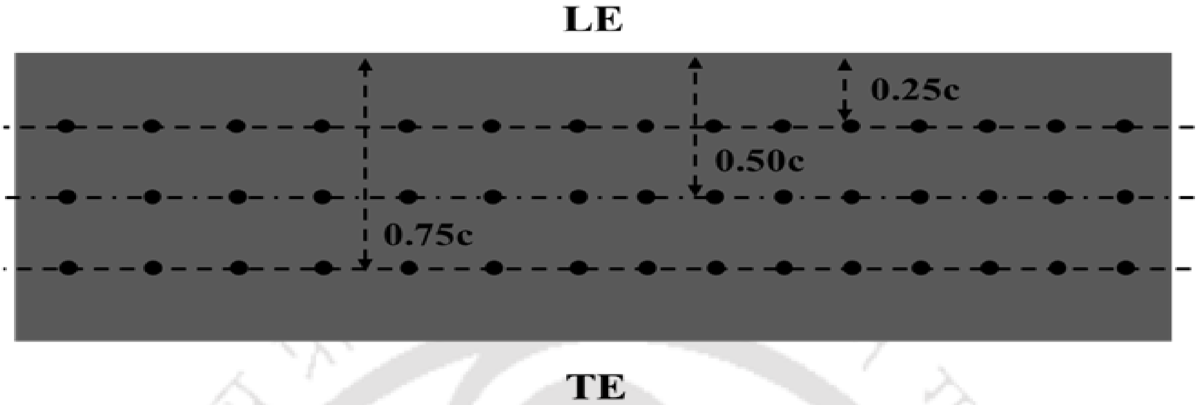

Figure 3.11: Location of inverted dimples on the suction side of wing

Figure 3.12: Flat-plate wing with inverted dimples at 0.25c location

In the second modification, various attachments are introduced in both planar and non-planar arrangements on wings with *AR* of 1.0 and 1.5. The attachment lengths are adjusted to maintain an overall *AR* of 2.0. The schematic diagrams illustrating different planar configurations of wing-tip attachments for the flat-plate of *AR* = 1.0 are depicted in Figure 3.11(a) through (d).

The planar configuration of the attachments bear resemblance to the wing-grid device introduced by La Roche (La Roche 1996; La Roche and Palffy 1996). While La Roche's device was tested at a higher *Re* of 2×10^6 and for conventional airfoil-shaped wings, the current study focuses on their application in low *AR* flat-plate winged *MAV*s. The positioning of the devices remains consistent in the *AR* = 1.5 plate, with the sole variation being its length, set at 37.5 mm to attain an overall *AR* = 2.0. A representative configuration for *AR* = 1.5 is illustrated in Figure 3.12.

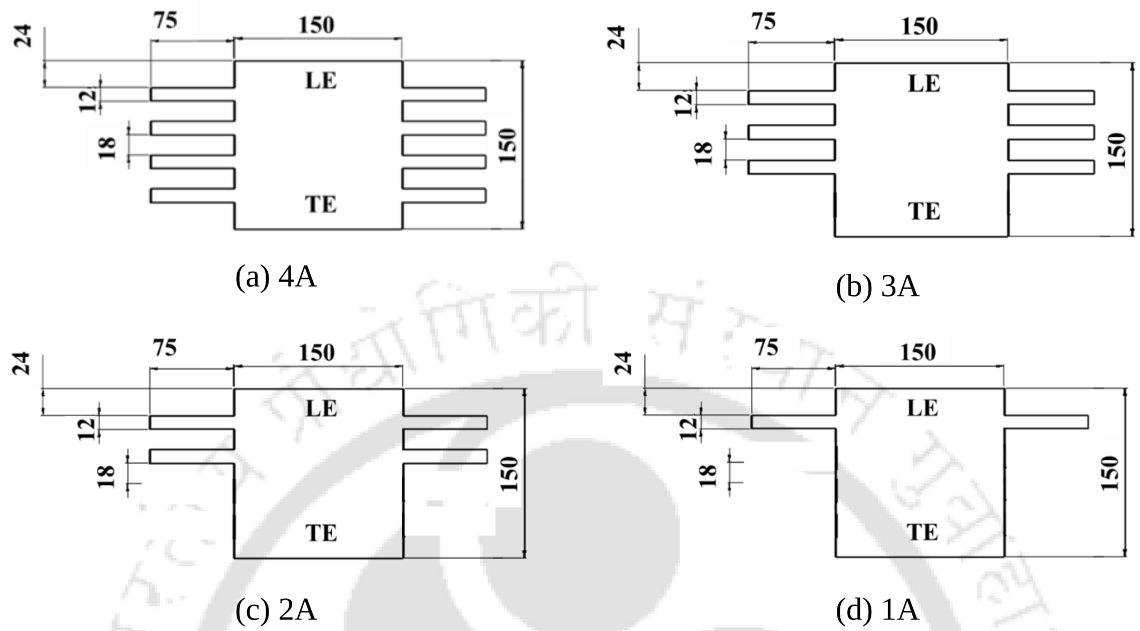

Figure 3.13: Planar configurations of the wing-tip attachments for *AR*=1.0 (all dimensions are in mm)

The attachment design is maintained consistently for both *AR*s, and its cross-sectional dimensions are illustrated in Figure 3.13. It's important to note that the winglet design is heuristic, emphasizing simplicity.

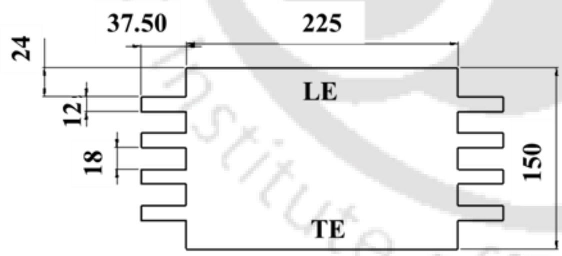

Figure 3.14: Wing-tip attachments on an *AR* = 1.5 flat plate (all dimensions are in mm)

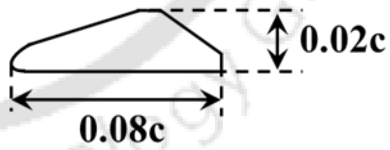

Figure 3.15: Cross sectional dimension of the wing-tip attachments

The attachment dimensions are inspired by the wingtip feathers of a Harris's hawk, with a wingspan typically ranging from 1000 mm to 1200 mm. Following Lynch et al. (2018), whose study featured attachments with a 25 mm chord length for wings with a semi-span of 312.5 mm, the chord length of the attachments in the present study is set at 12 mm, given the maximum span of the flat-plate wings is restricted to 300 mm. Given the study's emphasis on simplicity, a generic cross-section featuring a smooth leading and *TE* is chosen. The use of this straightforward biomimetic approach aims to yield results that can serve as a foundation for refining and optimizing future designs

Additionally, another attachment design was investigated within the non-planar arrangement. Four bionic attachments are incorporated into the wingtip of the flat plates, arranged in a dihedral configuration. These attachments are affixed using adhesive, ensuring an angle with the spanwise axis. The specific dihedral configurations under examination are detailed in Table 3.1, drawing inspiration from the work of Smith et al (Smith et al., 2001).

Table 3.1: Test matrix of dihedral configurations

Case	Range of dihedral angle	Configurations	Wing AR
A	20°, 10°, -10°, -20°	A1	1.0
		A2	1.5
B	-20°, -10°, 10°, 20°	B1	1.0
		B2	1.5

Smith and team demonstrated an enhanced lift curve slope using a similar combination, augmented by an extra central attachment at 0°. Both the flat plate and attachments are crafted from polystyrene material. Emphasizing simplicity, the attachment design features a straightforward cross-section, as depicted in Figure 3.13. Figure 3.14 provides a frontal view of the non-planar arrangement for the *AR* = 1.0 I configuration.

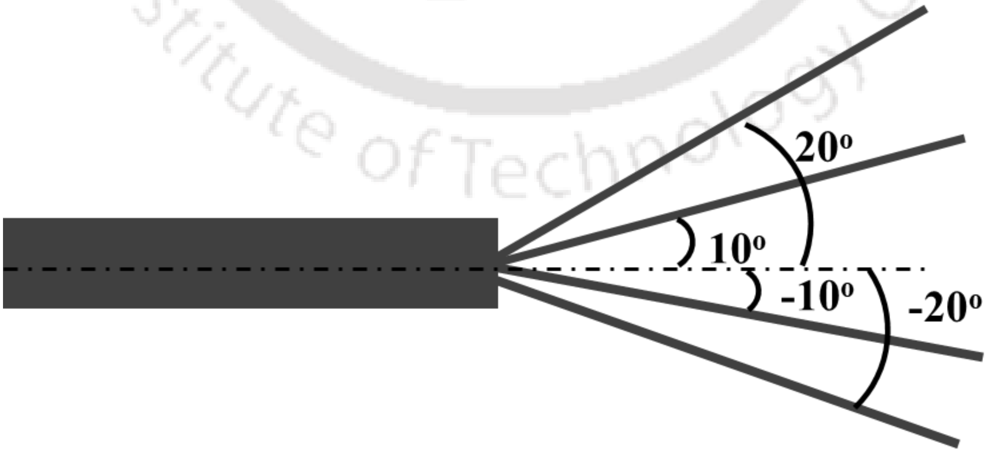

Figure 3.16: Non-planar winglet configuration (Front View)

The modifications implemented are geared towards *MAV* applications, where total weight is a critical parameter. Table 3.2 presents the volumetric form factor (V_f) of the modified wings relative to an unmodified wing of *AR* = 2.0.

Table 3.2: Volume factor of the modified flat-plates with planar devices

Aspect Ratio	**Configuration**	V_f
1.0	4A	0.60
	3A	0.57
	2A	0.55
	1A	0.52
1.5	4A	0.80
	3A	0.79
	2A	0.77
	1A	0.76

The volumetric form factor, defined in Eq. 3.4, offers insights into the weight savings achieved by each configuration compared to an unmodified *AR* = 2.0 flat-plate.

$$V_f = \frac{\text{Volume of modified wing with attachments}}{\text{Volume of } AR = 2.0 \text{ wing without attachments}} \quad (3.4)$$

Notably, the 4A configuration of *AR* = 1.0 (denoted as *AR* = 1-4A) and *AR* = 1.5 (denoted as *AR* = 1.5-4A) modified plates accounts for 60% and 80% of the total volume of the *AR* = 2.0 flat-plate, respectively. Consequently, weight reductions of approximately 40% and 20% can be realized with these configurations, potentially enhancing payload capacity, provided the performance of the modified flat-plates remains within specified limits. The significance of this factor will be elucidated in subsequent sections when discussing lift and drag per unit volume, highlighting the comparison of forces generated by lighter wings against those from heavier counterparts. For the non-planar configuration, the V_f for *AR* = 1.0 and 1.5, each equipped with four non-planar wingtip devices, is 0.58 and 0.79, respectively. These values indicate weight savings of approximately 42% and 21% for the modified *AR* = 1.0 and 1.5 flat plates compared to an unmodified *AR* = 2.0 flat plate. The configurations with four wingtip devices, both in planar and non-planar arrangements, are illustrated in Figure 3.15.

(a) Planar Wingtip Devices

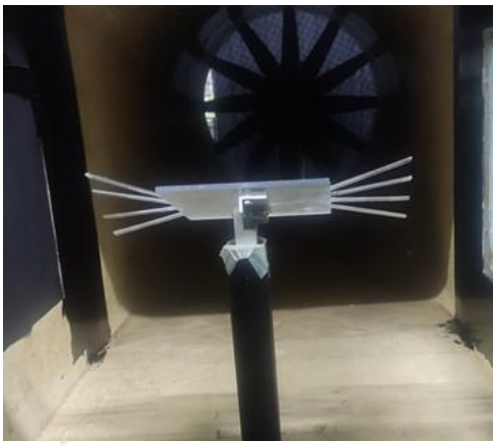

(b) Non-planar Wingtip Devices

Figure 3.17: Flat-plate wing setup in wind tunnel

3.3.5 Uncertainty Analysis

Uncertainty analysis is a critical component in experimental studies, aiming to assess and quantify potential errors in measurements. It involves evaluating the variations and standard deviations of data at different settings to estimate the reliability and precision of experimental results. In aerodynamic studies, such analysis helps provide a clearer understanding of the accuracy and confidence levels associated with parameters like lift and drag, enhancing the credibility of experimental findings.

In the current study, the force-balance system output undergoes analysis to identify and quantify potential errors. This involves calculating the standard deviation of the sample size at specific settings to gauge reading variations. In the current dataset, a maximum standard error of 0.8% for C_L and 0.24% for C_D is observed at a 95% confidence level (20:1 odds). The uncertainties in C_l and C_d are depicted with error bars in Figure 3.16, showcasing the analysis of the base wing (*AR* = 1.0) and the *AR* = 1.0-4A configuration at *Re* = 5×10^4.

3.3.6 Experimental Setup Validation

The validation of the experimental setup is a crucial step to ensure its conformity to intended specifications and proper functionality. In this study, validation is conducted by comparing results with those obtained by Shields and Mohseni (2012) and Mizoguchi et al. (2016). Despite variations in factors such as model material and mounting method, the outcomes exhibit a high correlation.

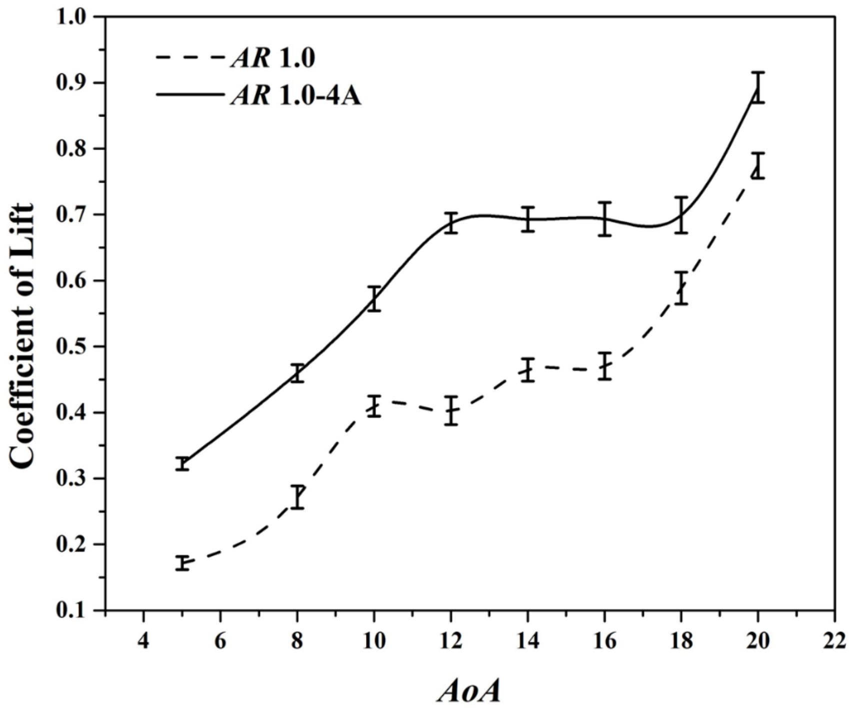

(a)

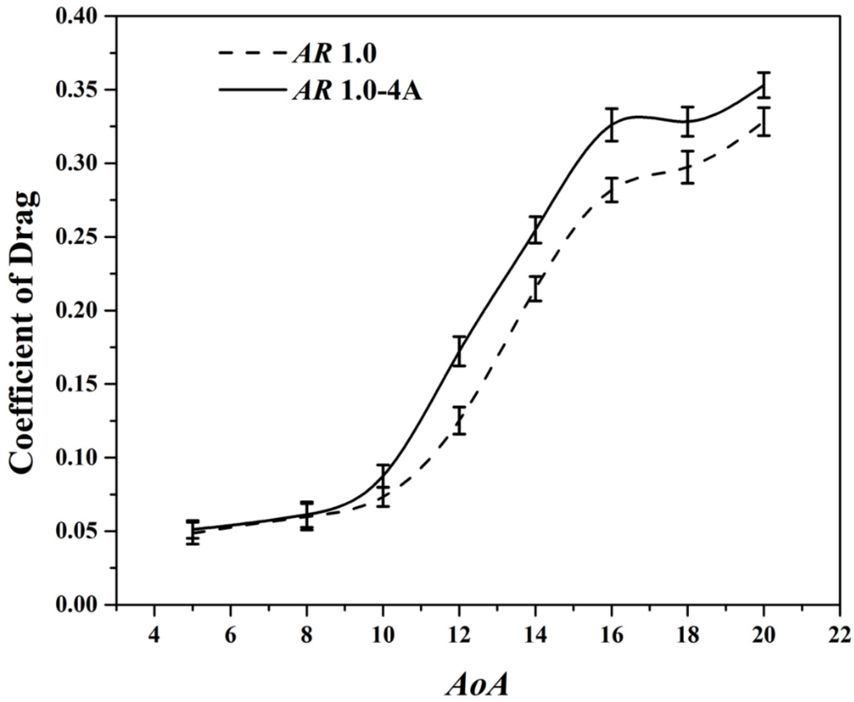

(b)

Figure 3.18: Uncertainties in (a) C_L and (b) C_D at Re = 5×10^4

The lift (C_L) and drag (C_D) data obtained by the current setup for an *AR* = 1.0 flat-plate wing at *Re* = 5×10^4 are employed for validation. Shields and Mohseni (2012) used a similar *AR* flat-plate wing at *Re* = 5×10^4 with an elliptically rounded *LE* (5:1 *AR*) and thickness-to-root chord ratios between 2.4% and 5.4%. Mizoguchi et al. (2016) utilized a flat-plate with a rectangular chordwise cross-section at AR = 0.9 and Re = 5.2×10^4. The results, depicted in Figure 3., show good agreement, with slight deviations attributed to differences in turbulence intensities and experimental setups.

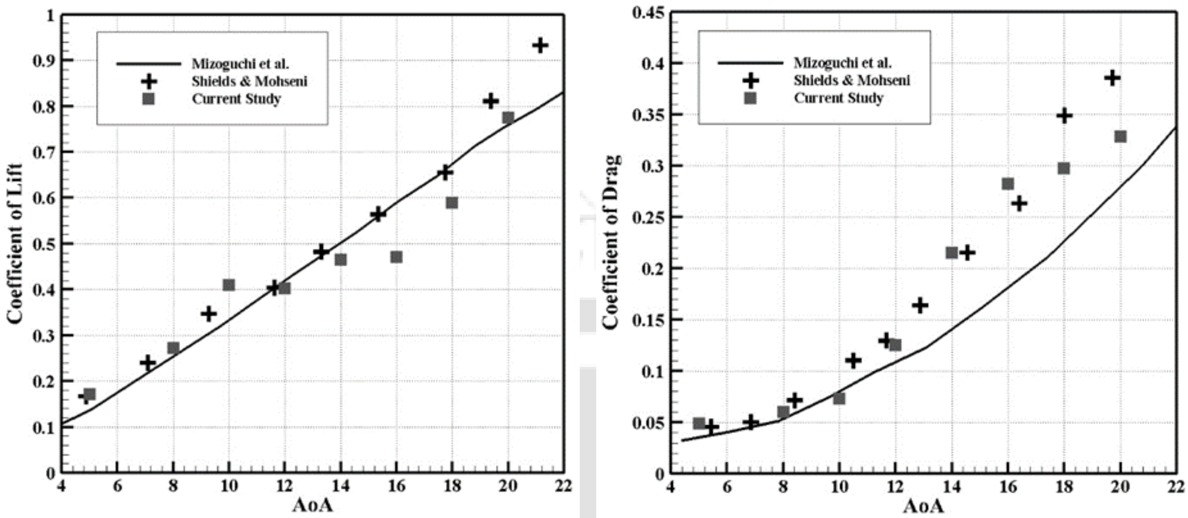

(a) C_L vs AoA (b) C_D vs AoA

Figure 3.19: Comparison of C_L and C_D of the present study with the reported data (Mizoguchi et al. 2016; Shields and Mohseni 2012)

3.4 Scaling Effects and Implications for Different MAV Sizes

Scaling effects play a critical role in the aerodynamic behaviour of *MAVs*, particularly because their performance is highly sensitive to changes in *Re*, surface roughness, and structural weight. The findings from this study, while based on a specific size and *Re* regime, offer insights that can be extended cautiously to *MAVs* of different scales.

- ***Re* Sensitivity:** The *Re*, which scales with the product of velocity and characteristic length (e.g., chord length), is a primary factor influencing aerodynamic behaviour at small scales. As *MAV* size increases, *Re* increases, leading to changes in boundary layer behaviour (from laminar to transitional or turbulent) and potentially delaying flow separation, which can improve lift and reduce drag. Lift mechanisms such as leading-edge vortex (LEV) attachment may weaken or become less effective at higher *Re*, altering the benefits observed with non-planar wingtip devices. This means that configurations optimized for low *Re* (e.g., 10^4–10^5) may not perform identically at higher *Re* values, and their aerodynamic benefits could diminish or shift in nature.

- **Structural Considerations:** Scaling up an *MAV* increases the structural mass disproportionately (volume scales with the cube of length), which can offset aerodynamic gains unless carefully managed. Larger *MAVs* must ensure that added mass does not negate performance improvements, particularly if the wingtip devices increase surface area or complexity. Conversely, scaling down may make the *MAV* more susceptible to viscous effects, such as increased skin-friction drag and lower *Re* efficiency, making the per-unit-weight aerodynamic performance metric (used in this study) even more critical.
- **Manufacturing and Integration:** As *MAV* size changes, so does the feasibility of manufacturing intricate wingtip attachments. Larger *MAVs* allow for more durable and complex structures using composite layups or CNC machining. Smaller *MAVs* may require micro-fabrication or high-resolution 3D printing to maintain geometric accuracy and minimize added weight. This influences not just the aerodynamic outcome but also the design-for-manufacture and assembly strategy, which must be tailored by scale.
- **Flow Physics:** Flow phenomena such as tip vortex behaviour, spanwise flow, and LEV stability do not scale linearly. Therefore, while the proposed configurations may demonstrate promising performance at the studied scale, their flow dynamics should be re-examined through either *CFD* simulations or flow visualization techniques when scaled to different *MAV* sizes.

3.5 Concluding Remark

The methodology employed in this study successfully integrates computational simulations and experimental testing to provide a robust framework for analyzing flat-plate wing configurations. The complementary nature of these approaches ensures the accuracy and reliability of the results, with computational models offering detailed insights into flow dynamics and experimental setups validating performance metrics under real-world conditions. This dual approach strengthens the credibility of the findings and establishes a solid foundation for future aerodynamic research and innovation.

Chapter 4: Computational Analysis

Chapter Outline

Overview:

The computational results provide a comprehensive understanding of the aerodynamic behavior of flat-plates in varying conditions. Through unsteady 2D simulations, the study investigates airflow around flat-plates with different thickness ratios at specific Reynolds numbers. The analysis includes variations in lift-to-drag ratio, Strouhal number, and vorticity magnitude contours, offering valuable insights into the complex flow patterns and aerodynamic characteristics of the flat-plates. These computational findings contribute to a deeper understanding of fluid dynamics and have implications for diverse applications in aerodynamics.

4.1 Prologue

Unsteady 2D simulations are conducted, focusing on incompressible airflow around flat-plates with thickness ratios of 1% and 3% at *Re* of 4.8×10^4 and 7.6×10^4. The free stream velocities are set at 5 ms^{-1} and 8 ms^{-1}, respectively. The results showcase variations in *L/D* ratio with *AoA*, *St* with *AoA*, and contours depicting vorticity magnitude. These outcomes offer insights into the aerodynamic behavior of the flat-plates under different flow conditions and geometric configurations. The simulations reveal the influence of thickness ratio and *Re* on the aerodynamic performance, emphasizing the critical role of free stream velocity. The variation in *L/D* ratio elucidates the plate's efficiency across different *AoA*s, while *St* trends highlight the frequency of shedding vortices. The vorticity magnitude contours offer a detailed visual representation of flow patterns, aiding in the understanding of the fluid dynamics around flat-plates.

In the subsequent sections, a comprehensive discussion on the aerodynamic parameters of the investigated flat-plate wings is presented. Various aspects, including lift, drag, and their corresponding coefficients, are analyzed to provide insights into the aerodynamic performance of these flat-plate configurations. Additionally, factors such as *AoA*, *Re*, and geometric characteristics are considered in the context of their impact on the aerodynamic behavior of the flat-plate wings.

4.2 Lift-to-Drag Ratio

The *L/D* ratio is a key aerodynamic parameter that signifies the efficiency of an airfoil or wing. It is calculated by dividing the C_L by the C_D, providing a measure of how effectively an aircraft generates lift relative to the drag it experiences.

At a *Re* of 10^4, flow separation begins at the sharp *LE* due to dominant viscous forces, exacerbated by the bluntness of the thicker plate. The *L/D* ratio variation with *AoA* (Figure 4.1) illustrates that the 1% thick plate outperforms the 3% thick plate, consistent with findings by Winslow et al. (2018). The thicker plate experiences more pronounced flow separation, leading to increased pressure drag. Winslow et al. attributed this to the heightened bluntness of the thicker plate causing a more adverse pressure gradient, resulting in flow separation closer to the *LE* and subsequently higher drag. The increased flow separation also impacts the lift force by reducing the pressure differential between the suction and pressure sides.

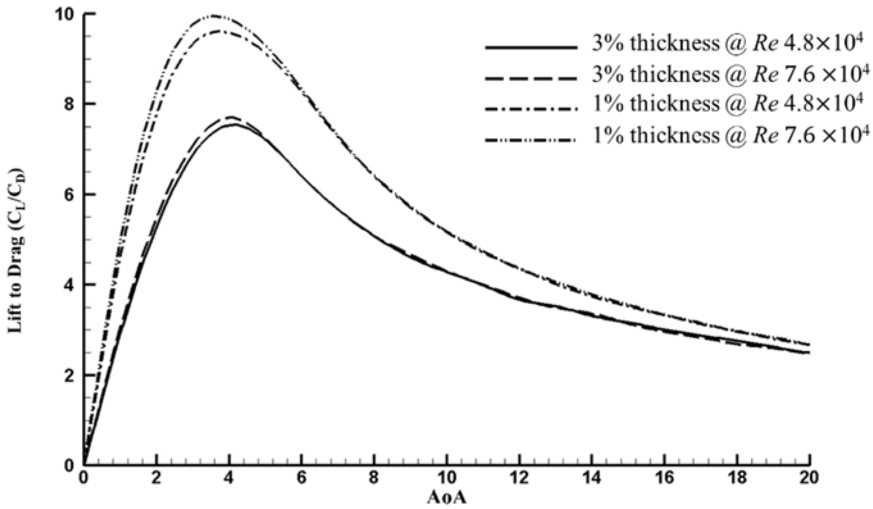

Figure 4.1: Variation of *L/D* ratio for a 1% and 3% thick flat plate

4.3 Strouhal Number

The Strouhal number, denoted by *St=fc/V*, serves as a dimensionless parameter crucial for interpreting flow oscillations, where *f* represents the shedding frequency, *c* is the chord length, and *V* denotes the free stream velocity magnitude. The vortex shedding frequency is derived through a Fast Fourier Transform applied to the x-component of velocity, *u*, measured at a location 0.1c downstream from the plate's *TE*. Figure 4.2 illustrates the periodic behavior of velocity after initial disturbances. The *St* variation with *AoA* is presented in Figure 4.3, showcasing a decrease as *AoA* increases within the simulated range. Smaller *AoA*s result in a narrower wake and vortices with smaller length scales, leading to an augmented vortex shedding frequency, as evidenced by the time history of u fluctuations. For the 3% thick plate, shedding frequencies are observed at *AoA*s of 9° and 10° for *Re* of 4.8×10^4 and 7.6×10^4, respectively. In contrast, for the 1% thick plate, similar frequencies are identified at *AoA*s of 12° and 13°, respectively. Figure 4.4 provides spectral representations of *u* at *AoA*s 17°, 18°, 19°, and 20°.

The variation in *St* with *AoA* indicates the influence of flow conditions on vortex shedding, with wider wakes and lower shedding frequencies at higher *AoA*s. The differences in shedding frequencies between the 1% and 3% thick plates highlight the impact of thickness on the flow behavior. The quantitative analysis of vortex shedding frequency offers valuable insights into the aerodynamic characteristics of the flat plates under different conditions. These findings contribute to a comprehensive understanding of the flow dynamics and shed light on the implications for the design and performance of flat-plate wings in various scenarios.

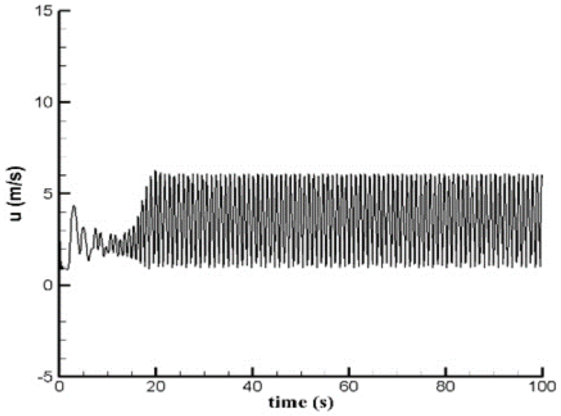

Figure 4.2: Oscillation of u at *AoA* 20° for 3% thick plate at *Re* 10^4

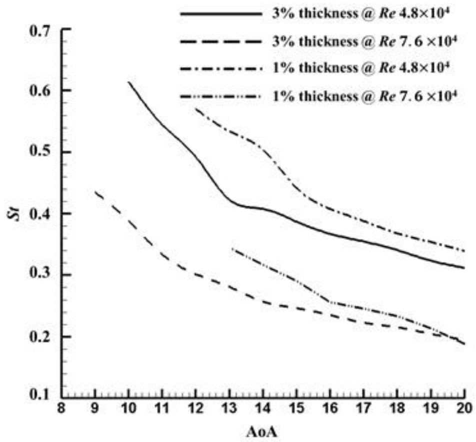

Figure 4.3: Variation of *St* with *AoA*

It was observed that the lift and drag exhibit synchronous fluctuations with the shedding frequency, as illustrated in Figure 4.5. This synchronization implies that the maximum values of lift and drag coincide, occurring simultaneously during the shedding cycle. This phase alignment of lift and drag oscillations indicates a close coupling between the aerodynamic forces and the shedding frequency. The coherent behavior between lift and drag provides insights into the dynamic interaction between the flow field and the wing surface, contributing to a comprehensive understanding of the aerodynamic response.

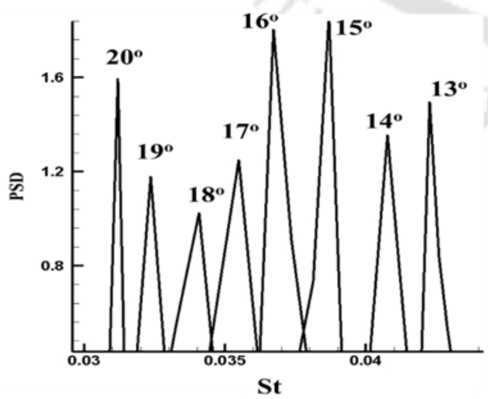

Figure 4.4: *St* vs *PSD* for 3% flat plate at *Re*=10^4

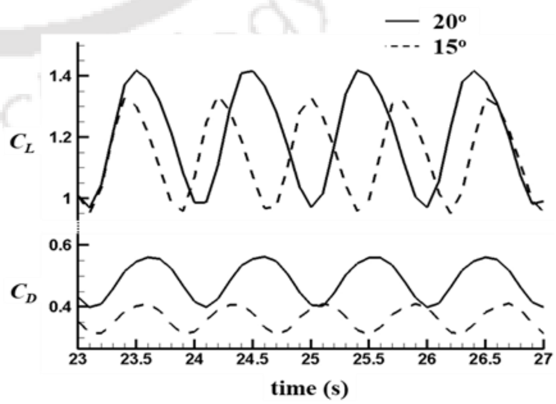

Figure 4.5: Fluctuating C_L and C_D for 3% thick flat plate at *Re* 10^4

4.4 Vortex Formation

Vortex dynamics play a central role in the lift generation mechanism, particularly in low *Re* regimes typical of *MAV* applications and unconventional wing configurations. When a wing moves through the air, pressure differences between the upper and lower surfaces result in the formation of vortices, especially at the wingtips and along the leading edge. These vortices contribute to the overall circulation around the wing, which, according to the Kutta–Joukowski theorem, is directly proportional to lift. In the case of flat-plate wings or wings with wingtip attachments, vortex structures such as *LE* vortices and tip vortices can enhance lift under certain conditions.

The process of vortex formation is elucidated through schematics, generated via simulations, in Figure 4.6, highlighting key flow features such as *LE* vortex roll-up, *LE* separation, and *TE* vortex. The clockwise rotation of the *LE* vortex initiates from the separated shear layer at the *LE*, extending streamwise until it reaches the *TE* (Figure 4.6 (a) and (b)). This leads to the creation of a low-pressure region around the *TE*, causing the flow to separate and curl up in an anticlockwise direction, resulting in maximum lift (Figure 4.6 (b)). As the anticlockwise vortex grows, it displaces the clockwise vortex towards the *LE* (Figure 4.6 (c)), causing the *LE* separated shear layer to expand upstream and eventually shed from the *TE*. *TE* shear layer separation occurs when the clockwise vortex reaches the *TE*. The separated shear layer then rolls into the anticlockwise vortex toward the suction side of the plate, driven by the low-pressure region created by the *LE* separated shear layer (Figure 4.6 (d)). This process leads to an increase in the size of the anticlockwise vortex, reaching its maximum, resulting in minimum lift. Subsequently, the vortex sheds from the *TE* (Figure 4.6 (e)). This cyclic process of vortex formation and shedding contributes to the periodic variation in lift and drag forces observed in the unsteady simulations. The interaction between the leading-edge and trailing-edge vortices plays a crucial role in shaping the aerodynamic performance of the flat plates. Understanding these flow phenomena provides valuable insights into the complex fluid dynamics governing the lift and drag characteristics of the flat-plate wings.

Figure 4.7 presents vorticity magnitude contours and streamlines for both the 1% and 3% thick plates. Notably, the vortices originating from the *LE* on the suction side are prominently visible in the images. At lower *AoA*s, the adverse pressure gradient lacks the strength to induce flow separation.

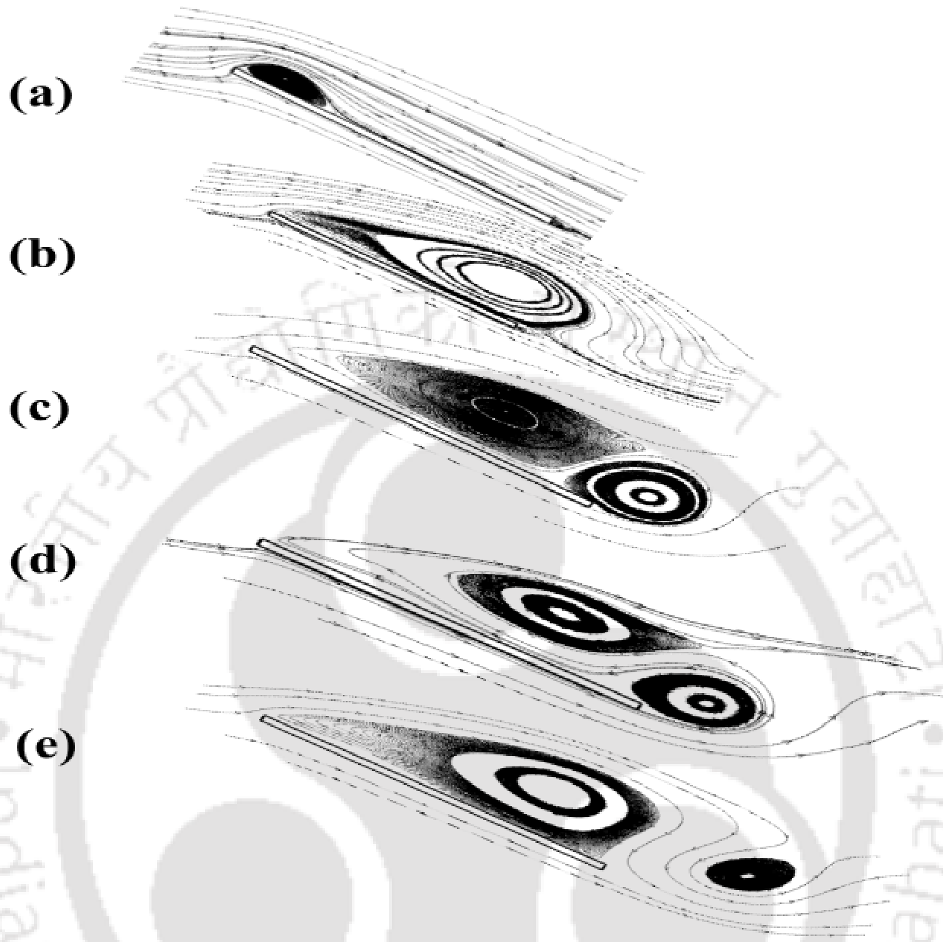

Figure 4.6: Schematic of vortex formation and shedding

The formation and propagation of *LE* and *TE* vortices contribute to variations in pressure distribution and other aerodynamic characteristics. The shedding phenomena significantly impact the alteration of lift and drag experienced by the plate. Particularly, at an *AoA* of 20^{o}, a distinct vortex emerges at the *TE*, a consequence of flow separation at that location. These vorticity patterns play a crucial role in influencing the overall aerodynamic performance of the flat plates. The visible vortices from the *LE* contribute to lift generation, while the shedding of vortices from the *TE* is indicative of flow separation. Understanding these flow phenomena is essential for comprehending the complex interactions and dynamic behavior of the flow around flat plates, especially at higher *AoA*s. The insights gained from these vorticity contours enhance our understanding of the intricate aerodynamic mechanisms governing the studied configurations.

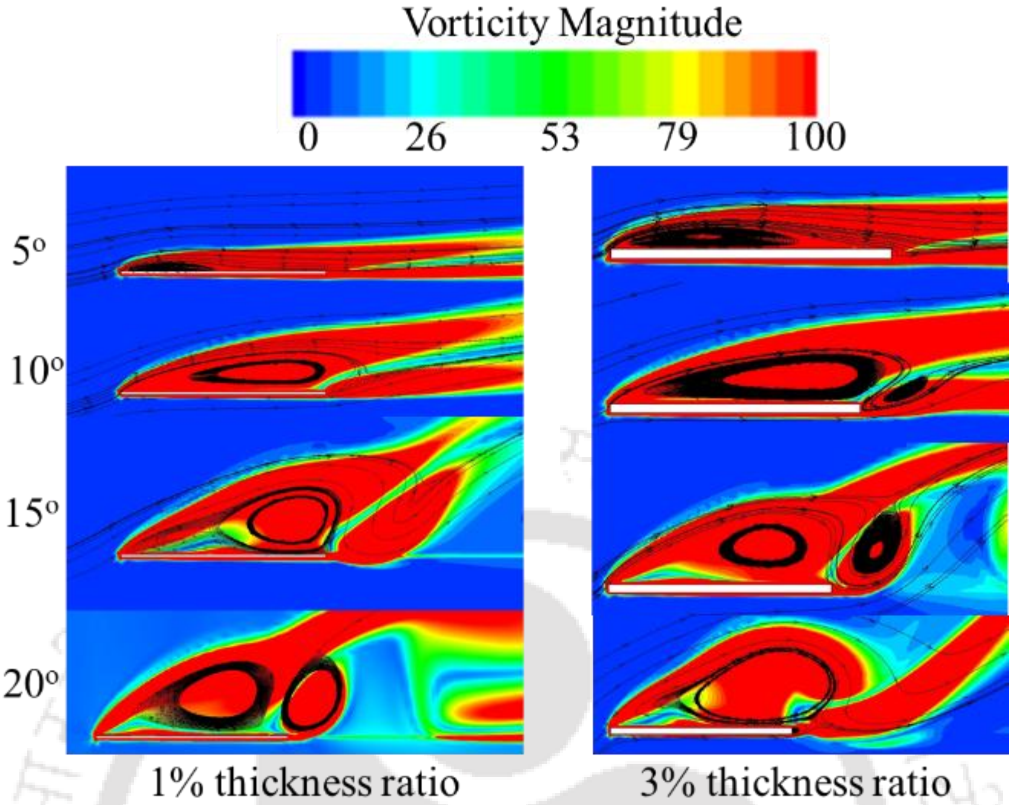

Figure 4.7: Vorticity magnitude contours with streamlines showing vortices for flat plate at *Re* = 1×10^4

4.5 Summary of the Chapter

The computational investigation of flat-plate wings with varying thickness ratios at *Re* of 4.8×10^4 and 7.6×10^4 reveals significant insights into their aerodynamic behavior. The *L/D* ratio analysis indicates that the 1% thick plate outperforms the 3% thick plate, aligning with the influence of thickness on flow separation and pressure drag. The examination of *St* variations with *AoA* unveils the impact of flow conditions on vortex shedding frequencies, showcasing distinct behaviors for different thickness ratios. Shedding frequencies and wake characteristics are found to be sensitive to thickness, providing valuable quantitative insights into the aerodynamic performance of flat plates. These findings contribute to a comprehensive understanding of flow dynamics and have implications for the design and optimization of flat-plate wings in diverse aerodynamic scenarios.

Chapter 5: Experimental Results with Inverted Dimples

Chapter Outline

Overview:

The first experimental study is conducted with the inverted dimples to investigate their potential to enhance aerodynamic performance by inducing an earlier transition to turbulent flow on a flat-plate wing. Positioned strategically on the suction side, these dimples, each about 1.0 mm in diameter and 0.5 mm in height, were arranged in specific patterns across three chordwise locations (0.25c, 0.5c, and 0.75c) to test their effects. By disrupting the boundary layer, these dimples aimed to reduce drag and improve flow stability. Various configurations were evaluated to determine the optimal layout for controlling flow separation and improving overall wing efficiency.

5.1 Prologue

The first experimental study investigates the use of inverted dimples on the suction side of the flat-plate wing. By promoting earlier turbulence through boundary layer disruption, inverted dimples could enhance flow attachment and reduce drag. The current study uses a flat-plate wing with an *AR* of 2 and places dimples at specific chordwise locations (0.25c, 0.5c, and 0.75c) as mentioned in Section 3.3.4. A total of 15 dimples were positioned in varied configurations across these chordwise locations to assess their effects on flow control and transition.

Inverted dimples can potentially reduce drag by altering boundary layer behavior and delaying flow separation, while planar and non-planar attachments can influence the distribution of lift and improve stability or reduce drag by changing the effective wing shape and airflow patterns. The attachment studies are explained in the later chapters, while this chapter seeks to provide insights into how inverted dimples may optimize flow control for wings, advancing knowledge on passive surface modifications and their practical applications in improving aerodynamic efficiency.

5.2 Aerodynamic Coefficients

The aerodynamic coefficients of wings with inverted dimples help evaluate performance changes from these surface modifications. Inverted dimples can increase the C_L by promoting turbulent flow and maintaining airflow attachment, especially at higher *AoA*, potentially delaying flow separation and enhancing lift. For the C_D, dimples may reduce drag by stabilizing the boundary layer, though added surface roughness could occasionally increase drag. The aim is often to improve the *L/D*, enhancing aerodynamic efficiency through an optimal dimple configuration. The variation of C_L and C_D with *AoA* at $Re = 15\times10^4$ is shown in Figure 5.1 and Figure 5.2, respectively, as these effects are more prominent at the higher *Re*.

From the C_L vs *AoA* plot (Figure 5.1), it is evident that among the modified wings, the 0.75c configuration achieves the highest lift values. At higher *AoA*, specifically when $AoA > 14°$, the 0.75c configuration notably surpasses the C_L of the base wing, indicating improved lift performance under these conditions. This configuration is closely followed by the 0.50c setup, which also shows enhanced lift but to a slightly lesser extent. In contrast, the other configurations consistently trail behind the base wing across all *AoA*s, with particularly poor performance at higher *AoA*s, where they fail to provide adequate lift compared to the base wing and the leading configurations.

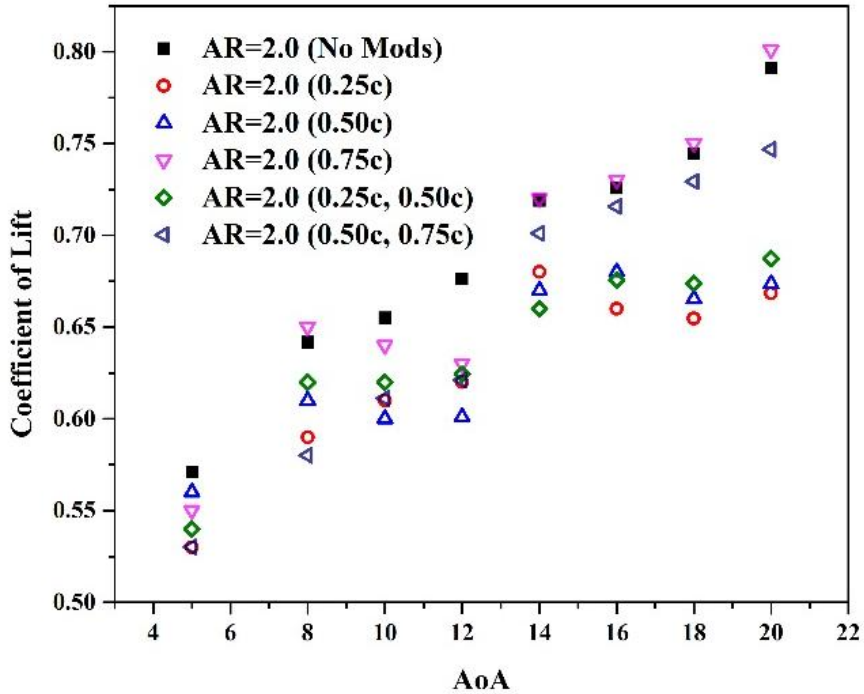

Figure 5.1: Variation of C_L with *AoA* at *Re* = 15×10^4

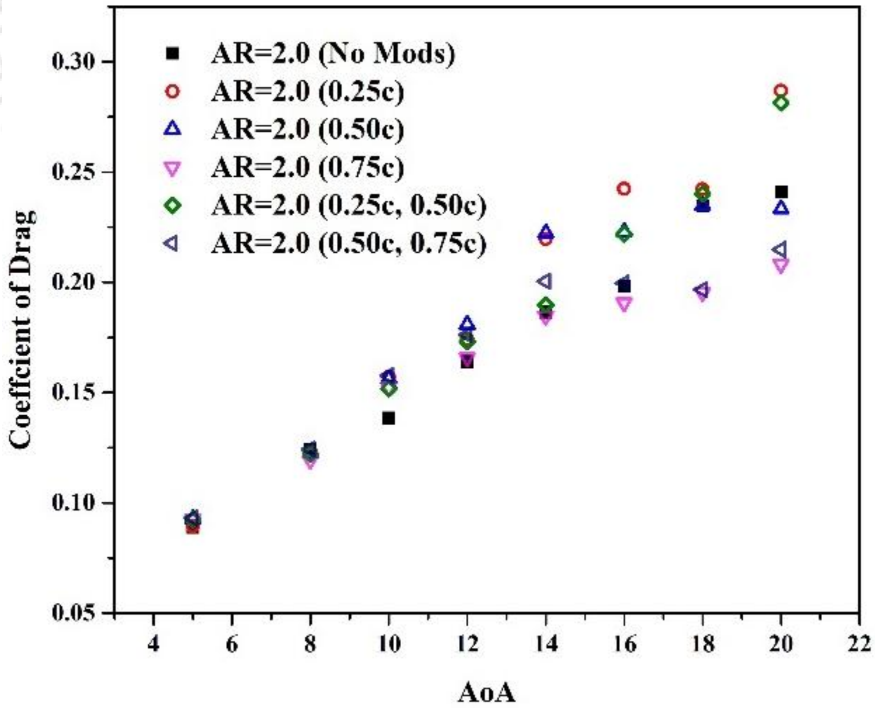

Figure 5.2: Variation of C_D with *AoA* at *Re* = 15×10^4

Regarding C_D values, as shown in Figure 5.2, the 0.75c configuration again demonstrates beneficial behavior, with consistently lower C_D values compared to the other modified wings and the base wing. Among the dual-row configurations of inverted dimples, the 0.50c, 0.75c setup shows improved aerodynamic performance, with better C_L and C_D values than the other dual-row configuration. However, both dual-row setups fall short of the top-performing single-row configurations. Notably, the 0.25c setup consistently exhibits the lowest lift values among all tested wings, likely due to premature boundary layer separation caused by the obstruction at this location. This suggests that the 0.25c configuration hinders aerodynamic efficiency, underscoring the importance of optimal dimple positioning for balancing lift and drag.

5.3 Oswald's Efficiency Factor

It is a parameter that measures the aerodynamic efficiency of a wing by quantifying how closely its actual performance approaches the ideal elliptical lift distribution. It is used in the calculation of induced drag and is part of the equation for C_D. A higher efficiency factor (closer to 1) indicates lower induced drag and higher aerodynamic efficiency, while lower values suggest increased drag. Factors affecting Oswald's efficiency include wing shape, *AR*, and flow conditions.

It appears in the equation for C_D related to lift, specifically in the formula for induced drag. The equation is:

$$C_D = C_{D0} + \frac{C_L^2}{\pi \times AR \times e} \tag{5.1}$$

where C_D is the total drag coefficient, C_{D0} is the profile drag coefficient (drag due to factors other than lift), C_L is the lift coefficient, *AR* is the wing's *AR* and *e* is Oswald's efficiency factor.

In equation (5.1), the 2nd term on the right hand side represents induced drag, the drag resulting from lift generation. A higher value of *e* (closer to 1) means the wing is more efficient, resulting in less induced drag for a given C_L and *AR*. Conversely, a lower *e* value indicates increased induced drag, often due to wing shape or flow disturbances that cause the lift distribution to deviate from the ideal elliptical shape.

Figure 5.3 illustrates the variation of *e* with *Re* for wings featuring inverted dimples across all configurations.

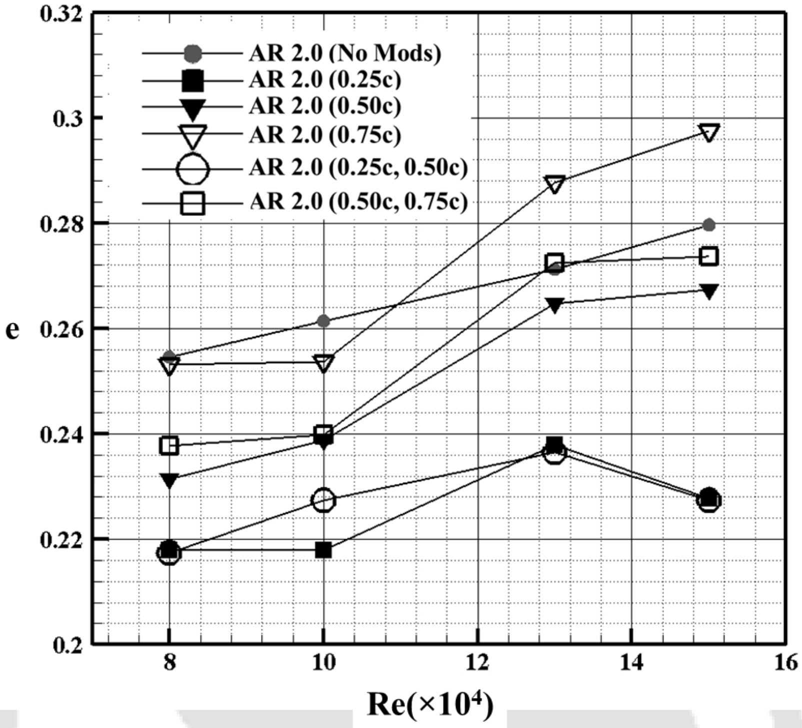

Figure 5.3: Effects of varying *Re* on *e* for flat-plate wings with inverted dimples

It is observed that the base wing of *AR* = 2.0 shows an increase in *e* with rising *Re*, as do the 0.75c, 0.50c, and dual-row (0.50c, 0.75c) configurations. A higher efficiency factor indicates reduced induced drag for a given lift, meaning these configurations effectively lower drag by better approximating an ideal lift distribution. Conversely, the placement of dimples at 0.25c appears less beneficial, as both the single-row (0.25c) and double-row (0.25c, 0.50c) configurations show lower *e* values than the base wing. This suggests that while certain dimple placements can enhance aerodynamic efficiency by reducing induced drag, the 0.25c location may disrupt optimal flow patterns, leading to increased drag. The results highlight the importance of dimple positioning in managing induced drag across various *Re*.

5.4 Lift-to-Drag Ratio

The *L/D* ratio for each modified wing configuration was measured and compared to that of an unmodified wing. Both lift and drag forces were recorded to calculate the *L/D* ratio, a critical metric in aerodynamics that reflects the efficiency of an aerofoil or wing. A higher *L/D* ratio indicates that the wing generates more lift for a given amount of drag, a desirable trait for enhancing performance, fuel efficiency, and overall aerodynamic effectiveness. Optimizing the *L/D* ratio is essential in applications where maximizing lift while minimizing drag is key to improved flight efficiency and stability.

The *L/D* ratio plots at different *Re* are presented in Figures 5.4(a) through (d). These plots reveal that the 0.75c configuration consistently demonstrates a superior *L/D* ratio compared to the unmodified wing, particularly at higher *AoA*.

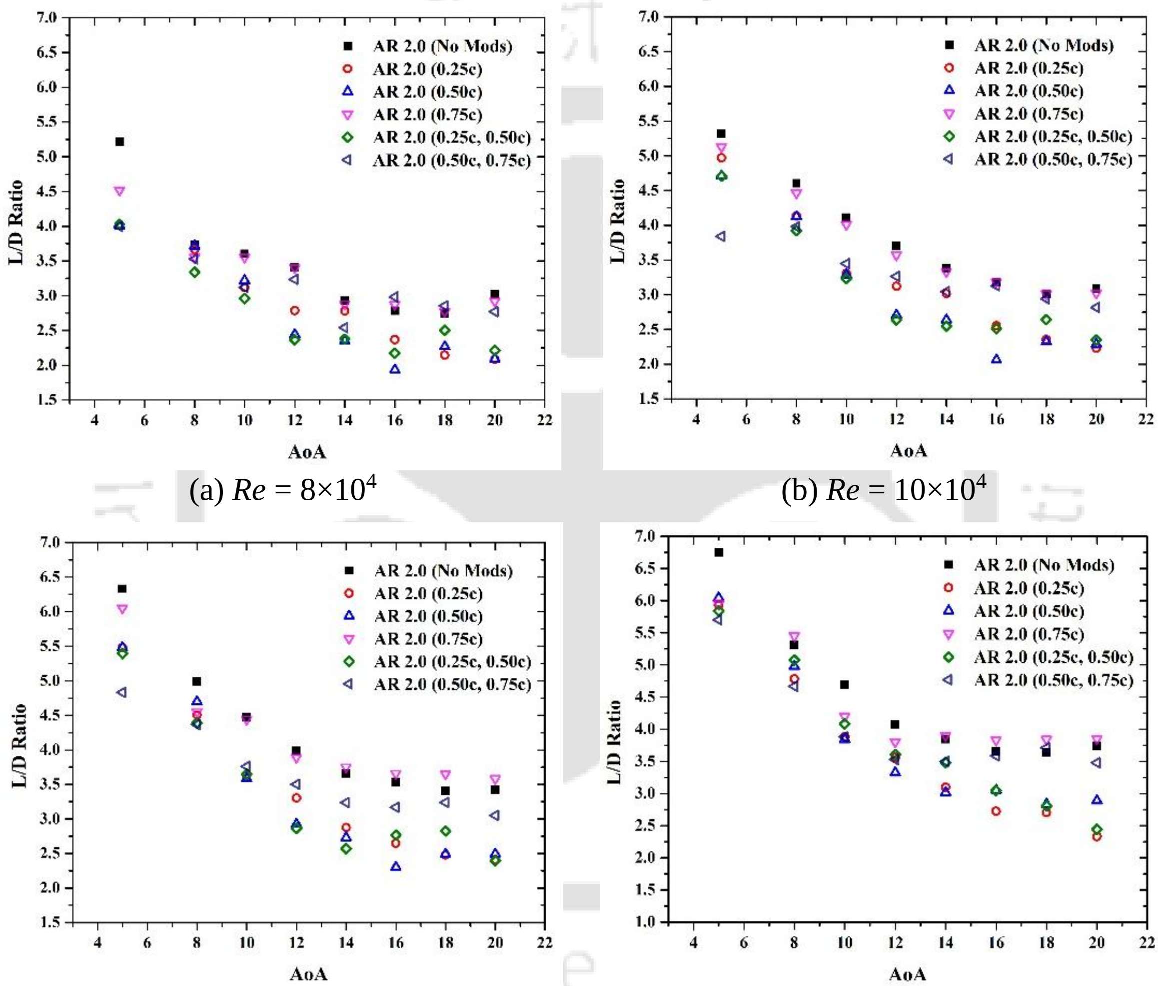

(a) *Re* = 8×10^4 (b) *Re* = 10×10^4

(c) *Re* = 13×10^4 (d) *Re* = 15×10^4

Figure 5.4: Variation of *L/D* with *AoA* at different free stream velocities (a) 8 ms^{-1} (b) 10 ms^{-1} (c) 13 ms^{-1} (d) 15 ms^{-1}

This improvement is especially notable at higher *Re* values of 13×10^4 and 15×10^4, where the 0.75c configuration outperforms the unmodified wing at *AoA*s of 14°, 16°, 18°, and 20°. At lower *Re* values of 8×10^4 and 10×10^4, the 0.75c configuration performs similarly to the unmodified wing, occasionally showing superior *L/D* at certain *AoA*s while being slightly lower at others. This suggests that while the 0.75c configuration is highly effective at higher *Re*, its advantages are less pronounced at lower *Re* but still observable.

The percentage improvements in *L/D* for the 0.75c configuration are listed in Table 5.1. No other configuration achieves performance gains over the unmodified wing at any *AoA* or *Re*. The 0.50c, 0.75c dual-row configuration shows the second-best performance; however, it consistently trails the unmodified wing by a considerable margin. These findings underscore the 0.75c configuration's unique capability to optimize aerodynamic efficiency, especially at higher *Re*.

Table 5.1: Percentage improvement for 0.75c inverted dimple configuration

AoA	Reynolds Number	Improvement of 0.75c over Unmodified wing
14°	15×10^4	1.42%
	13×10^4	2.44%
16°	15×10^4	4.83%
	13×10^4	3.46%
18°	15×10^4	5.49%
	13×10^4	7.25%
20°	15×10^4	2.90%
	13×10^4	4.64%

This trend indicates that placing the dimples at the 0.75c location is particularly advantageous for enhancing aerodynamic performance at critical *AoAs*. The significant performance advantage of the 0.75c configuration over other setups suggests that this placement is especially effective in delaying flow separation and reducing drag. At specific flow speeds and *AoAs*, the inverted dimples appear to energize the flow sufficiently to encourage boundary layer reattachment, likely due to the enhanced intermixing of fluid layers initiated by the dimples. By creating localized turbulence, the strategically positioned dimples increase momentum exchange within the boundary layer, thereby energizing the flow and preventing premature separation. This allows the boundary layer to stay attached to the wing surface for longer, improving lift and aerodynamic stability at higher *AoA*s.

At higher *Re* and *AoA*, this effect becomes even more pronounced, as the inverted dimples effectively disrupt laminar flow and induce an earlier transition to turbulence. This transition energizes the boundary layer, mitigating the effects of the adverse pressure gradient and promoting flow reattachment. As a result, the wing experiences reduced drag and enhanced lift characteristics, contributing to improved overall aerodynamic performance.

5.5 Summary of the Chapter

In this study, the aerodynamic effects of inverted dimples on flat-plate wings were examined, assessing different dimple placements to optimize lift, drag, and efficiency across various *Re* and *AoA*. Among the configurations tested, the 0.75c placement consistently outperformed others, demonstrating higher lift and lower drag, especially at higher *Re*. The 0.50c configuration also showed improved performance, while the 0.25c placement resulted in poorer outcomes, likely due to premature flow separation. Analysis of *e* indicated that the 0.75c and 0.50c configurations effectively reduced induced drag, underscoring the benefits of strategic dimple positioning in enhancing aerodynamic efficiency.

Chapter 6: Experimental Results for Planar Devices

Chapter Outline

Overview:

A comprehensive experimental study was undertaken to scrutinize the aerodynamic performance of flat plate wings featuring planar wingtip devices. The central focus was on evaluating how wingtip modifications influence the lift and drag characteristics of flat plate wings. Diverse configurations, incorporating different aspect ratios and wingtip attachments, were systematically investigated to discern their impact on aerodynamic forces. The experimental setups employed wind tunnel testing and force balance measurements to meticulously collect data on lift, drag, and other pertinent parameters. The study encompassed a range of angles of attack and Reynolds numbers, providing a thorough assessment of the aerodynamic behavior of the modified flat plate wings. The results contribute valuable insights into the potential optimization of the lift-to-drag ratio and overall efficiency of flat plate wings through strategic wingtip modifications, with potential applications in unmanned aerial vehicles and micro air vehicles.

6.1 Prologue

After implementing wingtip modifications on the flat-plate, wind tunnel experiments are conducted to assess their effectiveness. These modifications are designed to adjust the overall *AR* of the flat-plate to 2, as outlined in Section 3.3.4. The purpose of these attachments is to increase the *AR* without adding extra weight to the wing. Experiments take place in the wind tunnel under the specified operating conditions detailed in Section 3.3.6. The *L/D* is chosen as a superior parameter, considering its holistic representation of both aerodynamic force characteristics. The *L/D* ratios of the modified wings are calculated and compared across all four configurations, forming the basis for detailed discussions in the subsequent sections.

Following the implementation of modifications on the flat-plate, wind tunnel experiments were conducted to assess the effectiveness of these alterations. The adjustments were made to achieve an overall *AR* of 2, as outlined in Chapter 3. These modifications were strategically designed to enhance the *AR* without introducing additional weight to the wing. Experiments took place in the wind tunnel setup, operating under conditions detailed in Section 3.2. The *L/D* serves as a comprehensive parameter, encapsulating both individual aerodynamic force characteristics. Consequently, the *L/D* ratio of the modified wings was calculated and compared across all four configurations, providing insights discussed in the subsequent sections.

6.2 Aerodynamic Coefficients

The examination of aerodynamic coefficients with respect to *AoA* is a conventional method to showcase wing effectiveness. In this segment, the aerodynamic coefficients of unmodified flat-plates and those with the 4A configuration for both *AR*s are plotted against *AoA* at a *Re* of 15×10^4, as depicted in Figure 6.1 and 6.2. Additionally, data from Siddiqui et al. (2018) concerning the case of a rigid flat tip is presented to illustrate the similarities in the trend and behavior of aerodynamic coefficient variations with *AoA*. In the *AR* = 1.0-4A configuration, both C_L and C_D exhibit an increase compared to the base plate and the *AR* = 2.0 plate. For the *AR* = 1.5-4A arrangement, C_L demonstrates improvement only at higher *AoA*s, while C_D is lower at nearly all *AoA*s. The unmodified flat-plates exhibit the anticipated behavior of increasing C_L with rising *AR*, and conversely, a decrease is observed in C_D.

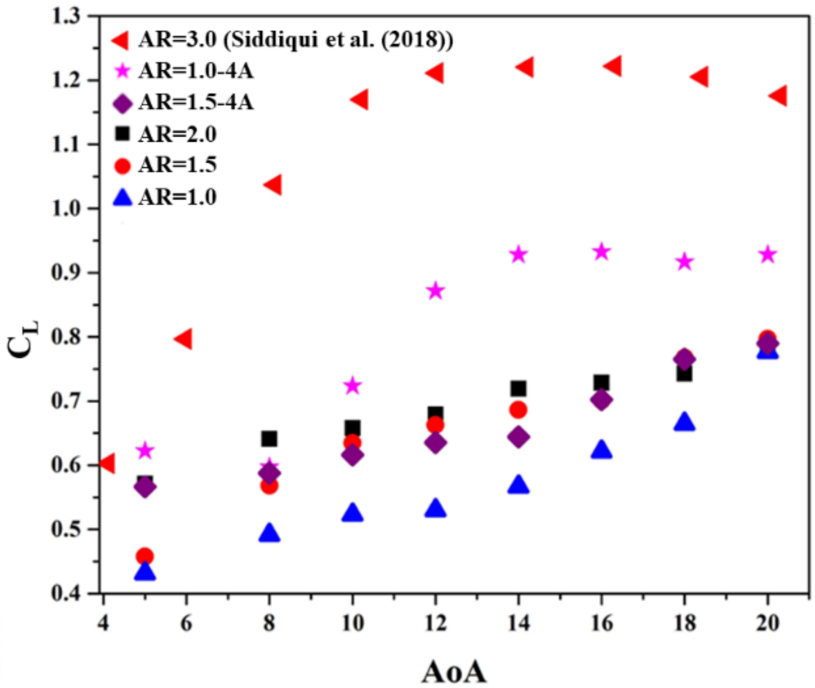

Figure 6.1: Variation of C_L with *AoA* at *Re* = 15×10^4

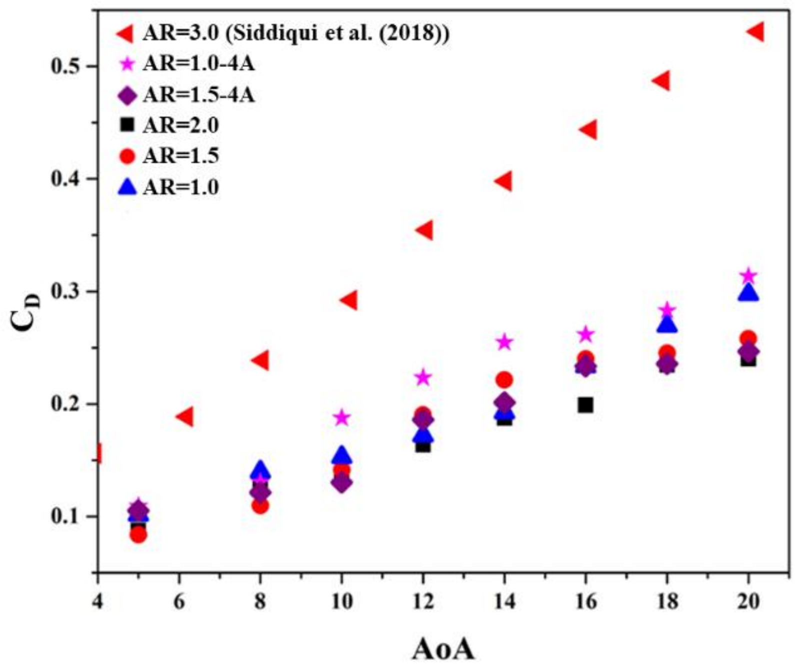

Figure 6.2: Variation of C_D with *AoA* at *Re* = 15×10^4

The *AR* = 1.0-4A configuration achieves a C_{Lmax} of 0.93 at *AoA* = 16°, outperforming the base plate's C_{Lmax} of 0.77 at *AoA* = 20°, despite having the same effective span as the *AR* = 2.0. This represents a notable 19% improvement in C_{Lmax}. However, it's essential to acknowledge that while the C_L is relatively higher in this configuration compared to others, the C_D is also elevated. This phenomenon can be attributed to the impact of the induced drag component of the total drag, which is directly influenced by the lift generated, as expressed in Eqn 6.1.

$$\text{Induced Drag} = \frac{C_L^2}{\pi \times AR \times e} \tag{6.1}$$

In the context of Eqn 6.1, where *e* represents Oswald's efficiency factor, the induced drag is directly proportional to the square of the C_L. The higher drag observed in the slotted wing-tip configuration is attributed to the separate functioning of each wing-tip as an individual airfoil, generating staggered vorticity that influences the preceding wing-tip (Siddiqui et al., 2018). This, coupled with an increase in overall wetted area, contributes to the significant drag observed in the flat-plate with attachments (Narayan and John, 2016). The higher C_L of the *AR* = 1.0-4A configuration results in elevated induced drag due to induced drag and staggered vorticity, leading to a higher C_D compared to other configurations. Specifically, the C_{Dmax} for *AR* = 1.0-4A is 6.9% and 29% higher than the C_{Dmax} of *AR* = 1.0 and *AR* = 2.0 plates, respectively. Unlike the base plate, the C_L for *AR* = 1.0-4A plate reaches a plateau from *AoA* = 14° onwards. The differences in absolute values compared to Siddiqui et al. (2018) are primarily attributed to variations in base wing dimensions and *Re*. Nevertheless, the trend of C_L for *AR* = 1.0-4A mirrors the observed increase with *AoA* reaching a plateau, consistent with findings by Bardera et al., (2023) in a simulation study.

In the case of the model with *AR* = 1.5-4A, the C_{Lmax} reaches 0.79 at *AoA* = 20°, demonstrating a similarity to its base configuration and *AR* = 2.0 plate. However, this model with attachments exhibits a reduced lift generation capability compared to the flat-plate model with *AR* = 2.0. Additionally, the drag experienced by this model is consistently higher across various *AoA* arrangements compared to the base configuration of *AR* = 2.0. Notably, the C_{Dmax} of this modified arrangement aligns closely with the C_{Dmax} values of the *AR* = 1.5 base plate and *AR* = 2.0.

Figure 6.3 provides a comprehensive view of the aerodynamic coefficients for various wings, both with and without attachments. Notably, the *AR* = 1.0-4A configuration stands out with higher C_D values corresponding to elevated C_L values at $Re = 15\times10^4$. In contrast, the *AR* = 2.0 exhibits a low C_D across all C_L values below 0.80, indicating superior lift generation and drag reduction. The linear trends observed in other configurations contrast with the sudden nonlinearity in C_L and C_D for the AR = 1.0-4A plate. This configuration surpasses others in terms of aerodynamic coefficient values. Additionally, Figure 6.3 highlights the lower aerodynamic coefficients for AR = 1.5-4A compared to AR = 1.0-4A, emphasizing the nuanced impact of wingtip attachments on aerodynamic performance.

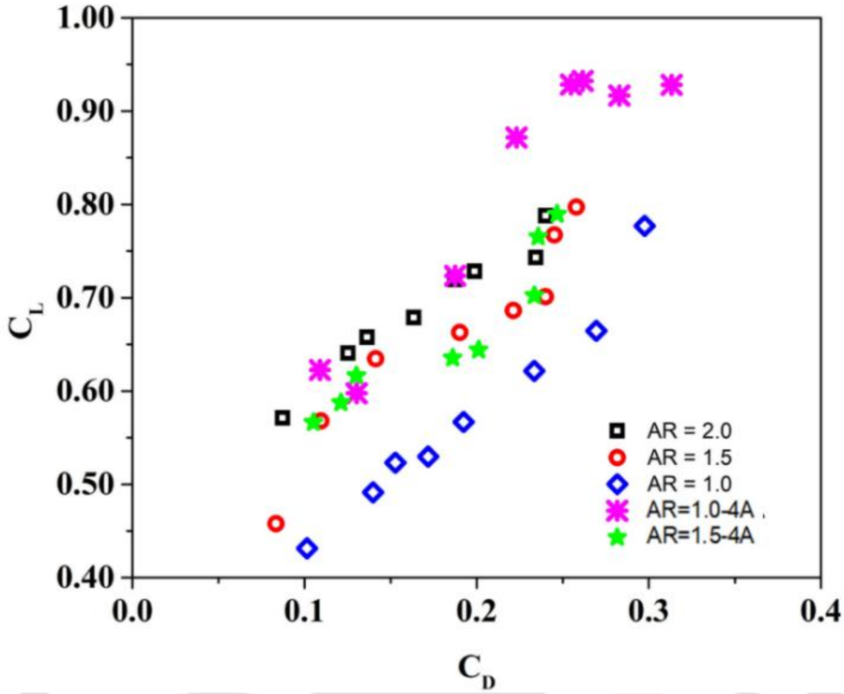

Figure 6.3: C_L vs C_D at $Re = 15\times10^4$

6.3 Oswald's Efficiency Factor

To assess the rise in induced drag, e, as described in Eqn. 6.1, is examined. Calculating this factor involves establishing a linear fit of C_D versus C_L^2 using wind tunnel data. The selection of the C_L range for this linear fit is crucial, aiming to achieve a higher coefficient of determination (R-squared value) through regression analysis. An exemplar linear fit is illustrated in Figure 6.4 using data from an AR = 1.0 flat-plate at $Re = 15\times10^4$. The R-squared value of 0.9945 indicates a strong agreement between the data and the linear fit. Analogously, this calculation procedure is applied to all other configurations for a comprehensive analysis.

The e, depicted in Figure 6.5, exhibits an intriguing trend deviating from the conventional literature range of 0.6–0.9 (McCormick, 1995; Roskam and Lan, 1987). A noteworthy departure from typical behavior is evident in the experimented flat-plates, aligning with observations by Spedding and McArthur (Spedding; McArthur, 2010). The data showcases an increase in *e* with rising *Re* and decreasing AR. This pattern aligns with well-established findings in previous studies, such as Ananda et al. (Ananda et al., 2015). As elucidated earlier, *e* serves as an indicator of the drag increase proportional to lift augmentation. With lift escalation due to heightened *Re*, the corresponding *e* values reflect this rise. Ananda et al. (2015) provided a comprehensive explanation, linking the rate of drag rise to the extent of flow separation on the wing. Particularly in low *AR* wings, intensified wingtip vortices contribute to disturbances in the flow over the wing, resulting in elevated drag.

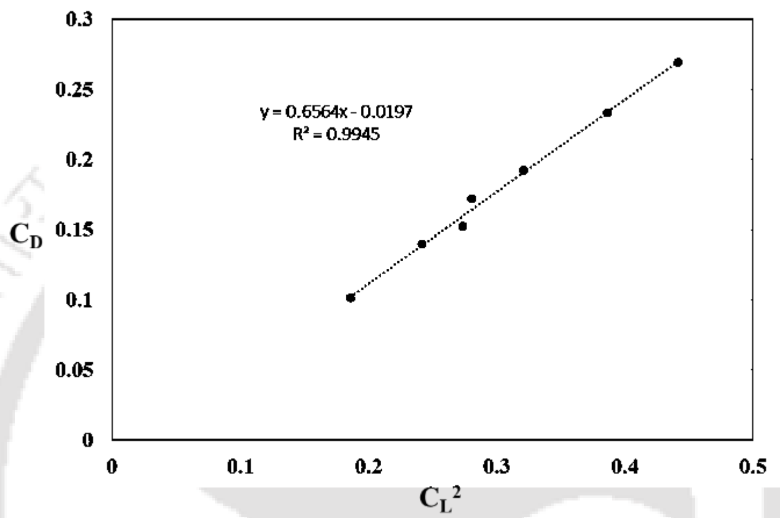

Figure 6.4: Variation of C_L^2 with C_D for *AR* = 1.0 flat-plate at *Re* = 15×10^4

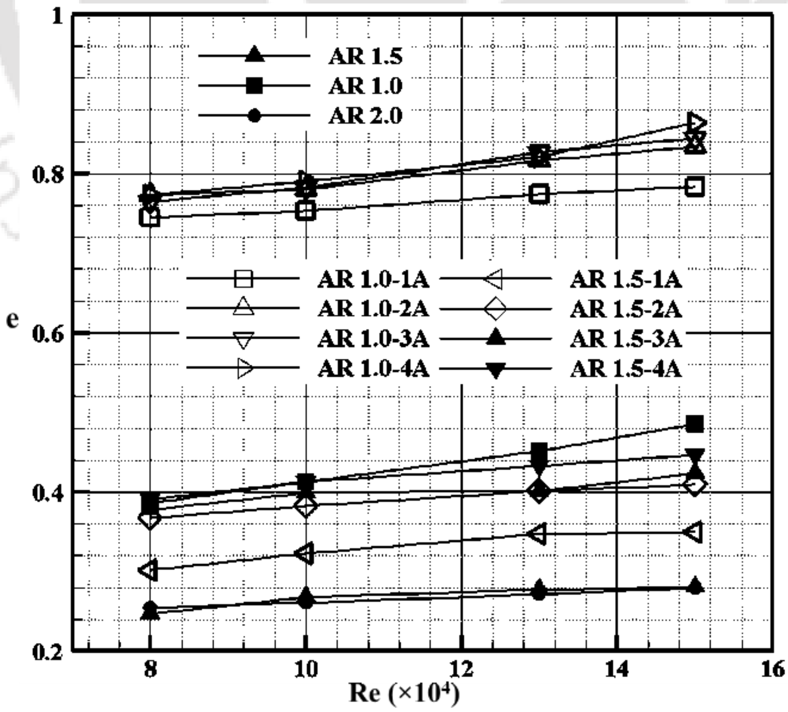

Figure 6.5: Effects of varying *Re* on *e* for flat-plate wings

Figure 6.5 reveals notable variations in the *e* among different configurations. The *AR* 1.0-4A stands out with the highest *e* values, ranging from 0.77 to 0.86, in stark contrast to the simpler *AR* = 1.0 base flat-plate, which exhibits a narrower range of 0.38-0.48. The unmodified *AR* = 1.5 and *AR* = 2.0 flat-plates present lower ranges of 0.24−0.28 and 0.25−0.28, respectively. While these absolute values differ from Ananda et al.'s observations, the overall trend aligns with previous studies. Importantly, the addition of wingtip attachments leads to an enhanced e, with the *AR* = 1.0 wing experiencing a more pronounced improvement compared to the *AR* = 1.5 wing. These variations underscore the sensitivity of *e* to wing modifications and emphasize the role of experimental setups and model differences in influencing results.

6.4 Lift-to-Drag Ratio

The *L/D* ratio, a crucial metric in assessing wing efficiency, establishes the relationship between aerodynamic forces. Utilizing force data acquired from the force balance, this parameter is calculated to gauge the effectiveness of the wing design.

The bio-inspired winglets demonstrate superior *L/D* ratios compared to their respective base wings, as illustrated in Figure 6.6 and Figure 6.7 for the *AR* = 1.0 and 1.5 modified flat-plates, respectively. The figures also present comparisons with unmodified *AR* = 1.0, 1.5, and 2.0 flat-plates. In the case of the *AR* = 1.0 flat-plate with attachments, the 4A configuration consistently outperforms other modified configurations, following the performance trend 4A > 3A ≥ 2A ≥ 1A. This trend becomes more pronounced with increasing *Re*. Across all flat-plates, modified and unmodified, the *L/D* value decreases with higher *AoA* and increases with higher *Re*. At *Re* = 15×10^4, the 4A, 3A, and 2A configurations exhibit maximum *L/D* (L/D_{max}) values that are 29%, 13%, and 2.6% higher than the base *AR* = 1.0 flat-plate, respectively. The *AR* = 1.0-4A plate consistently demonstrates improved *L/D* compared to the base plate across all *AoA*s and *Re*. Notably, the 4A configuration outperforms or matches the *L/D* of the base *AR* = 1.5 wing at specific *AoA*s, especially at higher *Re*. This improvement is evident at *AoA*s of 12°, 14°, 16°, and 18° for *Re* =10×10^4, 13×10^4, and 15×10^4, with an average improvement of 23% observed at *Re* = 15×10^4. The 4A configuration showcases enhancements of 29% and 10% at *AoA*s of 16° and 20°, respectively (Figure 6.6(d)). Similar improvements are observed at *Re* = 13×10^4, 10×10^4, and 8×10^4, with average enhancements of 21%, 14%, and 15%, respectively (Figure 6.6(a) through (c)).

Nevertheless, in the comparison of aerodynamic coefficients, the improvements are still less significant compared to an unmodified *AR* = 2.0 flat-plate. The *AR* = 1.0-1A configuration exhibits a lower *L/D* value when compared to the base *AR* = 1.0 plate at *AoA* = 10^o and 20^o for *Re*= 8×10^4, *AoA* = 20^o for *Re* = 10×10^4, *AoA* = 8^o, 10^o, and 12^o for *Re* = 13×10^4, and *AoA* = 8^o, 10^o, and 12^o for *Re* = 15×10^4. The introduction of the wingtip attachment may have resulted in a higher proportion of drag force compared to the lift force generation, which could be the reason for the observed lower performance. This aligns with the findings of Narayan and John (Narayan & John, 2016), who observed that added wingtips led to an increase in drag force, particularly parasitic drag force, due to an increase in overall wetted area.

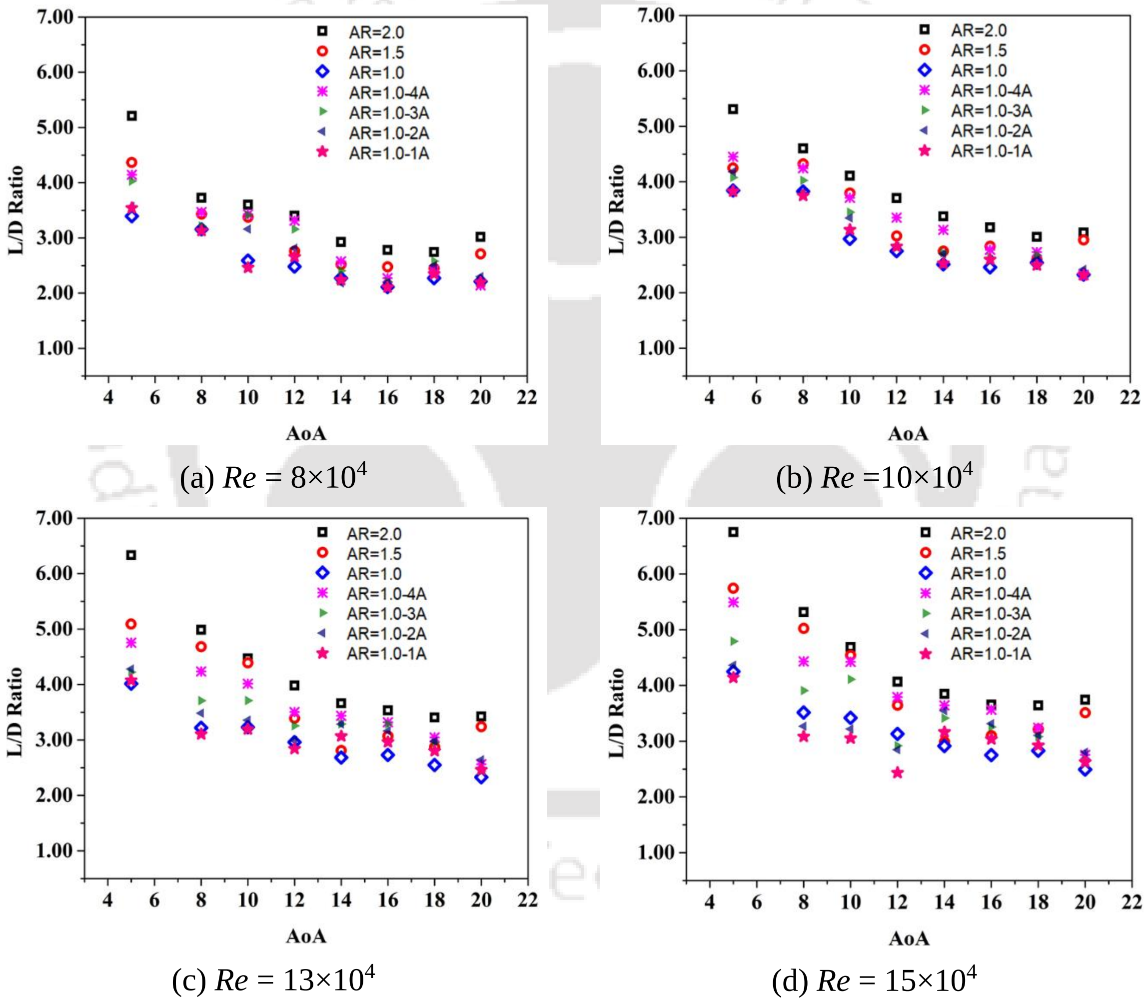

Figure 6.6: Variation of *L/D* with *AoA* at different free stream velocities for modified *AR* = 1.0 (a) 8 ms^{-1} (b) 10 ms^{-1} (c) 13 ms^{-1} (d) 15 ms^{-1}

Similarly, the *AR* = 1.5-4A configuration demonstrates the best performance among all the modified *AR* = 1.5 flat-plates. The 4A arrangement provides comparable or even superior results compared to the *AR* = 2.0 plate for *AoA* = 10^o, 12^o, 8^o, and 10^o at *Re* = 13×10^4 and

15×10^4, respectively (Figure 6.7(c) and (d)). At *Re* = 15×10^4, an average improvement of around 7% is observed from the 4A configuration compared to the base *AR* = 1.5 plate, with a maximum improvement of 20% at *AoA* = 14^o (Figure 6.7(d)). Similarly, the 3A and 2A arrangements offer an average improvement of 2.9% and 1% over the base plate at *Re* = 15×10^4. It is evident from Figure 6.7(a) through (d) that, apart from the 4A configuration, the other three arrangements do not follow a consistent pattern and provide a mix of superior or inferior *L/D* values compared to the base plate.

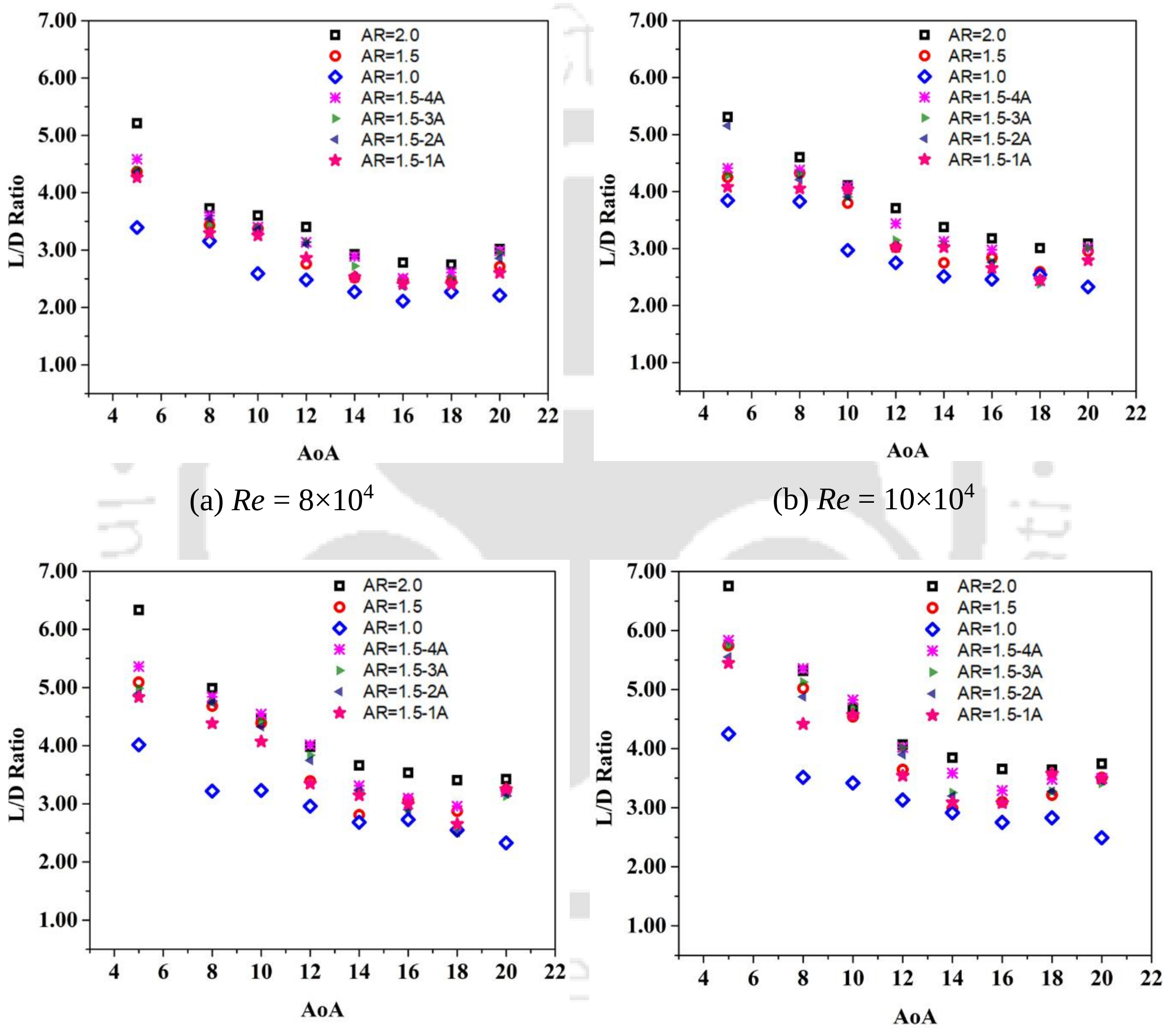

(a) *Re* = 8×10^4 (b) *Re* = 10×10^4

(c) *Re* = 13×10^4 (d) *Re* = 15×10^4

Figure 6.7: Variation of *L/D* with *AoA* different free stream velocities for modified *AR* = 1.5 (a) 8 ms^{-1} (b) 10 ms^{-1} (c) 13 ms^{-1} (d) 15 ms^{-1}

Similarly, to the *AR* = 1.0-1A case, the 1A configuration of the modified *AR* = 1.5 plate exhibits performance deficiencies compared to the base plate. This specific configuration consistently lags behind its base plate in *L/D* values at almost all *AoA*s, attributed to the increased overall wetted surface area that likely heavily influences parasitic drag generation.

Regarding the *L/D* parameter, for both *AR*s, the 4A arrangement demonstrates the maximum improvement over the other three configurations. The cases with *AR* = 1.0-4A and *AR* = 1.5-4A achieve superior *L/D* values compared to their individual base plates across the entire *AoA* and *Re* range under study, occasionally even surpassing flat-plates of higher *AR*s. Hence, the incorporation of wing-tip devices proves to significantly enhance the flat plate's lift generation capacity. The L/D_{max} values for the base wings and 4A configuration of both the modified *AR* wings are presented in Table 6.1 for clarity, along with the improvements achieved in L/D_{max} by the 4A configuration over the base wing.

Table 6.1: Comparison of L/D_{max}

Re ($\times 10^4$)	**AR=2.0**	**AR=1.5**	**AR=1.0**	**AR=1.0-4A**	**AR=1.5-4A**	**% Improvement over Base Wing**	
						AR=1.0-4A	**AR=1.5-4A**
15	6.75	5.74	4.25	5.49	5.83	29.17	1.56
13	6.33	5.09	4.01	4.75	4.83	18.45	-5.10
10	5.31	4.32	3.84	4.45	4.40	15.88	1.85
8	5.21	4.36	3.39	4.14	4.58	22.12	5.04

6.5 Lift and Drag Force per Unit Volume

The conventional approach of characterizing a wing's performance through aerodynamic coefficients and the *L/D* ratio is invaluable for full-scale airfoil-sectioned wings at high *Re*. However, given the primary focus of this study on understanding the effects of wingtips for *MAV* applications, the wing's weight must be considered when analyzing its performance metrics. A connection between the forces experienced and weight is established by linking force parameters with the volume factor from Table 3.2. The modifications implemented are geared towards MAV applications, where total weight is a critical parameter. Table 3.2 presents the V_f of the modified wings relative to an unmodified wing of AR = 2.0.

Assuming uniform material density across all wings, this parameter provides insight into the forces generated per unit weight of the wing. Figure 6.8 illustrates the variation of lift and drag force per unit volume with *AoA* for *AR* =1.0, 1.5, and 2.0 plain flat-plates, as well as the 1A and 4A configurations of *AR* = 1.0 and 1.5 flat-plates at *Re* = 15×10^4. A higher value of this parameter signifies an efficient wing design relative to its weight, a crucial consideration for implementing flat-plates as lift-generating devices for *MAV*s with specific weight and size constraints.

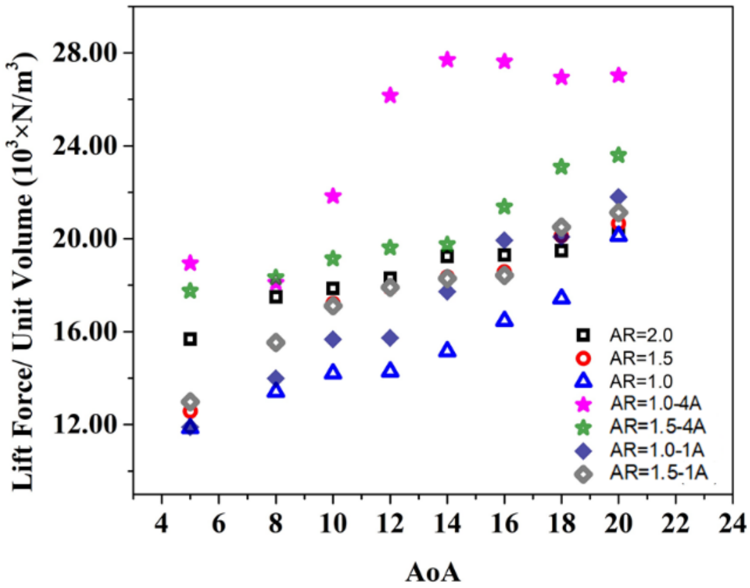

(a)

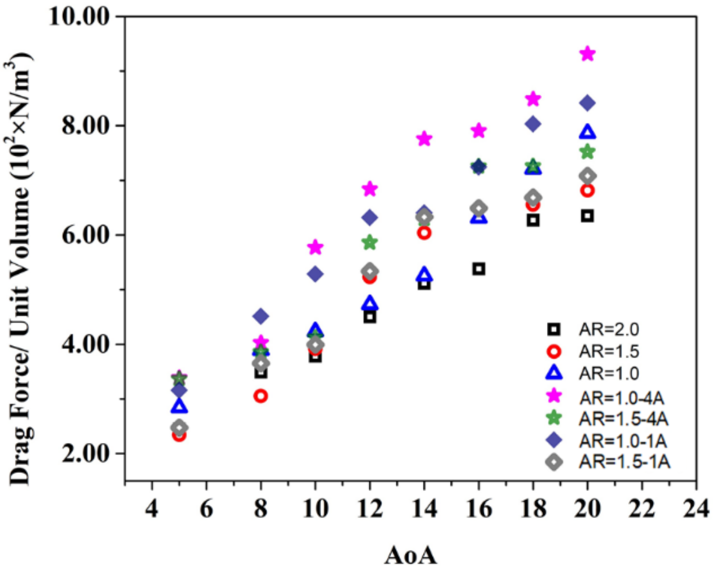

(b)

Figure 6.8: Variation of (a) lift and (b) drag forces per unit volume with *AoA* for the different *AR*, plain and modified wings at *Re* = 15×10^4

In Figure 6.8(a), it is evident that the *AR* = 1.0-4A configuration exhibits the best value among all configurations, closely followed by *AR* = 1.5-4A. These configurations achieve weight reductions of 40% and 20%, respectively, compared to the larger unmodified *AR* = 2.0 wing, while simultaneously offering average improvements of 30% and 10% over it. In comparison to their respective base plates, the *AR* = 1.0-4A shows a substantial average improvement of 58%, while the *AR* = 1.5-4A achieves an average increment of 17%. This suggests that the 4A combination for both ARs outperforms their individual base plates as well as the longer-spanned *AR* = 2.0 flat-plate. Consequently, it can be inferred that the lift force generated in these configurations surpasses the weight gained due to the addition of wing-tip attachments.

The 1A arrangement demonstrates an average improvement of 10% and 3.4% for the *AR* = 1.0 and 1.5, respectively, over their individual base plates. Notably, the *AR* = 1.5-1A configuration exhibits inferior values compared to its base plate at *AoA*s of 10^o, 12^o, 14^o, and 16^o. Likewise, when compared to the *AR*=2.0 flat-plate, this configuration for both *AR*s achieves superior values only at higher *AoA*s of 18^o and 20^o.

A significant increase in the drag force per unit volume is evident in the 4A configurations, as illustrated in Figure 6.8 (b). In comparison to the *AR* = 2.0 flat-plate, this configuration for the *AR* = 1.0 and 1.5 modified plates exhibits a 42% and 22% higher value, respectively. Conversely, the 1A configuration of the *AR* = 1.0 and 1.5 plates has 32% and 11% higher drag force per unit volume over the *AR* = 2.0 flat-plate. When considered individually against their original base plates, the drag force parameter of the *AR* = 1.0's 4A and 1A arrangements is higher by 26% and 17%, respectively. Similarly, for the *AR*=1.5, the figures for the modified configurations, namely *AR* = 1.5-4A and *AR* = 1.5-1A, are 15% and 12%, respectively. Nonetheless, it is observed that for *AR* = 1.5, the modified configurations have a lower value compared to its base plate at *AoA*s of 8^o, 10^o, and 20^o. These observations are summarized in Table 6.2, indicating that the 1A configuration for both *AR*s exhibits a slightly reduced lift force per unit volume value when compared with a stock *AR* = 2.0 flat-plate.

In a comparative analysis between the modified plates, the *AR* = 1.0 plate outperforms the *AR* = 1.5 in the case of the 4A configuration by an average value of 22% for the lift force per unit volume parameter. Meanwhile, the same configuration of the *AR* = 1.0 plate also exhibits a higher drag force per unit volume by an average value of 16%. For the 1A arrangement, the *AR*=1.5 modified plate holds an advantage over the *AR* = 1.0 modified plate, although a clear pattern is not discerned concerning the lift force.

Acceptable performance, even if slightly inferior, is justifiable if accompanied by a substantial weight reduction. The *AR* = 1.0-4A and 1.5-4A configurations occupy 60% and 80% of the volume compared to a plain *AR* = 2.0 flat-plate, respectively, yet these configurations are capable of generating a greater amount of lift force. It can also be inferred that the wing's performance is contingent on the number of attached devices. For a specific *AR*, the general performance trend, based on the number of attachments, is 4A>3A>2A>1A.

Table 6.2: Force/volume observations

Aspect Ratio	Parameter	Configuration	Improvement w.r.t.	
			AR=2.0	**Base Plate**
AR=1.0	Lift Force/Unit Volume	4A	30%	58%
		1A	-2.3%	10%
	Drag Force/Unit Volume	4A	42%	26%
		1A	32%	17%
AR=1.5	Lift Force/Unit Volume	4A	10%	17%
		1A	-3.6%	3.4%
	Drag Force/Unit Volume	4A	22%	15%
		1A	11%	12%

6.6 Summary of the Chapter

In the experimental study of modified flat-plate wings with wingtip devices, various configurations were analyzed for their aerodynamic performance. The study focused on assessing the impact of wingtip modifications on lift and drag characteristics. Wind tunnel experiments were conducted, and the results revealed that the 4A configuration, featuring four bionic attachments, outperformed other arrangements. The *AR* = 1.0-4A and *AR* = 1.5-4A configurations demonstrated weight savings of 40% and 20%, respectively, compared to an unmodified *AR* = 2.0 flat-plate, while exhibiting superior lift generation. The *L/D* ratio was a key parameter, showcasing the effectiveness of the modifications. Despite some variations in drag force per unit volume, the overall trend suggested that the addition of wingtip devices led to improved lift with acceptable trade-offs in weight and drag, emphasizing the significance of such modifications for *MAV* applications.

Chapter 7: Experimental Results for Non-planar Devices

Chapter Outline

Overview:

The experimental study with non-planar wingtip devices focused on investigating their impact on the aerodynamic performance of flat plate wings. These devices were strategically added to the wingtips in a dihedral arrangement. The study aimed to understand how these modifications affect lift and drag characteristics compared to unmodified flat plates. Wind tunnel experiments were conducted to measure aerodynamic coefficients such as lift and drag, along with the lift-to-drag ratio. Results indicated that the non-planar wingtip devices led to improvements in lift generation while maintaining acceptable levels of drag. The study provided valuable insights into the effectiveness of these modifications for enhancing the aerodynamic performance of flat plate wings.

7.1 Prologue

Following the integration of non-planar wingtip devices onto the flat-plate, wind tunnel experiments are conducted to evaluate their efficacy. These modifications are engineered to as described in Section 3.3.4. The A1, A2, B1 and B2 configurations are setup as per the dihedral arrangement of Smith et al. (Smith et al., 2001). In continuation of the planar attachment study, four distinct winglet configurations, A1, A2, B1 and B2 were examined to explore the aerodynamic effects of non-planar modifications. The objective of these attachments is to enhance the *AR* without introducing additional weight to the wing structure. Experimental trials are conducted in the wind tunnel under predefined operating conditions outlined in Section 3.3.6. The *L/D* is chosen as a superior parameter due to its comprehensive representation of both aerodynamic force characteristics. The *L/D* ratios of the modified wings are computed and compared across all four configurations, serving as the cornerstone for detailed discussions in subsequent sections.

7.2 Aerodynamic Coefficients

The lift and drag forces are quantified through experiments conducted within a subsonic wind tunnel, enabling the computation of force coefficients. Employing the classical method to examine the variation in C_L and C_D with respect to the *AoA* offers an effective means of comparing different wings. These trends elucidate the regions characterized by high lift production and drag generation. However, while the *L/D* ratio serves as a superior performance parameter, it overlooks the weight of the wing itself. To address this, the lift and drag forces per unit volume are calculated, facilitating the comparison of wing performance across different *AR*s while accounting for mass. Prior studies on planar winglets have highlighted the utility of this modified parameter, providing a standardized reference for comparing wings of varying span lengths.

Figure 7.1 and Figure 7.2 illustrate the variation of C_L and C_D with the *AoA* at different *Re*, respectively, comparing modified flat-plates with dihedral wingtips to base flat-plates of *AR* 1.0, 1.5, and 2.0. These plots compare the performance of modified flat plates with dihedral wingtips against base flat plates with *AR*s of 1.0, 1.5, and 2.0. The general observation is that the modified wings exhibit better C_L values compared to the base flat plates.

For the *Re* under consideration, the configuration A2 demonstrates the highest C_L values, followed closely by the configuration A1. This indicates that the modifications under the configuration A result in higher lift forces compared to the configuration B. Apart from the results at *Re* = 15×10^4 (Figure 7.1 d), for other *Re*, the configuration B2 shows higher C_L values than the B1 at lower *AoA*s. However, at *AoA*s greater than 12° or 14°, this difference diminishes, and in certain cases (Figure 7.1 c), the B1 configuration surpasses the B2 in C_L values. Despite these variations, all modified wings consistently display higher C_L values compared to their base counterparts, indicating that the dihedral wingtip modifications significantly enhance lift performance. This enhanced performance is especially evident at lower *AoA*s, where the modifications seem to provide the most benefit.

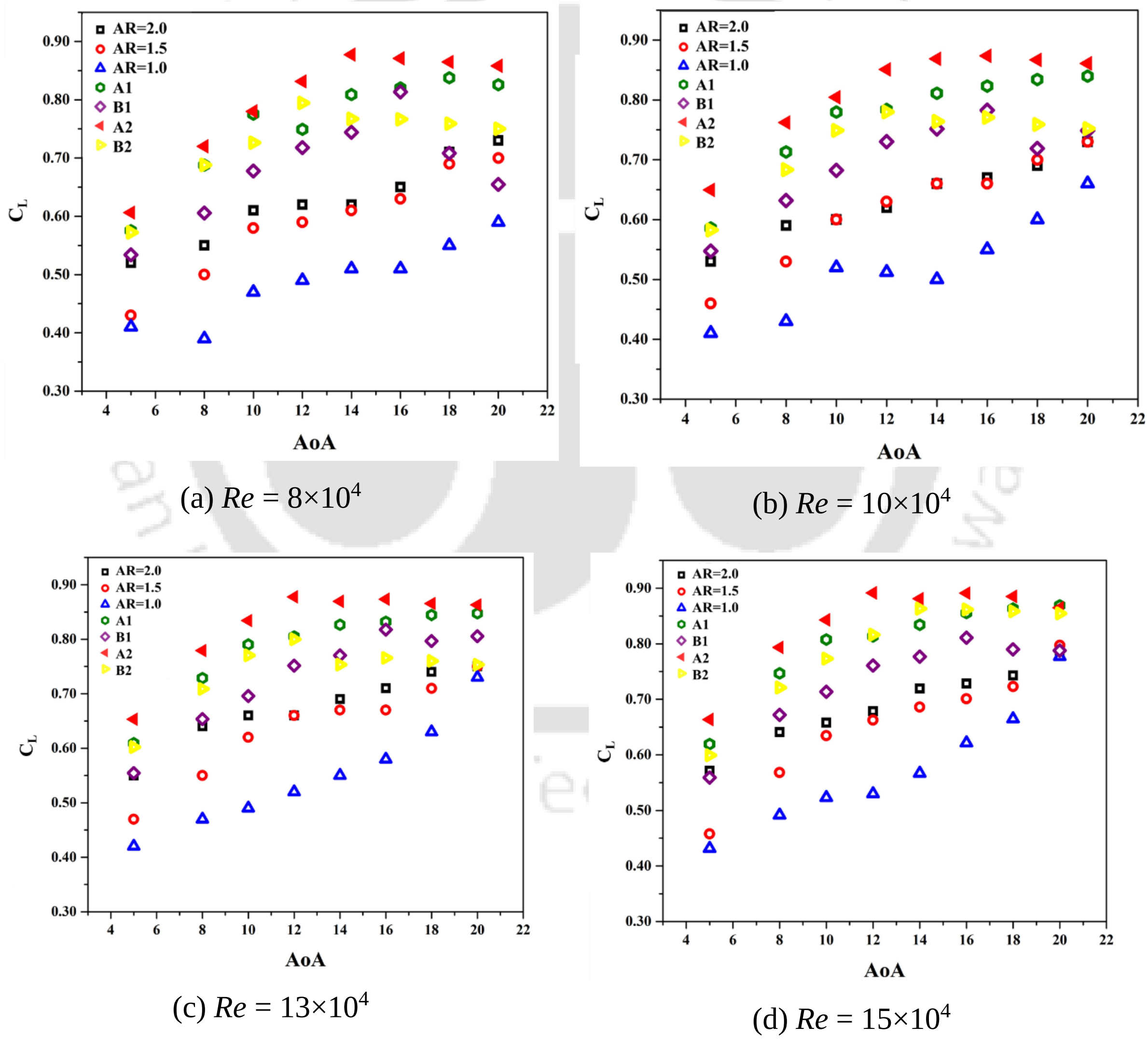

(a) *Re* = 8×10^4

(b) *Re* = 10×10^4

(c) *Re* = 13×10^4

(d) *Re* = 15×10^4

Figure 7.1: Variation of C_L at Different *Re* for modified flat-plate wings with non-planar devices

When comparing the C_{Lmax} values, it is observed that the A2 configuration shows an improvement of 16.8%, 16.4%, 14.5%, and 11.6% over the AR = 2.0 wing at Re of 8×10^4, 10×10^4, 13×10^4, and 15×10^4, respectively. At the lower Re, the improvement achieved is similar as is also evident from Figure 7.1(a) and (b).

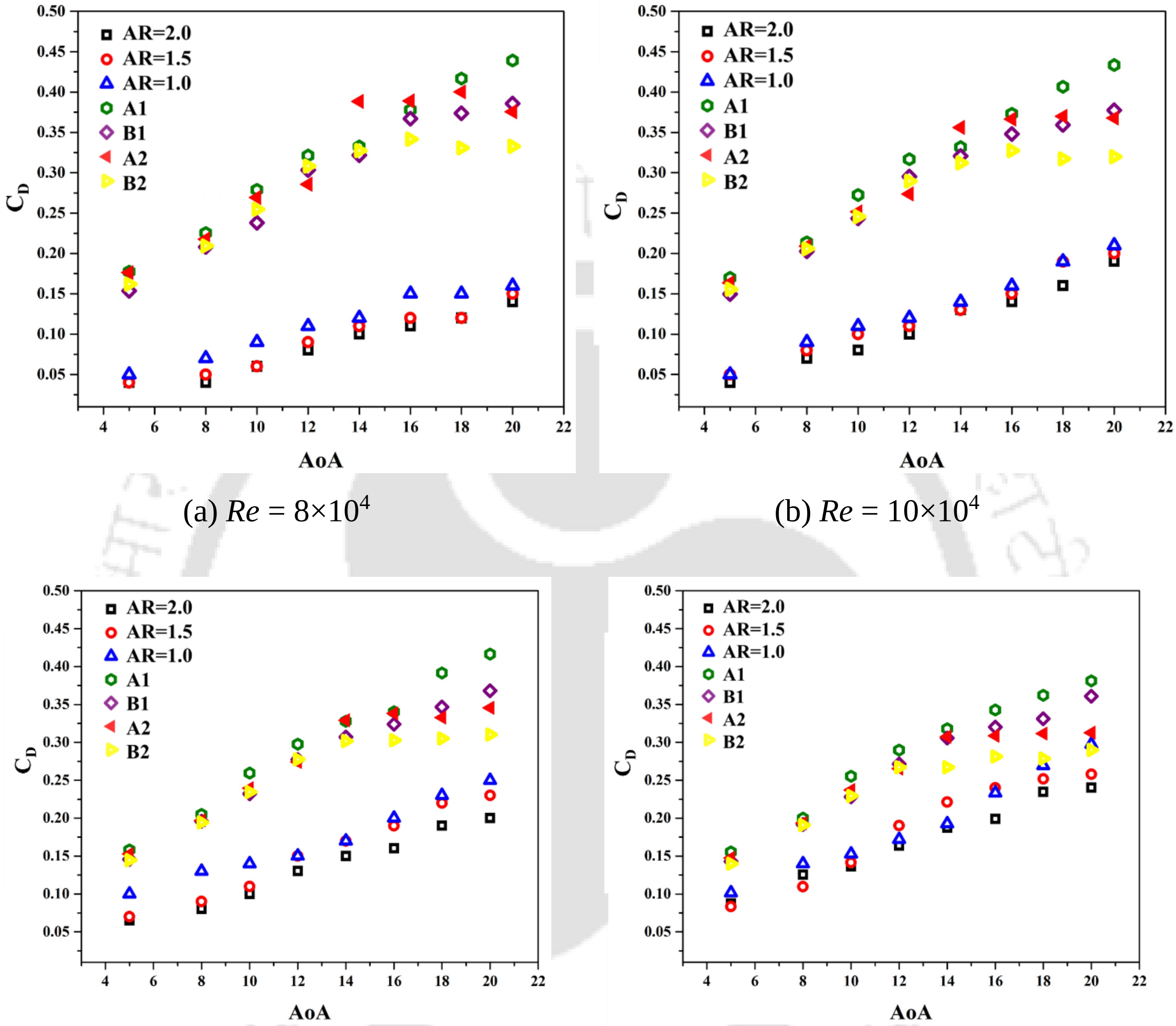

(a) $Re = 8 \times 10^4$ (b) $Re = 10 \times 10^4$

(c) $Re = 13 \times 10^4$ (d) $Re = 15 \times 10^4$

Figure 7.2: Variation of C_D at Different Re for modified flat-plate wings with non-planar devices

The improvement percentages for other modified wings compared to the baseline AR = 2.0 wing at different Re values are summarized in Table 7.1. It can be observed that generally, with an increase in Re, the improvement figures show a downward trend. Another key observation from Figure 7.1 is that the difference in C_L between the modified and baseline wings decreases with increasing AoA and this behaviour is more prominent at the higher Re (Figures 7.1(c) and (d)). This is due to the baseline wings showing an upward trajectory in the C_L vs AoA plot, whereas the modified wings behave like conventional wings by reaching stall at around *AoA* = 12°−16°.

When compared with their baseline wings, the configurations A2 and B2 exhibit a maximum C_{Lmax} improvement of 20.2% and 11.9%, respectively, at *Re* = 8×10^4 (Figure 7.1(a)). Similarly, the configurations A1and B1 show improvements of 29.7% and 27.4%, respectively, over their base plate at *Re* = 8×10^4. These results indicate that the modifications on the *AR* = 1.0 wing yield better performance enhancements compared to those on the *AR* = 1.5 wing.

Table 7.1: C_{Lmax} Improvement of modified wings over *AR* = 2.0

Modified Wing	**Re**	**C_{Lmax} Improvement over (%) *AR*=2.0**	**Average C_{Lmax} Improvement**
A1	8×10^4	12.8	11.7
	10×10^4	13.1	
	13×10^4	11.5	
	15×10^4	9.3	
A2	8×10^4	16.8	14.8
	10×10^4	16.4	
	13×10^4	14.5	
	15×10^4	11.6	
B1	8×10^4	10.2	7.0
	10×10^4	6.7	
	13×10^4	8.2	
	15×10^4	2.8	
B2	8×10^4	8.1	7.3
	10×10^4	6.3	
	13×10^4	6.2	
	15×10^4	8.7	

Upon modification, the C_D of the wings has also increased considerably, as shown in Figure 7.2. Among the modified wings, the A1 configuration is observed to have the highest C_D values. The general trend indicates that with increasing *Re*, the C_D values decrease, as evident at the higher *Re* (Figure 7.2(c) and (d)). Similar to the behavior in C_L, the configuration A exhibits higher C_D values than the configuration B. This is due to the induced drag component, which is directly related to the square of the lift generated. The individual attachments act to increase the drag force experienced by the overall wing by behaving as separate airfoils.

For the modified wings, the configuration A2 shows an average increment of 44.7% and 39.8% in C_{Dmax} over the AR = 2.0 and AR = 1.5 wings, respectively. Similarly, the B2 wing has average increments of 38.1% and 32.6%. The A1 wing exhibits an average C_{Dmax} value that is 53.3% and 44.2% higher than the AR = 2.0 and AR = 1.0 wings, respectively. For the B1 wing, these values are 48.1% and 38.1%, respectively. The configuration A generates higher drag because the staggered vorticity created by the individual wingtips increases the induced drag. The modifications lead to an overall increase in drag, but this is expected due to the enhanced lift characteristics, as the drag is partially a function of the increased lift generated by the wingtip modifications. One particular observation is that at the lower Re (Figure 7.2(a) and (b)), the difference in C_D values between the modified and baseline wings is considerably greater than at the higher Re (Figure 7.2(c) and (d)).

7.3 Oswald's Efficiency Factor

The e serves as a crucial indicator for assessing the drag experienced by a body. In Figure 7.3, the e values for wings equipped with dihedral attachments are presented, alongside those for unmodified wings and wings with planar wingtip devices. While it's noted that the e values for wings with dihedral arrangements are not as high as those for wings with planar attachments, they still surpass the values for the unmodified base wing. The e is compared with the test models, both modified (wings with dihedral wingtips) and unmodified (base wings), along with two specific models (AR = 1.0-4A and AR = 1.5-4A) from the study of Borah et al. (2024). Here, AR = 1.0-4A signifies an AR = 1.0 wing with four planar wingtip attachments; and similar is the case with AR = 1.5-4A where there are four planar wingtip attachments to a wing of AR = 1.5. It is observed that while the e values for wings with dihedral arrangements are generally lower than those with planar attachments, they still surpass the values for the baseline wing configurations (Borah et al., 2024). Notably, among the dihedral modified wings, the AR = 1.0 configuration consistently demonstrates superior e values compared to the AR = 1.5 wing. For the AR = 1.0 wing, the e ranges between 0.48 and 0.72 across both the configurations, whereas for the AR = 1.5 wing, it ranges between 0.29 and 0.43. These values represent an improvement over their respective base wings and the *AR* = 2.0 base wing. Importantly, the incorporation of dihedral wingtip attachments leads to an enhancement in *e*, with *AR* = 1.0 wing showing a more significant improvement compared to *AR* = 1.5 wing.

These findings underscore the sensitivity of *e* to wing modifications and highlight the influence of experimental setups and model differences on the results obtained. The variations of *e* underscore the nuanced effects of different wing configurations on aerodynamic efficiency. While the wing of *AR* = 1.0 consistently demonstrates higher *e* values across both dihedral and planar configurations, the wing of *AR* = 1.5 exhibits lower but still improved *e* values compared to its base configuration. This suggests that the effectiveness of wing modifications in enhancing the aerodynamic efficiency may depend on factors such as *AR* and attachment design. Additionally, the observed improvements in *e* highlight the potential of dihedral wingtip attachments to mitigate the induced drag and optimize the overall aerodynamic performance. These insights contribute to a deeper understanding of how a subtle change in design can influence the aerodynamic characteristics and underscore the importance of tailored modifications for specific application requirements.

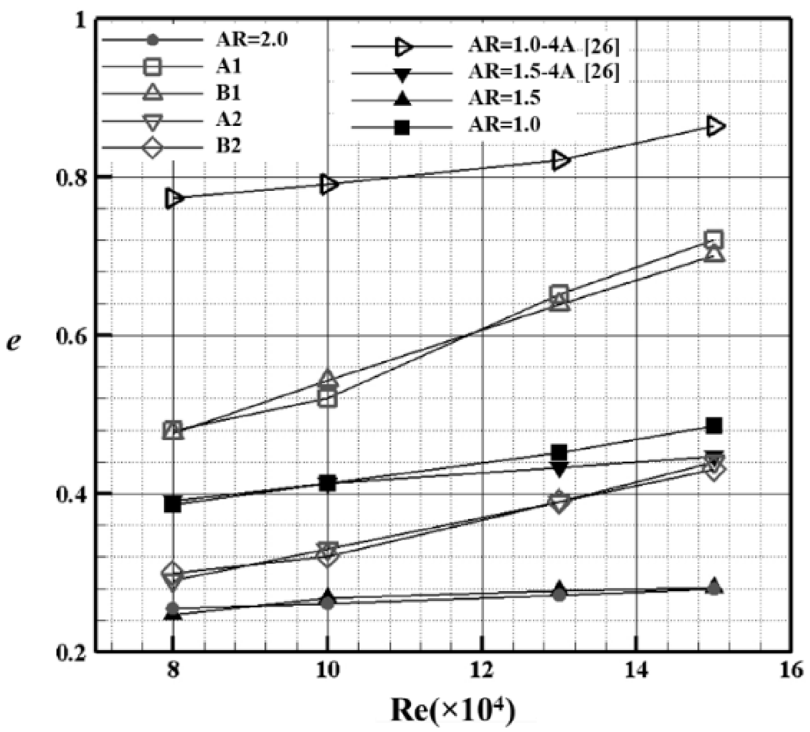

Figure 7.3: Variation of *e* with *Re*

7.4 Lift and Drag Force per Unit volume

While the analysis of C_L and C_D provides valuable insights into the performance of conventional airfoil-sectioned wings, these parameters overlook the weight of the wing itself, which is crucial for *MAV* applications. In this study, modifications are applied to flat-plate wings to assess their suitability for low *Re MAV* operations. To account for the wing's weight, a relationship between the forces experienced and the weight is established by relating force parameters to volume. Figure 7.4 illustrates the variation of lift force per unit volume with *AoA* for the different flat-plate wings under investigation. Similarly, Figure 7.5 showcases the variation of drag force per unit volume with *AoA*. These results shed light on the effectiveness of the wings relative to their weight, considering the specific weight and size constraints of *MAV*s.

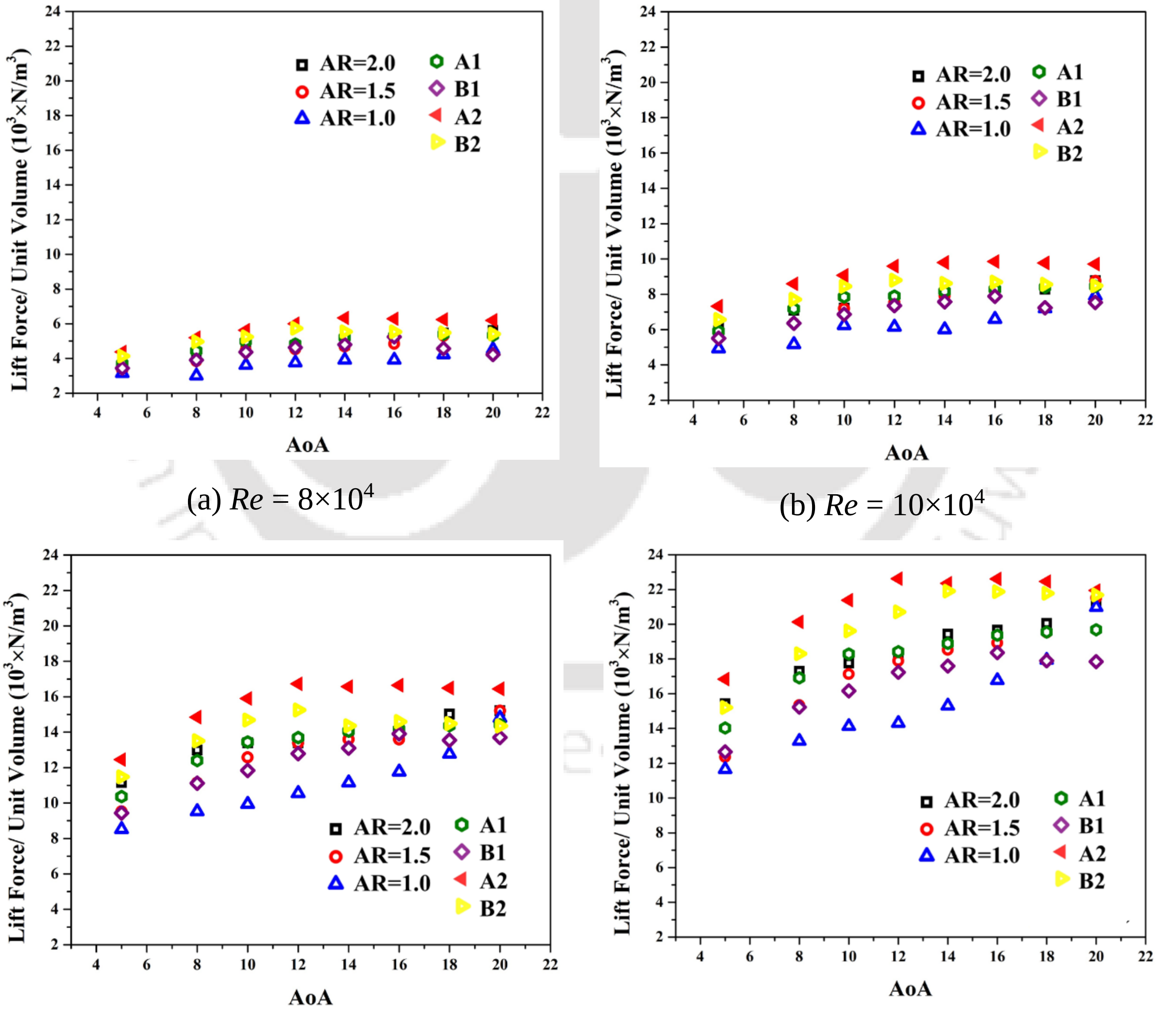

(a) *Re* = 8×10^4

(b) *Re* = 10×10^4

(c) *Re* = 13×10^4

(d) *Re* = 15×10^4

Figure 7.4: Variation of lift force per unit volume with *AoA*

From Figure 7.4, it is evident that the B1 configuration consistently exhibits superior lift values across all *Re* compared to rest of the wings. Following closely behind is the configuration B of the same *AR* = 1.5 modified wing. Similarly, for the *AR* = 1.0 wing, the configuration A demonstrates better values compared to the configuration B. Throughout the range of *AoA*s studied, the lift force per unit volume values appear to plateau around an *AoA* of 12° for all *Re* considered. However, it is worth noting that the improvements observed with the non-planar attachments are relatively smaller compared to the enhancements achieved with flat-plate wings equipped with planar attachments (Borah et al., 2024). This suggests that while the non-planar designs provide a benefit, the incremental gains are less pronounced than those obtained with the planar configurations.

The improvement achieved by the A2 configuration over the unmodified *AR* = 2.0 wing varies from a maximum average of 21% at *Re* = 15×10^4 (Figure 7.4(d)) to a minimum average of 5% at *Re* = 8×10^4 (Figure 7.4(a)). At *Re* = 13×10^4 (Figure 7.4(c)) and 10×10^4 (Figure 7.4(b)), this configuration shows average improvement figures of 16% and 7%, respectively. Following closely is the B configuration of the *AR* = 1.5 modified wing, which demonstrates average improvements of 18%, 13%, 6%, and 3.5% at *Re* = 15×10^4, 13×10^4, 10×10^4, and 8×10^4, respectively. These data are also shown in Table 7.2. Meanwhile, the A1 configuration consistently outperforms the base *AR* = 1.0 wing across all the *Re* investigated, occasionally showing the superior performance compared to the *AR* = 2.0 wing at certain *AoA*s. Conversely, the B1 configuration consistently falls short of the *AR* = 2.0 wing's performance and only exhibits an improved performance compared to the base *AR* = 1.0 wing.

Table 7.2:Average lift force per unit volume improvement

Re	**Average lift force/ unit volume improvement over *AR* = 2.0**	
	Configuration A2 (%)	**Configuration B2 (%)**
15×10^4	21	18
13×10^4	16	13
10×10^4	7	6
8×10^4	5	3.5

These findings underscore the effectiveness of the A2 configuration in enhancing the lift performance across the tested *Re*, with significant improvements observed especially at higher

Re values. The A1 configuration also shows promise, outperforming its counterparts in most scenarios. However, the B1 configuration, while showing some improvement over the base *AR* = 1.0 wing, does not consistently match the performance levels of the *AR* = 2.0 wing.

The results indicate that while non-planar attachments contribute to lift augmentation, their effectiveness may be somewhat constrained compared to planar attachments. Nevertheless, they still offer improvements in lift characteristics, especially in specific configurations such as A2 at the higher *Re* (Figure 7.4(c) and (d)). In summary, the B1 configuration consistently demonstrates notable improvements over the unmodified *AR* = 2.0 wing. The A1 configuration also shows promising performance, particularly when compared to its base wing. However, the B1 configuration generally underperforms, showing limited improvement over its base wing and inferior performance compared to the *AR* = 2.0 wing.

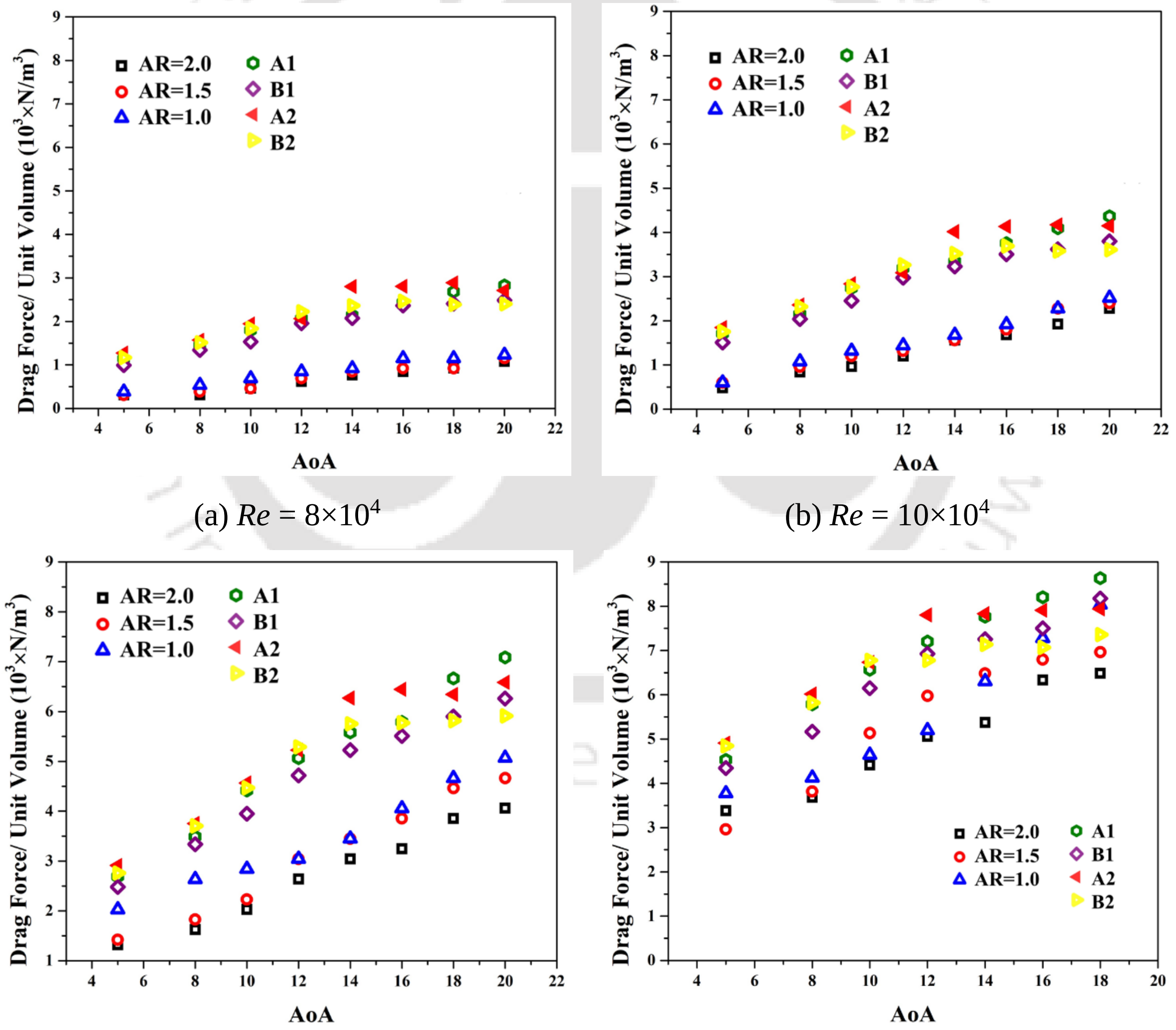

(a) *Re* = 8×10^4 (b) *Re* = 10×10^4

(c) *Re* = 13×10^4 (d) *Re* = 15×10^4

Figure 7.5: Variation of drag force per unit volume with *AoA*

Figure 7.5 illustrates that beyond an *AoA* of 12°, both the modified *AR* = 1.0 and 1.5 wings in the configuration A experience higher drag force per unit volume. This trend persists across all *Re* under investigation. In contrast to lift force, the drag force per unit volume consistently exceeds that of the unmodified wings for both configurations and all *Re*. Specifically, the B2 wing exhibits an average drag force higher by 6%, 7%, 11%, and 9% compared to the *AR* = 2.0 wing at *Re* of 8×10^4, 10×10^4, 13×10^4, and 15×10^4, respectively. Additionally, all modified wings show similar values, particularly at *Re* of 8×10^4 and 10×10^4. Contrary to the lift force per unit volume, at the lower *Re* (Figure 7.5(a) and (b)), the drag force per unit volume for the modified wings are higher than the unmodified baseline wings.

Consequently, while lift force per unit volume improves with the modified configurations, there is a significant increase in drag forces. This will result in less favourable *L/D* ratios for the modified wings compared to the unmodified ones. This trade-off between the increased lift and the higher drag underscores the complexity of optimizing wing designs for the *MAV*s, where achieving a balance between lift enhancement and drag minimization is crucial for overall performance. The consistent trend of higher drag forces indicates that the modifications, especially in the configuration A, introduce additional aerodynamic resistance. This increase in drag, alongside the improvement in lift force, highlights the critical need to balance aerodynamic performance metrics for achieving optimal design outcomes in *MAV*s.

7.5 Summary of the Chapter

In conclusion, the study demonstrates that non-planar dihedral wingtip attachments can effectively enhance the aerodynamic performance of *MAV* flat-plate wings, particularly in terms of lift generation. The A2 configuration consistently showed the highest C_L and lift force per unit volume, especially at lower *Re*, suggesting its suitability for low-speed applications meant for *MAV*s. However, these modifications also resulted in increased drag forces, highlighting the need for a careful balance between lift augmentation and drag minimization. The analysis of *e* further revealed that while dihedral configurations do not outperform planar attachments, they still provide significant improvements over unmodified wings, with the *AR* = 1.0 configuration demonstrating the highest efficiency gains. These findings underscore the importance of *AR* and precise attachment design in optimizing aerodynamic efficiency.

Chapter 8: Conclusions and Future Scope

Chapter Outline

Overview:

In this chapter, the culmination of the research journey is presented, encapsulating the core findings and their broader implications. Through a succinct summary of the experimental results, including notable trends and observations, the chapter offers insights into the effectiveness and limitations of the studied flat-plate wings with non-planar wingtip devices. Consideration is given to the practical relevance of the research outcomes, with discussions on potential applications and implications for engineering design. Additionally, the chapter acknowledges any limitations encountered during the study and suggests avenues for future research to address unresolved questions or further explore the identified phenomena. A reflective synthesis, reaffirming the significance of the research and its contribution to advancing scientific knowledge and informing practical endeavours in the field is presented.

8.1 Key Highlight of the Research Work

The present study investigates the utilization of flat-plate wings as lift-generating components, particularly targeting low *Re* applications like fixed-wing *MAV*s. The selection of flat-plate wings stems from their simplicity in geometry, making them a straightforward and cost-effective alternative to airfoil wings. This research endeavours to explore the feasibility and effectiveness of flat-plate wings in fulfilling the lift generation requirements for *MAV*s operating under low *Re* conditions. By focusing on flat-plate wings, the study aims to uncover their potential advantages and limitations in *MAV* design. Through comprehensive experimental and computational analysis, including wind tunnel tests, 2D simulations and performance evaluations, the research strives to provide valuable insights into optimizing flat-plate configurations for enhanced aerodynamic performance in low *Re* environments. Ultimately, the findings aim to contribute to the ongoing advancements in *MAV* technology by offering novel approaches to wing design and optimization.

Initially, a 2D computational analysis is conducted to investigate the flow characteristics surrounding a flat-plate wing. Using the Ansys FLUENT application and employing the Spalart-Allmaras turbulence model, simulations are performed to examine various aspects such as the *L/D* ratio, wake flow variations, and vortex formation. These simulations offer valuable insights into the flow dynamics associated with flat-plate wings, providing a foundational understanding of their potential as lift-generating devices.

Having gained a fundamental understanding of the flow dynamics around a flat-plate, wind tunnel experiments are conducted to validate the computational findings and evaluate the aerodynamic performance of flat-plate wings in real-world conditions. Through a series of modifications by implementing planar and non-planar wingtip attachments on *AR* = 1.0 and 1.5 flat-plate wings, a number of experiments are conducted to access the effectiveness of these modifications in enhancing lift generation and reducing drag. These experiments provide empirical data to complement the computational analysis, offering a comprehensive understanding of the aerodynamic behavior of flat-plate wings and their potential applications in low *Re* environments. The research explores the impact of various configurations of these wingtip devices on aerodynamic performance, shedding light on their efficacy in improving *L/D* ratios. The experimental results are analyzed to identify trends and patterns, providing insights into the most effective designs for enhancing lift while minimizing drag. Moreover, the study investigates the trade-offs between lift augmentation and increased drag associated with the use of wingtip devices, offering valuable guidance for optimizing wing designs for MAVs and similar applications.

8.2 Contribution of Present Work

The principal discoveries of this investigation are outlined in the following sections.

8.2.1 2D Unsteady Computational Simulations

Dynamic 2D simulations were conducted to explore the incompressible airflow patterns surrounding flat-plates featuring thickness ratios of 1% and 3% at *Re* of 4.8×10^4 and 7.6×10^4. The results unveil the varying *L/D* ratios with changes in *AoA*, the evolution of the *St* with *AoA*, and visual representations of vorticity magnitude across the flow field. The main points are outlined as follows:

- The thinner plate exhibited a higher *L/D* ratio compared to the thicker plate, aligning with observations made by earlier studies. The thicker plate exhibits more noticeable flow separation, resulting in higher pressure drag.
- The heightened flow separation affects the lift force by diminishing the pressure differential between the suction and pressure sides.
- With respect to *St*, it is observed to decrease with increasing *AoA*, for the studied flat-plates.
- For the 3% thick plate, vortex shedding frequencies occur at *AoA* of 9° and 10° for *Re* of 4.8×10^4 and 7.6×10^4, respectively.
- Conversely, for the 1% thick plate, corresponding frequencies are detected at *AoA* of 12° and 13°.
- The lift and drag showed synchronous fluctuations with the shedding frequency. This synchronization suggests that the peak values of lift and drag align, occurring concurrently during the shedding cycle. This coherence between the oscillations of lift and drag implies a tight coupling between the aerodynamic forces and the shedding frequency.

- The shedding frequencies and wake characteristics exhibit sensitivity to thickness, offering valuable quantitative insights into the aerodynamic performance of flat plates.

8.2.2 Flat-plate Wings with Inverted Dimples

The first experimental study involved placing arrays of inverted dimples strategically along the suction side of the flat-plate wing to examine their influence on aerodynamic performance. The dimples were positioned to induce early transition to turbulence, with the goal of enhancing lift and reducing drag by promoting better boundary layer control.

- The 0.75c dimple configuration showed the highest C_L and lowest C_D values among all configurations, particularly effective at higher *AoA* and *Re* (13×10^4 and 15×10^4).
- The 0.50c configuration also improved aerodynamic performance, though to a lesser extent than the 0.75c configuration.
- The 0.25c dimple placement performed poorly, showing lower lift and higher drag, likely due to premature flow separation.
- Dual-row dimple configurations (e.g., 0.50c, 0.75c) improved performance but did not surpass the single-row 0.75c configuration.
- Oswald's efficiency factor (*e*) indicated that the 0.75c and 0.50c configurations effectively reduced induced drag at higher *Re*, while the 0.25c placement had inferior efficiency.
- Overall, the results emphasize that optimal dimple placement, especially at the 0.75c location, enhances aerodynamic efficiency by reducing drag and improving lift.

8.2.3 Flat-plate Wings with Planar Attachments

Wind tunnel experiments were conducted on flat-plate wings modified with planar wingtip devices, drawing inspiration from avian aerodynamics. These experiments aimed to replicate real-world scenarios to enhance understanding.

- At $Re = 15\times10^4$, the *AR* = 1.0-4A configuration achieves a C_{Lmax} of 0.93 at *AoA* = 16°, outperforming the base plate's C_{Lmax} of 0.77 at *AoA* = 20°. This represents a notable 19% improvement in C_{Lmax}.

- In the case of the model with *AR* = 1.5-4A, the C_{Lmax} reaches 0.79 at *AoA* = 20°, demonstrating a similarity to its base configuration and *AR* = 2.0 plate at *Re* = 15×10^4.
- It's essential to acknowledge that while the C_L is relatively higher for the modified wings, the C_D is also elevated. This phenomenon can be attributed to the impact of the induced drag component of the total drag, which is directly influenced by the lift generated.
- Hence, it is observed that at *Re* = 15×10^4, the C_{Dmax} for *AR* = 1.0-4A is 6.9% and 29% higher than the C_{Dmax} of *AR* = 1.0 and *AR* = 2.0 plates, respectively.
- The experimental data reveals that *e* increases as *Re* rises and *AR* decreases, consistent with well-established findings in previous studies.
- At *Re* = 15×10^4, the *AR* 1.0-4A stands out with the highest *e* values, ranging from 0.77 to 0.86, in stark contrast to the simpler *AR* = 1.0 base flat-plate, which exhibits a narrower range of 0.38-0.48. The unmodified *AR* = 1.5 and *AR* = 2.0 flat-plates present lower ranges of 0.24–0.28 and 0.25–0.28, respectively.
- The inclusion of wingtip attachments is observed to enhance e, with the *AR* = 1.0 wing showing a more significant improvement compared to the *AR* = 1.5 wing.
- At *Re* = 15×10^4, the 4A, 3A, and 2A configurations of the modified *AR* = 1.0 wing exhibit L/D_{max} values that are 29%, 13%, and 2.6% higher than the base *AR* = 1.0 flat-plate, respectively. The *AR* = 1.0-4A plate consistently demonstrates improved *L/D* compared to the base plate across all *AoA*s and *Re*. It achieved average enhancements of 21%, 14%, and 15%, at *Re* = 13×10^4, 10×10^4, and 8×10^4, respectively.
- Similarly, at *Re* = 15×10^4, an average improvement of around 7% is observed from the 4A configuration of the modified *AR* = 1.5 wing compared to the base *AR* = 1.5 plate, with a maximum improvement of 20% at *AoA* = 14°. The 3A and 2A arrangements offer an average improvement of 2.9% and 1% over the base plate at *Re* = 15×10^4.
- Concerning the *L/D* parameter, the 4A arrangement exhibits the most significant improvement over the other three configurations for both *AR*s. Specifically, the *AR* = 1.0-4A and *AR* = 1.5-4A configurations achieve superior *L/D* values compared to their respective base plates across the entire *AoA* and *Re* range under study, occasionally outperforming flat-plates of higher *AR*s also.

- With respect to the parameter, lift force per unit volume, the *AR* = 1.0-4A configuration exhibits the best value among all configurations, closely followed by *AR* = 1.5-4A. These configurations achieve weight reductions of 40% and 20%, respectively, compared to the larger unmodified *AR* = 2.0 wing, while simultaneously offering average improvements of 30% and 10% over it.
- Regarding the drag force per unit volume parameter, compared to the *AR* = 2.0 flat-plate, this configuration for the *AR* = 1.0 and 1.5 modified plates demonstrates a 42% and 22% higher value, respectively.
- .It can also be inferred that the wing's performance is contingent on the number of attached devices. For a specific *AR*, the general performance trend, based on the number of attachments, is 4A>3A>2A>1A

8.2.4 Flat-plate Wings with Non-planar Attachments

After examining the planar attachments, non-planar dihedral wingtip devices are affixed to the flat-plate wings for further investigation. The key results from this study is summarised below.

- It is evident that for the *AR* = 1.5 wing, the A2 configuration exhibits improvements in C_{Lmax} values of 16.8%, 16.4%, 14.5%, and 11.6% over the *AR* = 2.0 wing at *Re* = 8×10^4, 10×10^4, 13×10^4, and 15×10^4, respectively.
- Comparing with their unmodified base wing of *AR* = 1.5, configurations A2 and B2 show maximum C_{Lmax} improvements of 20.2% and 11.9%, respectively, at *Re* = 8×10^4.
- For the *AR* = 1.0 modified wing, the A1 and B1 configurations bring improvements in C_{Lmax} of 29.7% and 27.4%, respectively, at *Re* = 8×10^4.
- In the modified wings, the A2 wing shows an average increment of 44.7% and 39.8% in C_{Dmax} over the *AR* = 2.0 and *AR* = 1.5 wings, respectively. Correspondingly, for the B2 wing, these figures stand at 38.1% and 32.6%.
- The C_{Dmax} value of the A1 wing is, on average, 53.3% and 44.2% higher than the *AR* = 2.0 and *AR* = 1.0 wings, respectively, while for the B1 wing, it is 48.1% and 38.1%.
- For the *AR* = 1.0 wing, *e* ranges between 0.48 and 0.72 across both configurations, whereas for the *AR* = 1.5 wing, it ranges between 0.29 and 0.43. These values represent an improvement over their respective base wings and the *AR* = 2.0 base wing.

Importantly, the incorporation of dihedral wingtip attachments leads to an enhancement in e, with the AR = 1.0 wing showing a more significant improvement compared to the AR = 1.5 wing.

- With regards to lift force per unit volume, the improvement achieved by the A2 configuration over the unmodified AR = 2.0 wing ranges from a maximum average of 21% at $Re = 15\times10^4$ to a minimum average of 5% at $Re = 8\times10^4$.
- For the drag force per unit volume, the B2 wing exhibits an average drag force higher by 6%, 7%, 11%, and 9% compared to the AR = 2.0 wing at Re of 8×10^4, 10×10^4, 13×10^4, and 15×10^4, respectively.

8.3 Application Potential

The application potential for modified flat-plate wings extends across various fields, including *UAV*s, *MAV*s, and small-scale aircraft. These wings offer improved aerodynamic performance, characterized by enhanced L/D ratios and reduced C_D, making them ideal for applications where efficiency and manoeuvrability are crucial. Their simple design and cost-effectiveness further enhance their attractiveness for industries seeking to optimize performance while minimizing costs.

Additionally, the versatility of these modified wings allows for customization to meet specific requirements, such as payload capacity, flight range, and operating conditions. Their lightweight construction and enhanced aerodynamic characteristics make them particularly suitable for missions demanding agility, endurance, and efficiency. As advancements in materials and manufacturing techniques continue, the potential applications for modified flat-plate wings are set to expand across various industries and sectors, paving the way for innovative aerial solutions.

As industries increasingly focus on sustainable aviation practices, the energy efficiency of modified flat-plate wings aligns well with the goals of reducing carbon footprints and operational costs. The growing demand for aerial logistics and delivery services further amplifies the need for high-performance, cost-effective wing designs. Overall, the future of modified flat-plate wings looks promising, with the potential to revolutionize aerial vehicle designs across multiple sectors, driving innovation and enhancing capabilities in flight technology.

8.4 Potential Manufacturing Techniques

A detailed discussion of potential manufacturing techniques for the proposed wing configurations in *MAV* applications is essential to assess their practical viability. The bird-inspired, feather-like wingtip devices and flat-plate wings require precise fabrication to ensure aerodynamic accuracy and structural integrity at small scales. Below are several viable manufacturing methods suitable for such components with the advantages and suitability/limitations mentioned accordingly:

1. **3D Printing (Additive Manufacturing):** 3D printing offers significant advantages for MAV component fabrication, especially when dealing with complex geometries like non-planar wingtips. Technologies such as Fused Deposition Modelling (*FDM*) and Stereolithography (*SLA*) can produce lightweight, high-resolution parts using polymers like *PLA*, *ABS*, or advanced composites.
    - Advantages: Rapid prototyping, customizability, minimal tooling.
    - Suitability: Ideal for low-volume production, testing various design iterations, and integrating intricate feather-like structures.
2. **Laser Cutting and Lamination:** For flat-plate wings, laser cutting of lightweight sheet materials (e.g., balsa wood, carbon fiber sheets, or foam board) offers precision and repeatability. These layers can be laminated together to form the desired wing shape.
    - Advantages: High precision, low material waste, simple setup.
    - Suitability: Best for producing flat, lightweight structures with consistent thickness.
3. **Micro Molding:** Micro-injection molding or soft lithography techniques can be used for mass production of small-scale components, particularly the non-planar tip devices if produced separately.
    - Advantages: High repeatability, fast production once molds are made.
    - Limitations: High initial cost for mold design, less flexible for design changes.

4. **CNC Machining:** *CNC* micro-machining can be employed for fabricating wing components from lightweight metal or composite materials. Although less commonly used for *MAV* wings due to weight concerns, it is useful for high-strength, load-bearing parts.
    - Advantages: High accuracy, strong material choices.
    - Limitations: Higher cost, not ideal for extremely thin or delicate parts.
5. **Composite Layup:** Traditional manual or vacuum-assisted composite layup techniques using carbon fiber or fiberglass can be used to fabricate thin, strong wings with integrated non-planar features. Molds would be required to form the feather-like geometry.
    - Advantages: Excellent strength-to-weight ratio.
    - Limitations: Labour-intensive, less suited for highly intricate tip shapes without advanced tooling.
6. **Hybrid Approaches:** Combining 3D printing for wingtip attachments with laser-cut or molded flat plates allows for modular assembly, flexibility in design, and efficient material usage. Adhesive bonding or snap-fit mechanisms can be used for integration.

Weight minimization is paramount in the case *MAVs*, hence, material selection (e.g., carbon fiber-reinforced polymers, lightweight foams) and design for manufacturability are critical. Structural integrity at low *Re* numbers must be maintained, requiring tight tolerances and smooth surface finishes, especially at the wingtips where vortex control is sensitive to geometry. Scalability and cost-effectiveness are also important for moving from prototypes to operational MAVs. In conclusion, additive manufacturing and laser cutting offer the most accessible and flexible solutions for prototyping the proposed designs, while composite layup and micro-molding become more relevant in production stages. Future work may explore which combinations yield the best trade-off between aerodynamic performance, manufacturability, and structural efficiency

8.5 Limitations of Current Work

While this study provides valuable insights into the aerodynamic performance of flat-plate wings equipped with bird-inspired wingtip attachments, several limitations should be acknowledged (Sumpter et al. 2023). First, the analysis is restricted to wind tunnel measurements at low *Re* and does not incorporate direct flow visualization or numerical simulations to elucidate the detailed flow physics, such as vortex formation, separation behaviour, or spanwise flow patterns. This limits the depth of understanding regarding the mechanisms driving observed aerodynamic improvements.

Second, the structural and dynamic aspects of the *MAV*—such as wing flexibility, aeroelastic effects, and flight control responses—were not considered. These factors could influence real-world performance and should be addressed in future studies to evaluate the full system-level behaviours of *MAVs* with such modifications.

Third, the results are scale-specific and may not directly translate across *MAVs* of different sizes without accounting for scaling effects. Parameters such as *Re*, structural weight, and material properties vary significantly with scale and may alter the aerodynamic outcomes.

Lastly, the manufacturing feasibility and durability of the proposed wingtip configurations were not experimentally validated. While design concepts show aerodynamic promise, their robustness under real flight conditions and environmental stressors remains to be tested.

Future work will aim to address these limitations by incorporating high-fidelity simulations, flow visualization techniques, structural modelling, and fabrication trials to assess both aerodynamic performance and practical applicability.

8.6 Scopes for Future Work

- **Integration of Advanced Materials**: Investigate the incorporation of advanced materials, such as composites and lightweight alloys, into modified flat-plate wings to enhance both aerodynamic performance and structural integrity. This can lead to more durable designs that withstand operational stresses while maintaining efficiency.
- **Attachment Geometries and Configurations**: Explore the effects of various attachment geometries and configurations on aerodynamic efficiency and stability. By optimizing these design elements, researchers can enhance wing performance across a range of flight conditions and improve overall vehicle handling.
- **Testing at Higher Reynolds Numbers**: Conduct experiments at higher *Re*s and in diverse environmental conditions, such as varying temperatures and humidity levels, to gain a

comprehensive understanding of how modified flat-plate wings behave under real-world scenarios. This could lead to improved design guidelines and performance predictions.

- **Active Control Systems**: Incorporate active control systems, such as morphing structures or adaptive wing surfaces, to enable real-time adjustments during flight. These systems can enhance performance by dynamically optimizing wing shape in response to changing aerodynamic conditions, thus improving efficiency and manoeuvrability.
- **Automation and AI in Design**: Leverage automation and artificial intelligence in the design and testing processes to rapidly iterate and optimize wing configurations based on performance data, leading to faster innovation cycles.

References

Ananda, G. K., Sukumar, P. P., & Selig, M. S. (2012). Low-to-moderate Aspect Ratio Wings Tested at Low Reynolds Numbers. *30th AIAA Applied Aerodynamics Conference 2012, June*, 1516–1534. https://doi.org/10.2514/6.2012-3026

Ananda, G. K., Sukumar, P. P., & Selig, M. S. (2015). Measured Aerodynamic Characteristics of Wings at Low Reynolds Numbers. *Aerospace Science and Technology*, *42*, 392–406. https://doi.org/10.1016/j.ast.2014.11.016

Badrya, C., Govindarajan, B., & Chopra, I. (2018). Basic Understanding of Unsteady Airfoil Aerodynamics at Low Reynolds Numbers (10^4 - 10^5). *2018 AIAA Aerospace Sciences Meeting*. https://doi.org/10.2514/6.2018-2061

Bardera, R., Rodríguez-sevillano, A. A., Barroso, E., & Matias, J. C. (2023). Numerical Analysis of a Biomimetic UAV with Variable Length Grids Wingtips. *Results in Engineering*, *18*(April). https://doi.org/10.1016/j.rineng.2023.101087

Barroso-Barderas, E., Rodriguez-Sevillano, A. A., Bardera-Mora, R., Crespo-Moreno, J., & Matias-Garcia, J. C. (2022). Design of Non-Conventional Flight Control Systems for Bioinspired Micro Air Vehicles. *Drones*, *6*(9), 248.

Ceron-Munoz, H. D., Cosin, R., Coimbra, R. F. F., Correa, L. G. N., & Catalano, F. M. (2013). Experimental Investigation of Wing-Tip Devices on the Reduction of Induced Drag. *Journal of Aricraft*, *50*(2), 441–449. https://doi.org/10.2514/1.C031862

Chen, J. M., & Fang, Y.-C. (1996). Strouhal Numbers of Inclined Flat Plates. *Journal of Wind Engineering and Industrial Aerodynamics*, *61*, 99–112.

Chen, P. W., Bai, C. J., & Wang, W. C. (2016). Experimental and Numerical Studies of Low Aspect Ratio Wing at Critical Reynolds Number. *European Journal of Mechanics, B/Fluids*, *59*, 161–168. https://doi.org/10.1016/j.euromechflu.2016.06.005

Cosyn, P., & Vierendeels, J. (2006). Numerical Investigation of Low-aspect-ratio Wings at Low Reynolds Numbers. *Journal of Aircraft*, *43*(3), 713–722. https://doi.org/10.2514/1.16991

Devoria, A. C., & Mohseni, K. (2017). On The Mechanism of High-incidence Lift Generation for Steadily Translating Low-aspect-ratio Wings. *Journal of Fluid Mechanics*, *813*, 110–126. https://doi.org/10.1017/jfm.2016.849

Dong, L., So, K., & Xuerui, C. (2020). Interplay of The Leading-edge Vortex and The Tip Vortex of a Low-aspect-ratio Thin Wing. *Experiments in Fluids*, *61*(9), 1–15. https://doi.org/10.1007/s00348-020-03023-4

Epple, P., Steppert, M., & Florschuetz, M. (2022). Effect of Winglets on Wing Tip Vortices. *ASME J. Fluids Eng.*, *144*(4: 040906).

Fluck, M., & Crawford, C. (2014). A Lifting Line Model to Investigate The Influence of Tip Feathers on Wing Performance. *Bioinspiration and Biomimetics*, *9*(4). https://doi.org/10.1088/1748-3182/9/4/046017

Giguère, P., & Selig, M. S. (1997). Low Reynolds Number Airfoils for Small Horizontal Axis Wind Turbines. *Wind Engineering*, *21*(6), 367–380.

Gopalarathnam, A., Broughton, B. A., McGranahan, B. D., & Selig, M. S. (2003). Design of Low Reynolds Number Airfoils with Trips. *Journal of Aircraft*, *40*(4). https://doi.org/10.2514/6.2001-2463

Grasmeyer, J. M., & Keennon, M. T. (2001). Development of The Black Widow Micro Air Vehicle. *39th Aerospace Sciences Meeting and Exhibit*. https://doi.org/10.2514/6.2001-127

Gresham, N. T., Wang, Z., & Gursul, I. (2010). Low Reynolds Number Aerodynamics of Free-to-roll Low Aspect Ratio Wings. *Experiments in Fluids*, *49*(1), 11–25. https://doi.org/10.1007/s00348-009-0726-2

Gutierrez-Castillo, P., Aguilar-Cabello, J., Alcalde-Morales, S., Parras, L., & del Pino, C. (2021). On The Lift Curve Slope for Rectangular Flat Plate Wings at Moderate Reynolds Number. *Journal of Wind Engineering and Industrial Aerodynamics*, *208*(July 2020), 104459. https://doi.org/10.1016/j.jweia.2020.104459

Helal, H. S. M., Khalil, E. E., Abdellatif, O. E., & M.Elhariry, G. (2017). Aircraft-Blended Winglet Performance Analyses. *55th AIAA Aerospace Sciences Meeting*. https://doi.org/10.2514/6.2017-1838

Hoerner, S. F. (1985). *Fluid-Dynamic Lift* (L. A. Hoerner (ed.); 2nd Editio).

Hossain, A., Rahman, A., Iqbal, A. K. M. P., Ariffin, M., & Mazian, M. (2011). Drag Analysis of an Aircraft Wing Model with and without Bird Feather like Winglet. *International Journal of Aerospace and Mechanical Engineering*, *6*(1), 8–13.

Khan, F. N., Batul, B., & Aizaz, A. (2019). A *CFD* Analysis of Wingtip Devices to Improve Lift and Drag Characteristics of Aircraft Wing. *IOP Conf. Series: Materials Science and Engineering*, *642*. https://doi.org/10.1088/1757-899X/642/1/012006

Kroo, I. (2001). Drag Due to Lift: Concepts for Prediction. *Annual Review of Fluid Mechanics*, *33*, 587–617.

Kroo, I. (2005). Nonplanar Wing Concepts for Increased Aircraft Efficiency. *Innovative Configurations and Advanced Concepts for Future Civil Aircraft*, 1–29. http://www-aa.stanford.edu/Reports/VKI_nonplanar_Kroo.pdf

La Roche, U. (1996). *Wing with a Wing Grid as The End Section* (Patent No. US5823480A).

Laitone, E. V. (1995). Aerodynamic Lift at Reynolds Numbers Below 70,000. *33rd Aerospace Sciences Meeting and Exhibit*.

Laitone, E. V. (1997). Wind Tunnel Tests of Wings at Reynolds Numbers below 70000. *Experiments in Fluids*, *23*, 405–409.

Lam, K. M., & Leung, M. Y. H. (2005a). Asymmetric vortex shedding flow past an inclined flat plate at high incidence. *European Journal of Mechanics, B/Fluids*, *24*(1), 33–48. https://doi.org/10.1016/j.euromechflu.2004.05.004

Lam, K. M., & Leung, M. Y. H. (2005b). Asymmetric Vortex Shedding Flow Past an Inclined Flat Plate at High Incidence. *European Journal of Mechanics, B/Fluids*, *24*(1), 33–48. https://doi.org/10.1016/j.euromechflu.2004.05.004

Lam, K. M., & Wei, C. T. (2010). Numerical Simulation of Vortex Shedding from an Inclined Flat Plate. *Engineering Applications of Computational Fluid Mechanics*, *4*(4), 569–579. https://doi.org/10.1080/19942060.2010.11015342

Lamar, J. E. (1974). Extension of Leading-edge-suction Analogy to Wigns with Separated Flow Around The Side Edges at Subsonic Speeds. *NASA Technical Report*, *TR R-428*(October).

Lanchester, F. W. (1907). *Aerodynamics, Constituting the First Volume of a Complete Work on Aerial Flight* (1st ed.). A. Constable & Company.

Lee, T., & Su, Y. Y. (2012). Low Reynolds Number Airfoil Aerodynamic Loads Determination via Line Integral of Velocity Obtained with Particle Image Velocimetry. *Exp Fluids*, *53*, 1177–1190. https://doi.org/10.1007/s00348-012-1353-x

Lynch, M., Mandadzhiev, B., & Wissa, A. (2018). Bioinspired Wingtip Devices: A Pathway to Improve Aerodynamic Performance during Low Reynolds Number Flight. *Bioinspiration and Biomimetics*, *13*(3). https://doi.org/10.1088/1748-3190/aaac53

McCormick, B. W. (1995). *Aerodynamics, Aeronautics, and Flight Mechanics* (2nd Editio). John Wiley & Sons.

McMasters, J. H., & Henderson, M. L. (1979). Low-Speed Single-Element Airfoil Synthesis. *NASA. Langley Res. Center The Sci. and Technol. of Low Speed and Motorless Flight, Pt. 1*, 1–31.

Mizoguchi, M., & Itoh, H. (2013). Effect of Aspect Ratio on Aerodynamic Characteristics at Low Reynolds Numbers. *AIAA Journal*, *51*(7), 1631–1639. https://doi.org/10.2514/1.J051915

Mizoguchi, M., & Yamaguchi, Y. (2012). Aerodynamic Characteristics of Rectangular Flat Plate Wings in Low Reynolds Number Flows. *Journal of the Japan Society for Aeronautical and Space Sciences*, *60*(3), 121–127. https://doi.org/10.2322/jjsass.60.121

Mueller, T. J. (2004). Aerodynamic Measurements at Low Reynolds Numbers for Fixed Wing Micro-Air Vehicles. *Hessert Center for Aerospace Research University of Notre Dame*, *21*, 3–36. http://www.jstor.org/stable/20753438

Mueller, T. J. (1999). Aerodynamic Measurements at Low Reynolds Numbers for Fixed Wing Micro-Air Vehicles. *RTO AVT/VKI Special Course on Development and Operation of UAVs for Military and Civil Applications*, 1–32.

Nakamura, Y., Ohya, Y., & Tsuruta, H. (1991). Experiments on Vortex Shedding from Flat Plates with Square Leading and Trailing Edges. *Journal of Fluid Mechanics*, *222*, 437–447. https://doi.org/10.1017/S0022112091001167

Nakayama, R; Nakamura, Y; Ohya, Y; Ozono, S. (1993). A Numerical Study on the Flow around Flat Plates at Low Reynolds Numbers. *Journal of Wind Engineering and Industrial Aerodynamics*, *47*, 255–264.

Narayan, G., & John, B. (2016). Effect of Winglets Induced Tip Vortex Structure on The Performance of Subsonic Wings. *Aerospace Science and Technology*, *58*, 328–340. https://doi.org/10.1016/j.ast.2016.08.031

O'Meara, M. M., & Mueller, T. J. (1986). Experimental Determination of the Laminar Separation Bubble Characteristics of an Airfoil At Low Reynolds Numbers. *AIAA Paper*, *25*(8). https://doi.org/10.2514/6.1986-1065

Okamoto, Masata; Sasaki, Daisuke; Kamikubo, Masaya; Fujii, R. (2019). Disappearance of Vortex Lift in Low-Aspect-Ratio Wings at Very-low Reynolds Numbers. *Transactions of the Japan Society for Aeronautical and Space Sciences*, *62*(6), 310–317.

Okamoto, M., & Azuma, A. (2005). Experimental Study on Aerodynamic Characteristics of Unsteady Wings at Low Reynolds Number. *AIAA Journal*, *43*(12), 2526–2536. https://doi.org/10.2514/1.14813

Okamoto, M., & Azuma, A. (2011). Aerodynamic Characteristics at Low Reynolds Numbers for Wings of Various Planforms. *AIAA Journal*, *49*(6), 1135–1150. https://doi.org/10.2514/1.J050071

Pelletier, A., & Mueller, T. J. (2000). Low Reynolds Number Aerodynamics of Low-aspect-ratio, Thin/Flat/Cambered-plate Wings. *Journal of Aircraft*, *37*(5), 825–832. https://doi.org/10.2514/2.2676

Reddy, S. R., Dulikravich, G. S., Abdoli, A., & Sobieczky, H. (2015). Multi-Winglets: Multi-Objective Optimization of Aerodynamic Shapes. *53rd AIAA Aerospace Sciences Meeting*.

Roche, U. La, & Palffy, S. (1996). *Wing-grid a Novel Device for Reduction of Induced Drag on Wings*. ICAS-96-2.10 (R).

Roskam, J, & Lan, C. E. (1987). *Airplane Aerodynamics and Performance*.

Santos, L. M. dos, Gomes, G. F., & Coimbra, R. F. (2021). An Experimental Parametric Study on Planar Sheared Wings Tip Devices for Low-to-moderate Aspect Ratio Wings. *Aircraft Engineering and Aerospace Technology*, *93*(1), 227–238. https://doi.org/10.1108/AEAT-07-2020-0143

Savile, D. B. O. (1957). Adaptive Evolution in the Avian Wing. *Evolution*, *11*(2), 212–224.

Schmitz, F. W. (1967). Aerodynamics of the Model Airfoil Part I. In *Airfoil Measurements, Translated from German*. Redstone Scientific Information Center RSIC-721.

Selig, M. S;, Donovan, J. F., & Fraser, D. B. (1989). *Airfoils at Low Speeds*. H. A. Stokely.

Selig, Michael S., Guglielmo, J. J., Broeren, A. P., & Giguère, P. (1996). Experiments on Airfoils at Low Reynolds Numbers. *34th Aerospace Sciences Meeting and Exhibit, January*. https://doi.org/10.2514/6.1996-62

Sevillano, A. A. R., Mora, R. B., Montejano, M. A. B., Barderas, E. B., & Díez, I. (2019). Design of Multiple Winglets for Enhancing Aerodynamics in a Micro Air Vehicle . *8th European Conference for Aeronautics and Space Sciences (EUCASS)*. https://doi.org/10.13009/EUCASS2019-448

Shields, M., & Mohseni, K. (2012). Effects of Sideslip on the Aerodynamics of Low-aspect-ratio Low-reynolds-number Wings. *AIAA Journal*, *50*(1), 85–99. https://doi.org/10.2514/1.J051151

Siddiqui, N. A.; Asrar, W.; Sulaeman, E. (2017). Literature Review: Biomimetic and Conventional Aircraft Wing Tips. *International Journal of Aviation, Aeronautics and Aerospace*, *4*(2).

Siddiqui, N. A., Aldeeb, M., Asrar, W., & Sulaeman, E. (2018). Experimental Investigation of a New Spiral Wingtip. *International Journal of Aviation, Aeronautics, and Aerospace*, *5*(2). https://doi.org/10.15394/ijaaa.2018.1213

Smith, M. J., Komerath, N., Ames, R., Wong, O., & Pearson, J. (2001). Performance Analysis of a Wing with Multiple Winglets. *19th AIAA Applied Aerodynamics Conference, June*. https://doi.org/10.2514/6.2001-2407

Solis, P., Garrido-Martin, M., Duran, E., Gutierrez-Castillo, P., & Pino, C. del. (2024). On The Influence of Spanwise Deformation on Lift Coefficient and Trailing Vortices Properties at Low Reynolds Number. *Physics, 36,* 037122.1-037122.11. https://doi.org/10.1063/5.0195188

Soltani, M. R., Ghorbanian, K., & Nazarinia, M. (2004). Experimental Investigation of The Effect of Various Winglet Shapes on The Total Pressure Distribution Behind a Wing. *24th*

International Congress of The Aeronautical Sciences (ICAS).

Spedding, G. E.; McArthur, J. (2010). Span Efficiencies of Wings at Low Reynolds Numbers. *Journal of Aircraft*, *47*(1), 120–128.

Spillman, J. J.; Allen, J. E. (1978). The Use of Wing Tip Sails to Reduce Vortex Drag. *Aeronaut. J.*, *82*, 387.

Sumpter, J. P.; Runnalls, T. J.; Johnson, A. C.; Barcelo, D. (2023). A 'Limitations' section should be mandatory in all scientific papers. *Science of The Total Environment*, 857(2). https://dx.doi.org/10.1016/j.scitotenv.2022.159395

Sunada, S., Ozaki, K., Tanaka, M., Yasuda, T., Yasuda, K., & Kawachi, K. (2000). Airfoil Characteristics at a Low Reynolds Number. *Journal of Flow Visualization and Image Processing*, *7*(3), 207–215. https://doi.org/10.1615/jflowvisimageproc.v7.i3.20

Sunada, S., Yasuda, T., Yasuda, K., & Kawachi, K. (2002). Comparison of Wing Characteristics at an Ultralow Reynolds Number. *Journal of Aircraft*, *39*(2), 331–338. https://doi.org/10.2514/2.2931

Torres, G. E., & Mueller, T. J. (2004). *Low-Aspect-Ratio Wing Aerodynamics at Low Reynolds Numbers*. *42*(5). https://doi.org/10.2514/1.439

Traub, L. W. (2013). *Aerodynamic Impact of Aspect Ratio at Low Reynolds Number*. *March 2013*. https://doi.org/10.2514/1.C031980

Traub, L. W. (2023). Examination and Prediction of the Lift Components of Low Aspect Ratio Rectangular Flat Plate Wings. *Aerospace*, *10*(7), 597.

Tucker, V. A. (1993). Gliding Birds: Reduction of Induced Drag by Wing Tip Slots Between the Primary Feathers. *Journal of Experimental Biology*, *180*(1), 285–310.

Tucker, V. A. (1995). Drag Reduction by Wing Tip Slots in a Gliding Harris' Hawk, Parabuteo Unicinctus. *Journal of Experimental Biology*, *198*(3), 775–781. https://doi.org/10.1242/jeb.198.3.775

Whitcomb, R. T. (1976). A Design Approach and Selected Wind Tunnel Results at High Subsonic Speeds for Wing-tip Mounted Winglets. *NASA Tn D-8260*, *July*, 1–33. https://ntrs.nasa.gov/archive/nasa/casi.ntrs.nasa.gov/19760019075.pdf

Winslow, J., Otsuka, H., Govindarajan, B., & Chopra, I. (2018). Basic Understanding of Airfoil Characteristics at Low Reynolds Numbers (10^4–10^5). *Journal of Aircraft*, *55*(3), 1050–1061. https://doi.org/10.2514/1.C034415

Zhang, Z., Hubner, J. P., Timpe, A., Ukeiley, L., Abudaram, Y., & Ifju, P. (2012). Effect of Aspect Ratio on Flat-plate Membrane Airfoils. *50th AIAA Aerospace Sciences Meeting Including the New Horizons Forum and Aerospace Exposition*, *January*, 1–15. https://doi.org/10.2514/6.2012-1084

Zhu, Y., Wang, J., & Liu, J. (2024). Tip effects on Three-dimensional Flow Structures Over Low-aspect-ratio Plates : Mechanisms of Spanwise Fluid Transport. *Journal of Fluid Mechanics*, *983*, 1–27. https://doi.org/10.1017/jfm.2024.169

List of Publications

Journals

1. Borah, B., Verma, A., Kulkarni, V. and Saha, U. K., 2024, "Experimental Exploration of Bio-inspired Planar Wingtip Devices for a Flat-plate Wing in the Low Reynolds Number Regime," ASCE Journal of Aerospace Engineering (DOI: 10.1061/JAEEEZ.ASENG-5359)

2. Verma, A., Borah, B., Saha, U. K. and Kulkarni, V., 2024, "Wind tunnel investigation into the bio-inspired slotted winglets for micro air vehicles," Proceedings of the Institution of Mechanical Engineers, Part C: Journal of Mechanical Engineering Science (DOI: 10.1177/09544062241308358)

3. Borah, B., Verma, A., Kulkarni, V. and Saha, U. K., 2024, "Application of Bio-inspired Dihedral Wingtip Attachments on a Flat Plate Wing for Micro Aerial Vehicles," ASCE Journal of Aerospace Engineering (Submitted, under Review)

Conferences

4. Borah, B., Verma, A., Kulkarni, V. and Saha, U. K., 2021, "Vortex Shedding Analysis in the Wake of a Flat Plate at Low Incidence and Low Reynolds Number," ASME 2021 Gas Turbine India Conference. (DOI: 10.1115/GTINDIA2021-75959)

5. Borah, B., Kulkarni, V. and Saha, U. K., 2021, "Aerodynamic Analysis of Flat Plates as Lift Generating Devices for Micro Aerial Vehicles," ASME 2021 International Mechanical Engineering Congress and Exposition. (DOI: 10.1115/IMECE2021-69419)

6. Verma, A., Borah, B. and Kulkarni, V., 2021, "Cavity for Flow Control and Performance Improvement of Airfoil," ASME 2021 Gas Turbine India Conference. (DOI: 10.1115/GTINDIA2021-76415)

Book Chapter

7. Borah, B., Verma, A., Kulkarni, V. and Saha, U. K., 2024, "Experimental Analysis in The Wake of a Flat Plate at Low Reynolds Number," Springer Proceedings of the International Conference on Advances in Aerospace and Energy. (Accepted)